OPTIMIZATION OF CO_2 EOR AND STORAGE DESIGN UNDER UNCERTAINITY

A THESIS SUBMITTED TO
THE GRADUATE SCHOOL OF NATURAL AND APPLIED SCIENCES
OF
MIDDLE EAST TECHNICAL UNIVERSITY

BY

SERDAR BENDER

IN PARTIAL FULFILLMENT OF THE REQUIREMENTS
FOR
THE DEGREE OF DOCTOR OF PHILOSOPHY
IN
PETROLEUM AND NATURAL GAS ENGINEERING

DECEMBER 2016

Approval of the thesis:

OPTIMIZATION OF CO_2 EOR AND STORAGE DESIGN UNDER UNCERTAINITY

submitted by **SERDAR BENDER** in partial fulfillment of the requirements for the degree of **Doctor of Philosophy in Petroleum and Natural Gas Engineering Department, Middle East Technical University** by,

Prof. Dr. Gülbin Dural Ünver _____
Dean, Graduate School of **Natural and Applied Sciences**

Prof. Dr. Serhat Akın _____
Head of Department, **Petroleum and Natural Gas Engineering**

Prof. Dr. Serhat Akın _____
Supervisor, **Petroleum and Natural Gas Engineering**

Examining Committee Members:

Prof. Dr. Nurkan Karahanoğlu _____
Geological Engineering Dept., METU

Prof. Dr. Serhat Akın _____
Petroleum and Natural Gas Engineering Dept., METU

Asst. Prof. Dr. İsmail Durgut _____
Petroleum and Natural Gas Engineering Dept., METU

Prof. Dr. Abdurrahman Satman _____
Petroleum and Natural Gas Engineering Dept., ITU

Assoc. Prof. Dr. Ömer İnanç Türeyen _____
Petroleum and Natural Gas Engineering Dept., ITU

Date: 08/12/2016

I hereby declare that all information in this document has been obtained and presented in accordance with academic rules and ethical conduct. I also declare that, as required by these rules and conduct, I have fully cited and referenced all material and results that are not original to this work.

Name, Last name : SERDAR BENDER

Signature :

ABSTRACT

OPTIMIZATION OF CO_2 EOR AND STORAGE DESIGN UNDER UNCERTAINITY

Bender, Serdar
Ph.D., Department of Petroleum and Natural Gas Engineering
Supervisor: Prof. Dr. Serhat Akın

December 2016, 119 pages

The combination of CO_2 enhanced oil recovery (EOR) and permanent CO_2 storage in mature oil reservoirs have the potential to provide a critical near-term solution for reducing greenhouse gas emissions. In the literature, although there are many studies about CO_2 storage and EOR, only a few studies have focused on maximizing both the oil recovery and the CO_2 storage. Moreover, these studies are either experimental or conducted using synthetic reservoir models. Typically, pure CO_2 has the property of mixing with oil to swell it, make it lighter, detach it from the rock surfaces, and cause the oil to flow more freely within the reservoir to producer wells. The main aim of this research is to investigate the effects of immiscible CO_2 injection while maximizing CO_2 storage in a mature heavy oil carbonate reservoir located in south east Turkey. Three different nearby natural gas reservoirs with differing amounts of CO_2 (77.17%, 28.15% and 20.65%) and flue gas originating from a cement factory were considered as CO_2 sources. In order to realistically simulate several possible mechanisms such as CO_2 swelling and viscosity reduction a 3D compositional simulation model was built after a detailed fluid characterization study. Effect of injected gas composition, gas oil ratios and injection rates on CO_2 storage and oil recovery were investigated. Impact of these parameters on the project feasibility was studied using an economic model. The highest amount of CO_2 storage (1.63 billion sm^3) and cumulative oil production (1.57 $MMsm^3$) was achieved by pure CO_2 injection. As the amount of CO_2 present in the injected gas stream decreased, the oil recovery and the stored CO_2 decreased

as well. It has been observed that optimized GOR values and injection rates contributed to better sweep efficiency, pressure management and higher net present values.

Keywords: CO_2, Storage, EOR, Flue Gas

ÖZ

KARBONDİOKSİT KULLANIMI İLE GELİŞTİRİLMİŞ PETROL KURTARIMININ VE KARBONDİOKSİT DEPOLAMASININ BELİRSİZLİK DURUMUNDA DİZAYNININ OPTİMİZASYONU

Bender, Serdar
Doktora, Petrol ve Doğalgaz Mühendisliği Bölümü
Tez Yöneticisi: Prof. Dr. Serhat Akın

Aralık 2016, 119 Sayfa

Olgun petrol sahalarında karbondioksit ile geliştirilmiş petrol kurtarımının ve daimi karbondioksit depolamasının birleştirilmesi, sera gazı emisyonlarının düşürülmesine çözüm olabilir. Literatürde, CO_2 depolanmasına ve geliştirilmiş petrol kurtarımına ait birçok çalışma olmasına rağmen, sadece birkaçı petrol kurtarımının ve CO_2 depolanmasının arttırılmasına odaklanmıştır. Dahası, bu çalışmalar ya deneysel ya da sentetik rezervuar modellerinde yürütülmüştür. Genellikle, saf karbondioksit petrol ile karışma özelliği sayesinde petrolü şişirir, hafif hale getirir, kaya yüzeyinden ayırır ve petrolün rezervuardan üretim kuyularına daha özgürce akmasını sağlar. Bu çalışmanın amacı, Türkiye`nin güney doğusunda bulunan olgun bir ağır petrol karbonat rezervuarında karışmayan CO_2 enjeksiyonunun etkilerini incelemek ve aynı zamanda CO_2 depolanmasını arttırmaktır. CO_2 kaynağı olarak saha yakınında bulunan ve farklı miktarlarda CO_2 içeren (%77.17, %28.15 ve % 20.65) üç farklı doğal gaz kaynağı ve çimento fabrikasından gelen baca gazı kullanılmıştır. CO_2 şişirme ve viskozite düşürme gibi bazı olası mekanizmaları daha gerçekçi simüle etmek amacıyla detaylı akışkan karakterizasyon çalışması sonrasında 3D karışımsal simülasyon modeli oluşturulmuştur. Enjeksiyonu yapılan gaz bileşiminin, gaz petrol oranının ve enjeksiyon debilerinin CO_2 depolamasına ve petrol kurtarımına etkileri araştırılmıştır. Bu parametrelerin proje fizibilitesine etkileri ekonomik model kullanılarak çalışılmıştır. Saf CO_2 enjeksiyonu ile en yüksek CO_2 depolanması

(1.63 milyar sm^3) ve kümülatif petrol üretimi (1.57 milyon sm^3) elde edilmiştir. Enjeksiyonu yapılan gazdaki CO_2 miktarı azaldığında, petrol kurtarımı ve depolanan CO_2 miktarı da düşmektedir. Optimize edilmiş gaz petrol oranı değerlerinin ve enjeksiyon debilerinin daha iyi süpürme verimine, daha iyi basınç yönetimine ve daha yüksek net bugünkü değerine katkıda bulunduğu gözlemlenmiştir.

Anahtar Kelimeler: CO_2, Depolama, EOR, Baca Gazı

To My Family

ACKNOWLEDGMENTS

This thesis would not have been possible without the guidance and the help of several individuals who, by any means, contributed and provided their valuable assistance in the preparation and completion of this study.

First of all, I would like to present my truthful gratitude to Prof. Dr. Serhat Akın. Without his valuable guidance, this thesis would not have been completed.

Besides my advisor, I would like to thank the rest of my thesis committee; Prof. Dr. Nurkan Karahanoğlu, Prof. Dr. Abdurrahman Satman, Assoc. Prof. Dr. Ömer İnanç Türeyen, and Asst. Prof. Dr. İsmail Durgut for their encouragement, insightful comments and hard questions.

I would like to acknowledge scholarship support provided by The Scientific and Technological Research Council of Turkey (TUBITAK 2211-D).

I would like to express my gratitude to the TP Production Department since they assisted me obtaining the essential data.

I would like to acknowledge Schlumberger for providing the license of Eclipse and Petrel Software.

TABLE OF CONTENTS

ABSTRACT v

ÖZ vii

ACKNOWLEDGMENTS x

TABLE OF CONTENTS xi

LIST OF TABLES xiii

LIST OF FIGURES xiv

NOMENCLATURE xvi

CHAPTER 1 1

INTRODUCTION 1

CHAPTER 2 3

GEOLOGICAL CO_2 STORAGE & ENHANCED OIL RECOVERY 3

2.1 CO_2 Storage 3
2.1.1 CO_2 Storage Sites 3
2.1.1.1 Oil and Gas Reservoirs 3
2.1.1.2 Deep Saline Aquifers 4
2.1.1.3 Coal Seams 5
2.1.2 Trapping Mechanisms 5
2.1.2.1 Stratigraphical/Structural Trapping 6
2.1.2.2 Residual Trapping 7
2.1.2.3 Solubility Trapping 7
2.1.2.4 Mineral Trapping 9
2.1.3 CO_2 Sources and CO_2 Capture Systems 9
2.1.3.1 Sources of CO_2 9
2.1.3.2 CO_2 Capture Systems and Technologies 10
2.2 CO_2 EOR 13
2.2.1 CO_2 Properties 13
2.2.1 CO_2 EOR Displacement Mechanisms 15
2.2.1.1 Immiscible CO_2 EOR 15
2.2.1.2 Miscible CO_2 EOR 16
2.2.3 CO_2 Flooding Methods 17
2.2.3.1 Cyclic CO_2 Injection (Huff-N-Puff) 17
2.2.3.2 Continuous CO_2 Injection 18
2.2.3.3 Water Alternating Gas Injection (WAG) 18
2.2.3.4 Tapered Water Alternating Gas Injection 18
2.2.3.5 Carbonated Water Injection 19
2.2.4 Screening Criteria for CO_2 EOR 19
2.3 Co-Optimization of CO_2 EOR and Storage 21
2.4 Flue Gas 22

CHAPTER 3 27

STATEMENT OF PROBLEM 27

CHAPTER 4 29

SOURCES AVAILABLE FOR STORAGE & EOR APPLICATION AND PVT TESTS 29

4.1 Gas Source A 30

4.2 Gas Source B 31
4.3 Gas Source C 33
4.4 Cement Factory 34
4.5 Mature Oil Field PVT Tests 35
4.5.1 Constant Composition Expansion 36
4.5.2 Differential Liberation Expansion (DLE) 39
4.5.3 Viscosity Measurement 42

CHAPTER 5 43

NUMERICAL MODELING AND HISTORY MATCHING 43

5.1 Field Data 43
5.2 Geologic Description 45
5.3 Rock and Fluid Properties 47
5.4 Fluid Characterization for Compositional Simulation 51
5.5 Lumping Scheme 55
5.6 Equation of State Tuning 58
5.7 Model Construction and History Matching 61

CHAPTER 6 69

OPTIMIZATION OF GAS INJECTION AND OIL RECOVERY 69

6.1 Flue Gas Injection 69
6.1.1 Effect of CO_2 Solubility 72
6.1.2 Effect of GOR 75
6.1.3 Effect of Injection Rates 77
6.2 Pure CO_2 Injection 79
6.2.1 CO_2 Storage 80
6.2.2 CO_2 EOR 82
6.3 Natural Gas Injection for EOR 84
6.4 A Discussion on Gas Saturation Distributions 86
6.5 Economic Investigation of Flue Gas Injection, CO_2 Injection and Natural Gas Injection 93

CHAPTER 7 99

CONCLUSIONS 99

CHAPTER 8 103

RECOMMENDATIONS AND FUTURE WORK 103

REFERENCES 105

CURRICULUM VITAE 119

LIST OF TABLES

TABLES

Table 1 - Screening criteria for CO_2 EOR 20
Table 2 - Source A reservoir gas composition 30
Table 3 - Source A reservoir gas properties 31
Table 4 - Source A reservoir gas PVT properties 31
Table 5 - Gas source B gas composition 32
Table 6 - Gas source B gas properties 32
Table 7 - Gas source C gas composition 33
Table 8 - Gas source C gas properties 34
Table 9 - Flue gas stream gas composition and properties used for simulation 35
Table 10 - PVT Report summary 36
Table 11 - One phase oil isothermal compressibility 37
Table 12 - Relative volume 38
Table 13 - Bo, GOR, oil density 39
Table 14 - Oil gravity & density at standard conditions 40
Table 15 - Viscosity measurements for oil and gas mixture 42
Table 16 - Molar compositions of oil 52
Table 17 - Properties of components before regression and lumping 54
Table 18 - Properties of components after lumping 56
Table 19 - Properties of injected gas stream components after lumping 57
Table 20 - Summary of the reservoir model properties 62
Table 21 - Summary of simulation results 74
Table 22 - Economic model input data from the simulator 93
Table 23 - Economic inputs 94
Table 24 - Economic model outputs 94
Table 25 - Economic analysis results 97

LIST OF FIGURES

FIGURES

Figure 1 - Contribution of the trapping mechanisms to storage security with time 6
Figure 2 - CO_2 Solubility in water vs pressure and temperature 8
Figure 3 - United States CO_2 EOR project sources 10
Figure 4 - CO_2 Capture systems 11
Figure 5 - CO_2 Separation systems 12
Figure 6 - CO_2 Phase diagram 13
Figure 7 - CO_2 Density vs temperature and pressure 14
Figure 8 - CO_2 Viscosity vs temperature and pressure 15
Figure 9 - Cyclic CO_2 injection method 17
Figure 10- Global greenhouse emissions by gas 23
Figure 11 - Cement production process 24
Figure 12 - Distance of the sources to the main camp 29
Figure 13 - Oil properties vs pressure 41
Figure 14 - Oil & Gas mixture properties vs pressure 41
Figure 15- Field structure map 44
Figure 16 - Field production and injection history 45
Figure 17 - Petrographic and log characteristics of the reservoir 46
Figure 18 – Conceptual model of the reservoir 46
Figure 19 - Porosity distribution map 48
Figure 20 - Permeability and porosity relationship for Layers 1, 2, 3 48
Figure 21 - Relative permeability vs water & gas saturation for Layer 1 49
Figure 22 - Capillary pressure vs water saturation for Layer 1 50
Figure 23 - Relative volumes from CCE experiment vs calculated 59
Figure 24 - Liquid density from DLE experiment vs calculated 59
Figure 25 - GOR from DLE experiment vs calculated 60
Figure 26 - B_o from DLE experiment vs calculated 60
Figure 27 - Viscosity from viscosity experiment vs calculated 61
Figure 28 - History match of the field oil water gas production rate and pressure 64
Figure 29 - History match for Well #14 and Well #12 65
Figure 30 - History match analysis of oil production rate, oil production cumulative, water cut & pressure 67
Figure 31 - Field cumulative oil production, oil rate, pressure and water production rate for the base case 71
Figure 32 - Cumulative oil production, gas in place and CO_2 dissolved in aqueous phase with and without CO_2SOL 73
Figure 33 - Gas in place and CO_2 dissolved in aqueous phase, cumulative oil production and average reservoir pressure for the GOR Case 76
Figure 34 - Gas in place and CO_2 Dissolved in aqueous phase, cumulative oil production and average reservoir pressure for the injection rate case 78
Figure 35 - Amount of flue gas storage vs recovery factor 79
Figure 36 - Cumulative oil production, gas in place, CO_2 dissolved in aqueous phase and pressure for the CO_2 storage case 81
Figure 37 - Cumulative oil production, gas in place, CO_2 dissolved in aqueous phase and pressure for the CO_2 EOR case 83
Figure 38 - Cumulative oil production vs time 85
Figure 39 - 3D view of CO_2 saturation distribution from 2003 to 2016 (Real case) 87
Figure 40 - 3D view of CO_2 saturation distribution from 2021 to 2041 (Continuous CO_2 injection case) 89
Figure 41 - 3D view of CO_2 saturation distribution from 2061 to 2116 (Continuous CO_2 injection case) 90

Figure 42 - Cross sectional view of CO_2 saturation distribution, 01.01.2116 (Continuous CO_2 injection case) 91
Figure 43 - 3D view of gas saturation distributions for CO_2 injection case, flue gas injection case and Source A gas injection case, 01.01.2116 92

NOMENCLATURE

Abbreviations:

B_g	: Gas Formation Volume Factor
B_o	: Oil Formation Volume Factor
CAPEX	: Capital Expenditure
CCE	: Constant Composition Expansion
CWI	: Carbonated Water Injection
DLE	: Differential Liberation Expansion
$EF_{clinker}$	: Clinker Emission Factor
EOR	: Enhanced Oil Recovery
G_{inj}	: Gas Injection Rate
GOR	: Gas Oil Ratio
G_{pro}	: Gas Production Rate
G_t	: Gigatonne
K_{rg}	: Gas Relative Permeability
K_{ro}	: Oil Relative Permeability
K_{rw}	: Water Relative Permeability
M	: Match Value
MCN	: Multi Carbon Number
M_I	: Number of Carbon Atoms of the Plus Fraction
M_N	: Molecular Weight of the Last Component
M_n	: Molecular Weight of the + Component
M_w	: Molecular Weight
n	: Number of Carbon Atoms of the Plus Fraction
N	: Number of Carbon Atoms of the Last Component
N_c	: Number of Components
N_g	: Number of Multi Carbon Number Groups
NCF	: Net Cash Flow
NPV	: Net Present Value
O_i	: Observed Value
OPEX	: Operating Expenditure
O_{pro}	: Oil Production Rate
p	: Pressure
P_b	: Saturation Pressure
P_{bh}	: Bottom Hole Pressure
P_c	: Capillary Pressure
P_{pc}	: Critical Pressure
R	: Universal Gas Constant
RF	: Recovery Factor
S_i	: Simulated Value
S_w	: Water Saturation
T	: Temperature

T_{pc} : Critical Temperature
V : Volume
WAG : Water Alternating Gas Injection
W_{inj} : Water Injection Rate
W_{pro} : Water Production Rate
Z : Compressibility Factor

Greek Symbols:

γ_g : Specific Gravity of Gas
ω : Acentric Factor
μ_g : Gas Viscosity
σ : Normalization Parameter

CHAPTER 1

INTRODUCTION

Carbon dioxide (CO_2) is the primary anthropogenic greenhouse gas. One of the major CO_2 emitting sources is process industries and cement industry is one of them. Approximately 5% of the anthropogenic CO_2 emissions is released to the atmosphere by the cement industry (Arachchige et al., 2013). Flue gas containing high amount of CO_2 is emitted during cement clinker production and during fuel combustion. Composition of the flue gas depends on the fuel used for combustion process but it mainly consists of nitrogen (N_2), carbon dioxide (CO_2), water vapor (H_2O), oxygen (O_2) and sulfur dioxide (SO_2). Sulfur, nitrogen oxide (NO_x), carbon monoxide (CO), carbon dioxide and dust are some of the air polluting components that may be present in flue gases (Knopse and Walleser, 2004). CO_2 emissions and non-CO_2 emissions produced as flue gas during cement production can be sequestered in underground geologic formations. CO_2 can be sequestered into three geological areas: coal seams, mature or depleted hydrocarbon reservoirs and deep saline aquifers (Bender, 2011). There are four essential mechanisms that hold CO_2 in place: stratigraphic/structural, residual, solubility and mineral trapping (Zhang and Song, 2014). These mechanisms are required for successful geologic CO_2 storage for hundreds to thousands of years. With the lack of required trapping mechanisms, CO_2 will be released into the atmosphere. If there is a good seal, it can be stated that CO_2 will be trapped permanently and will be immobile with the contribution of the residual, solubility and mineral trapping mechanisms. Injecting flue gas into oil reservoirs is very attractive for flue gas sequestration because these reservoirs have structural seals for trapping, these are well studied and characterized fields, these fields have surface facilities and wells, which will also

decrease the capital investments of the storage project. Injecting flue gas into producing oil fields will result in incremental oil recovery and make the storage project more feasible due to reduced costs. In addition, availability of the flue gas source has strong effect on project economics.

The main aim of this research is to investigate the effects of immiscible CO_2 injection while maximizing CO_2 storage in a mature heavy oil carbonate reservoir located in south east Turkey. Three different nearby natural gas reservoirs with differing amounts of CO_2 (77.17%, 28.15% and 20.65%) and flue gas originating from a cement factory were considered as CO_2 sources. In order to realistically simulate several possible mechanisms such as CO_2 swelling and viscosity reduction a 3D compositional simulation model was built after a detailed fluid characterization study. Effect of injected gas composition, gas oil ratios and injection rates on CO_2 storage and oil recovery were investigated. Impact of these parameters on the project feasibility was studied using an economic model.

This thesis consists of seven chapters:

In Chapter 1, information about the scope of this study and each chapter is given. Chapter 2 presents literature review about geological CO_2 storage and information about CO_2 storage sites, CO_2 trapping mechanisms, CO_2 sources and CO_2 capture systems. Chapter 3 gives information about CO_2 properties, CO_2 EOR displacement mechanisms, CO_2 flooding method and screening criteria for CO_2 EOR. In Chapter 4, information about gas sources that can be used for EOR application is given. In Chapter 5, numerical modeling and history matching of the field are discussed. Chapter 6 discusses the optimization of the gas injection and oil recovery. The final chapter concludes the thesis. The work performed and main results are summarized.

CHAPTER 2

GEOLOGICAL CO_2 STORAGE & ENHANCED OIL RECOVERY

In this chapter, CO_2 storage and CO_2 EOR fundamentals are discussed.

2.1 CO_2 Storage

This section provides information about CO_2 storage sites, trapping mechanisms, CO_2 sources and CO_2 capture systems.

2.1.1 CO_2 Storage Sites

CO_2 can be sequestered into three geological structures; these are oil and gas reservoirs, deep saline aquifers and coal seams (Orr, 2004).

2.1.1.1 Oil and Gas Reservoirs

Oil and gas reservoirs are very attractive for CO_2 storage because these reservoirs already have structural seals, which trap oil and gas for millions of years. This demonstrates the safety of these seals for CO_2 sequestration. These reservoirs are also best candidates, because they are well studied and characterized. Most of the fields have seismic analysis, core data and log analysis, well test analysis, PVT analysis, static and dynamic models. These data can be used to design the project, to determine the storage capacity, and to establish project economics and risks. In addition, these fields have surface facilities that will also decrease the capital investments of the storage project. The benefits discussed above about storing CO_2

into oil and gas reservoirs are both for abandoned fields and mature fields. Injecting CO_2 into producing oil fields will result in incremental oil recovery and make the storage project more feasible. There are many reported CO_2 flooding research in the literature. CO_2 can be stored in most of the oil reservoirs however to make the project profitable, there are some screening criteria. Taber (1997) discusses the screening criteria for CO_2 EOR and Jessen et al. (2005) discuss the screening criteria for CO_2 storage.

2.1.1.2 Deep Saline Aquifers

For CO_2 storage, saline aquifers are advantageous in terms of storage capacity and availability. Oil and gas reservoirs or coal seams may not be around the CO_2 emission sources, but saline formations might be due to the fact that saline aquifers are widespread (Pruess et al., 2003). Another advantage is the CO_2 storage capacity of these formations, which is more than other geological storage areas. According to Parson and Keith (1998), storage capacity of deep saline aquifers is between 370-3700 G_t CO_2 while storage capacity of oil and gas reservoirs is between 740-1850 G_t CO_2 and storage capacity of coal beds is between 370-1100 G_t CO_2. However, there are some disadvantages of storing CO_2 in deep saline aquifers. Storing CO_2 in deep saline aquifers has no economic value when compared with EOR projects. According to Bender (2011), geopressured geothermal aquifers might contain dissolved methane and this gas can be produced while sequestering CO_2, which can possibly make the project profitable. Moreover, according to John et al. (1998), mechanical energy (brine rates), thermal energy (hot brine) and chemical energy (dissolved methane) can be obtained from geopressured geothermal aquifers and can be used to decrease the costs of the project. On the other hand, capital investments will be higher for CO_2 storage projects in saline aquifers because there is need to drill wells. Characterization is the other problem for saline aquifers, because aquifers are not thoroughly investigated and increasing the need to do extensive characterizations to decrease the project risk (Stausland, 2014).

2.1.1.3 Coal Seams

Unmineable coal seams are other natural options for geological CO_2 storage, because mining of the coal and combustion will release the sequestered CO_2 into the atmosphere. Coal seams contain methane on pore surfaces of the coal and in fractures as adsorbed gas or free gas. Here, CO_2 is stored by the mechanism of adsorption. Injected CO_2 induces coal matrix and as a result methane is desorbed because coal prefers the adsorption of carbon dioxide over methane (Ripepi, 2009). Injected CO_2 will go through fractures, diffuse into matrix system and then replace methane (Ohga, 2003). The process is called enhanced coal bed methane recovery (ECBM). Sequestering CO_2 into coal seams might be economic by producing methane from these formations (Gale and Freund, 2001).

2.1.2 Trapping Mechanisms

Four basic mechanisms may hold CO_2 in place. These are stratigraphical/structural, residual, solubility and mineral trapping (Zhang and Song, 2014). These mechanisms are required for successful geologic CO_2 storage for hundreds to thousands of years. With the lack of required trapping mechanisms, CO_2 will be released into the atmosphere. If there is a good seal, CO_2 will be trapped permanently and will be immobile with the contribution of the residual, solubility and mineral trapping mechanisms. Figure 1 shows the contribution of the trapping mechanisms to storage security with time (Metz et al., 2005). As can be seen from Figure 1, mineral trapping has the highest storage security, followed by solubility, residual and structural trapping. However, mineral trapping requires long CO_2 residence times (more than 100 years) compared to other trapping mechanisms. Time is a very important parameter while discussing these parameters. These are explained in the following sections.

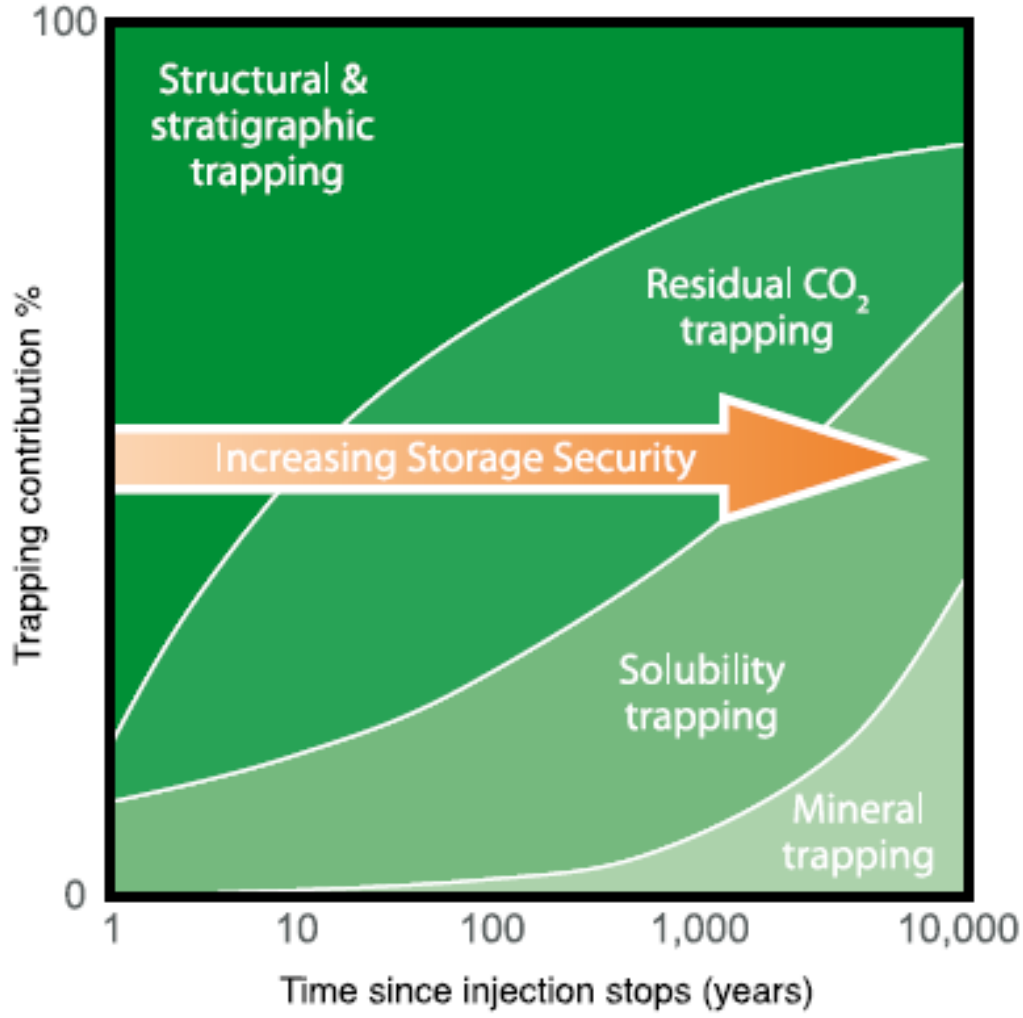

Figure 1 - Contribution of the trapping mechanisms to storage security with time (Metz et al., 2005)

2.1.2.1 Stratigraphical/Structural Trapping

The first basic mechanism required to store CO_2 as a gas or supercritical fluid is stratigraphical/structural trapping (hydrodynamic trapping) (Law and Bachu, 1996). During CO_2 injection, CO_2 will rise in the reservoir because of buoyancy. In structural trapping CO_2 is trapped under a low permeability cap rock which will prevent the migration of the CO_2 to the surface. There are many combinations of structural traps. Anticline traps, sealing fault traps, salt dome traps and unconformity traps are common examples for structural and stratigraphic traps.

2.1.2.2 Residual Trapping

When CO_2 is injected into reservoir it will flow as a nonwetting phase and invades pores which is a drainage process. As CO_2 continues to move, it will leave these pores and CO_2 saturation in the pores will decrease until gas saturation reaches to residual gas saturation which can be explained by relative permeability hysteresis (Juanes et al., 2006). Imbibition of brine starts when CO_2 leaves these pores and brine disconnects some of the CO_2 in pores where capillary forces are dominant and traps it. Methods like water alternating gas injection are cyclic injection mechanisms, which change the saturation direction and increase the effect of hysteresis (Ghomian, 2008). In this study, only continuous gas injection is discussed.

2.1.2.3 Solubility Trapping

Dissolution of injected CO_2 in formation fluid is called solubility trapping. Solubility of CO_2 will decrease with increase in formation water salinity, temperature and solubility of CO_2 will increase with the increasing pressure (Figure 2). With increasing depth, temperature and salinity will increase and amount of dissolved CO_2 will decrease (Bachu and Adams, 2003). When brine is saturated by CO_2, density of brine will increase and brine will start to move down which will increase the possibility to keep CO_2 underground. However, as can be seen from Figure 1, solubility trapping is a very slow process.

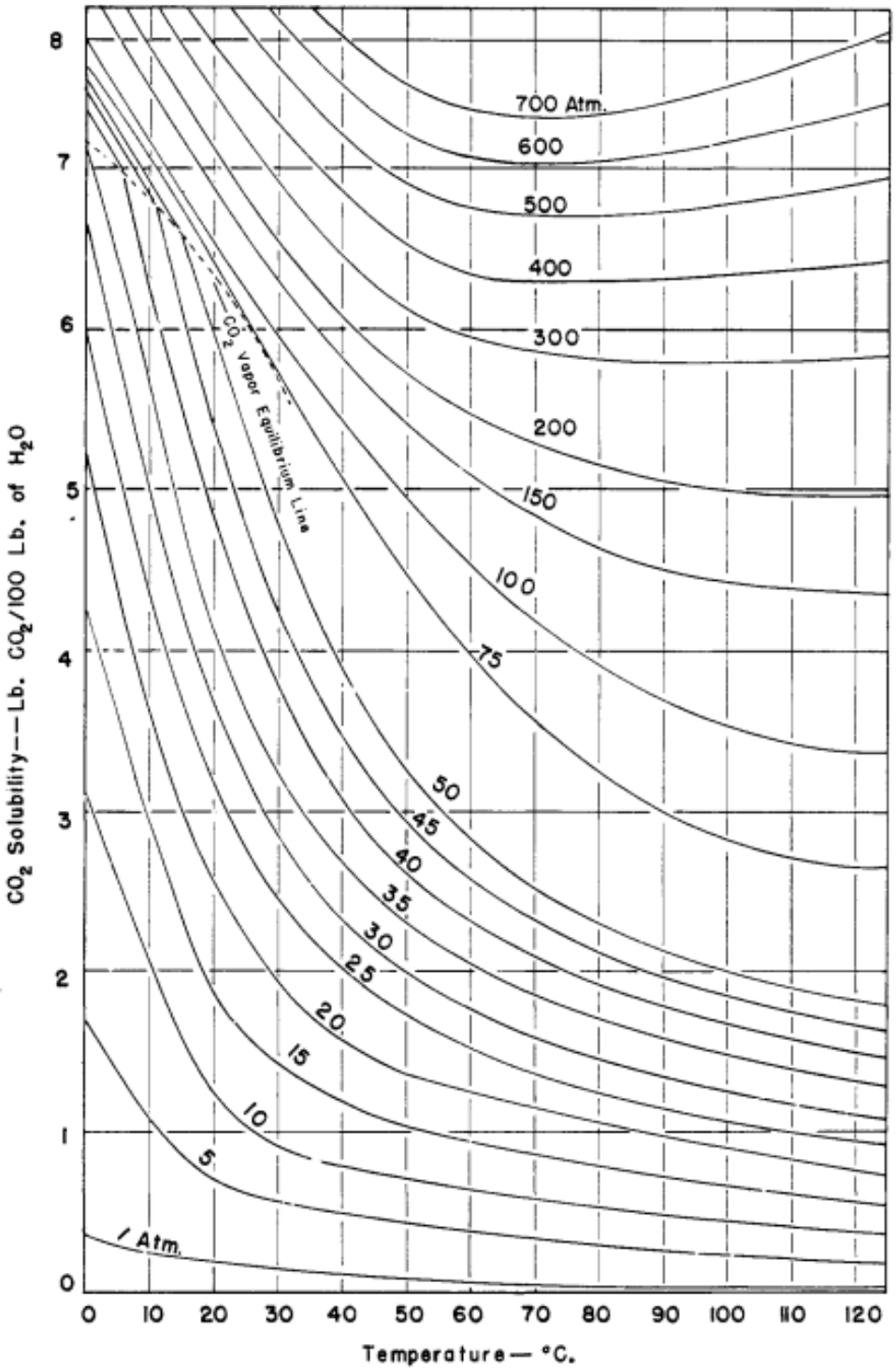

Figure 2 - CO_2 Solubility in water vs pressure and temperature (Dodds et al., 1956)

2.1.2.4 Mineral Trapping

With the dissolution of CO_2 in brine, carbonic acid (H_2CO_3) may form. As a result, pH will decrease and geochemical reactions will start. Carbonic acid will react with other dissolved species and minerals in formation. Dissolved CO_2 will react with divalent cations like Ca^{2+}, Mg^{2+} or Fe^{2+} to form carbonate mineral precipitates like calcite, magnesite and siderite (Nghiem et al., 2010). This type of trapping is the most stable one, but long residence times from hundreds to thousands of years (Figure 1) are required. Because of this slow process, contribution of mineral trapping is usually considered as negligible during CO_2 injection (Bachu et al., 2007). Therefore, mineral trapping is neglected in this study.

2.1.3 CO_2 Sources and CO_2 Capture Systems

This section provides information about CO_2 sources and CO_2 capture systems.

2.1.3.1 Sources of CO_2

There are three different sources of CO_2, which can be used for CO_2 EOR and storage purposes: anthropogenic sources, hydrocarbon reservoirs containing CO_2 and natural CO_2 reservoirs. These CO_2 sources might be impure and needs to be processed before injection to increase the efficiency of CO_2 EOR. United States CO_2 EOR projects are good examples where both natural and industrial CO_2 sources are used (Figure 3).

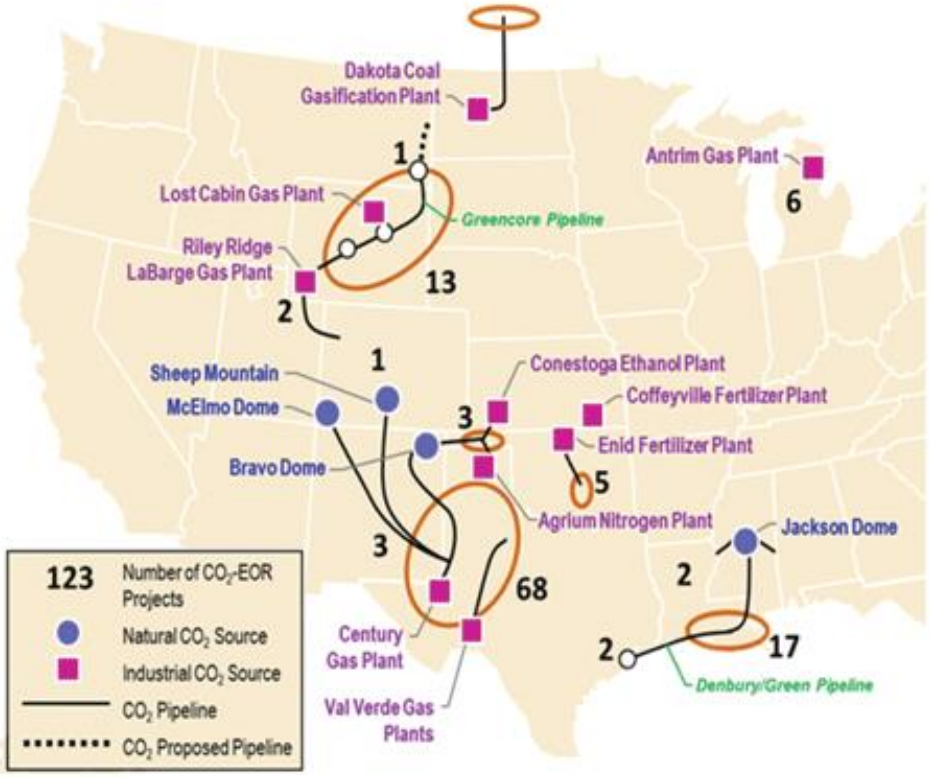

Figure 3 - United States CO_2 EOR project sources (Michael, 2014)

2.1.3.2 CO_2 Capture Systems and Technologies

CO_2 is generally captured from sources that are continuous and able to provide sufficient amount of CO_2. Fuel processing plants, fossil fuel power plants and other industrial plants that produce cement, chemicals, steel and iron etc. are typical candidates (Metz et al., 2005). Pre-combustion capture, oxy-fuel combustion capture, post combustion capture and capture from industrial sources are main CO_2 capture systems from fossil fuel/biomass use (Figure 4). These systems work together with three different separation technologies to separate CO_2 from other gases: separation with sorbents or solvents (chemical and physical absorption), separation with membranes, and cryogenic distillation (Figure 5).

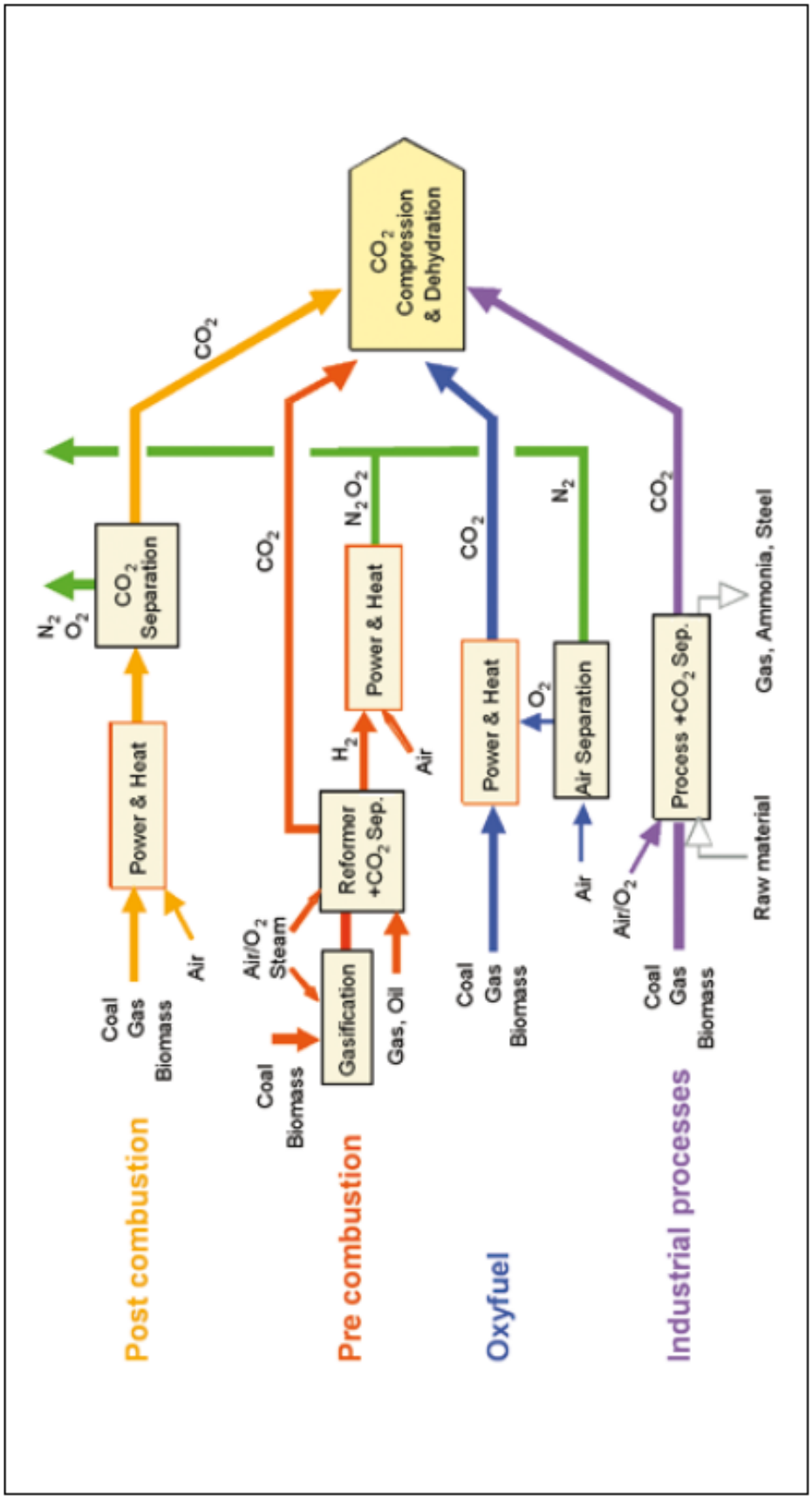

Figure 4 - CO_2 Capture systems (Metz et al., 2005)

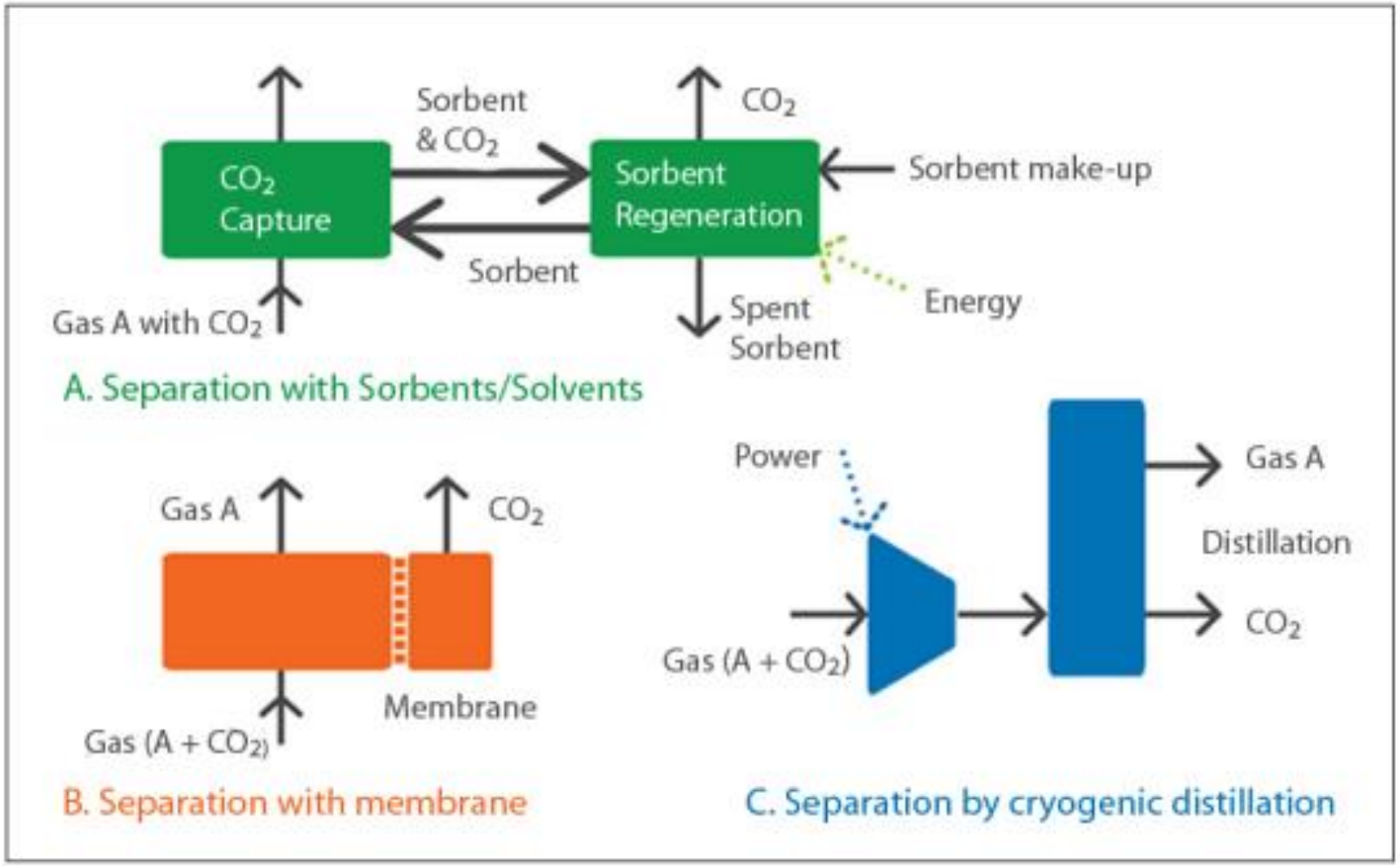

Figure 5 - CO_2 Separation systems (CO_2 Capture project, 2008)

2.2 CO_2 EOR

In this section information about CO_2 properties, CO_2 flooding methods and screening criteria for CO_2 EOR is given.

2.2.1 CO_2 Properties

CO_2 is a gas existing in atmosphere, that is composed of a carbon and two oxygen atoms and chemical formula is CO_2. It is important to understand physical properties of CO_2 and chemical reactions of CO_2 to design successful CO_2 EOR and storage projects. Atomic weight of CO_2 is 44.01 g/mol (Metz et al., 2005). CO_2 is in gas form at standard conditions, 1 bar and 0 ^oC. Liquid CO_2 forms when the pressure is above 5.18 bar and temperature is above -56.5 ^oC. Solid CO_2 forms at very high pressures when the temperature is above -56.5 ^oC. Carbon dioxide behaves like a supercritical fluid above critical point that is 31.1 ^oC and 73.9 bar. Relationship between the three states of CO_2 is presented on CO_2 Phase Diagram in Figure 6.

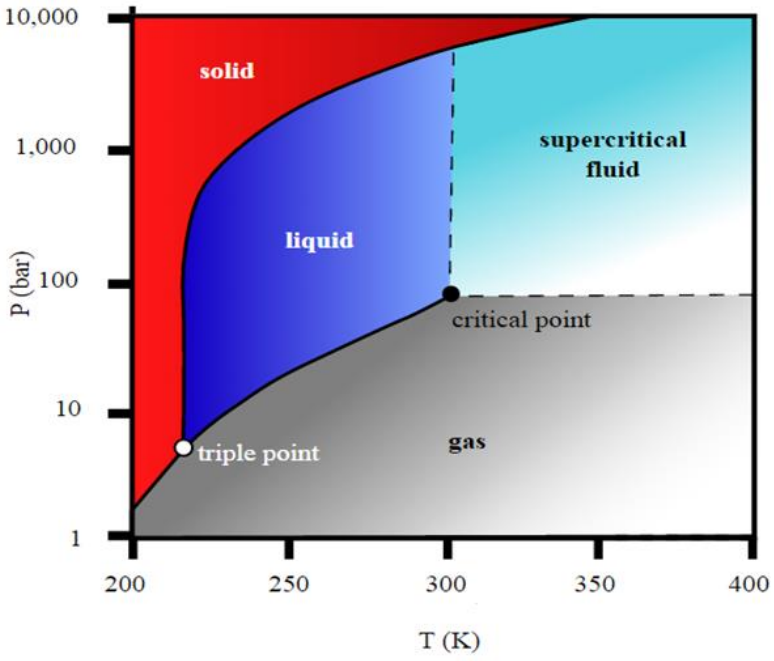

Figure 6 - CO_2 Phase diagram (Lower, 2016)

During CO_2 injection into reservoirs, CO_2 is injected in liquid form in wellbore because of low temperature and high pressure. However, in the reservoir CO_2 will be in gas or supercritical form because reservoir temperatures are generally higher than 31.1 ^oC. As a result, there is only gas or supercritical CO_2 should occur. Therefore, it is principal to understand supercriticality of CO_2. Supercritical carbon dioxide will diffuse like gas and it will dissolve in substances like liquid. Supercritical CO_2 is compressible like a gas and will fill and get the shape of a tank. However, it will dissolve in materials like a liquid. Density of supercritical CO_2 is close to density of liquid CO_2 (Figure 7); however, viscosity of CO_2 will always be smaller than the water viscosity but close to gas viscosity (Figure 8). Therefore, CO_2 mobility will be similar to gas mobility at reservoir conditions and it will be buoyant (Oldenburg, 2002). Around critical temperature and pressure, property of gas or supercritical fluid may change sharply with a little change in pressure (Figure 7). In supercritical state, CO_2 has a density like liquid and viscosity like gas.

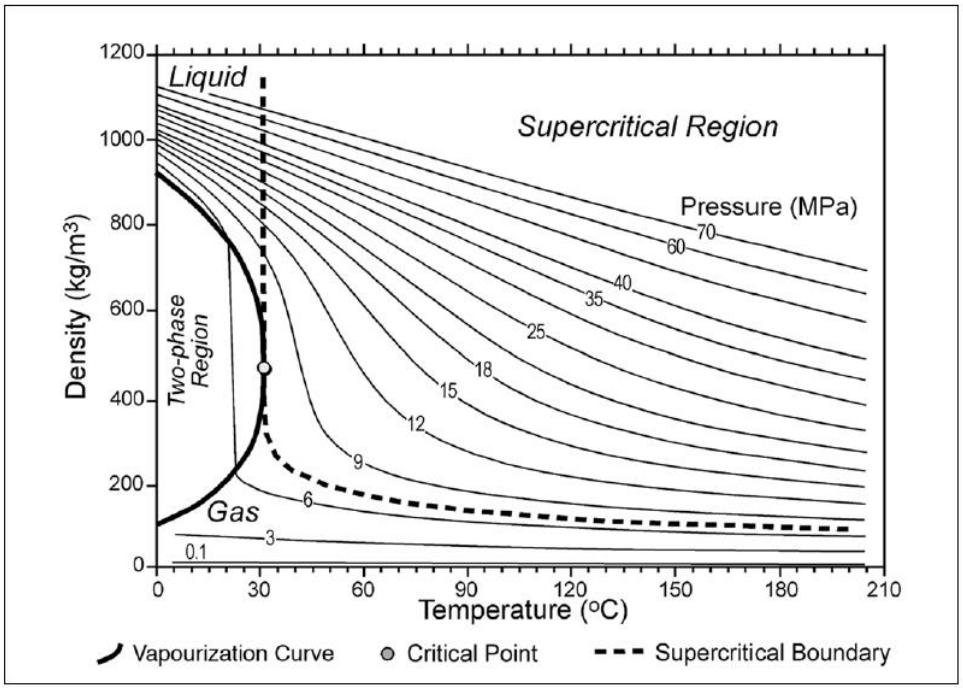

Figure 7 - CO_2 Density vs temperature and pressure (Bachu, 2003)

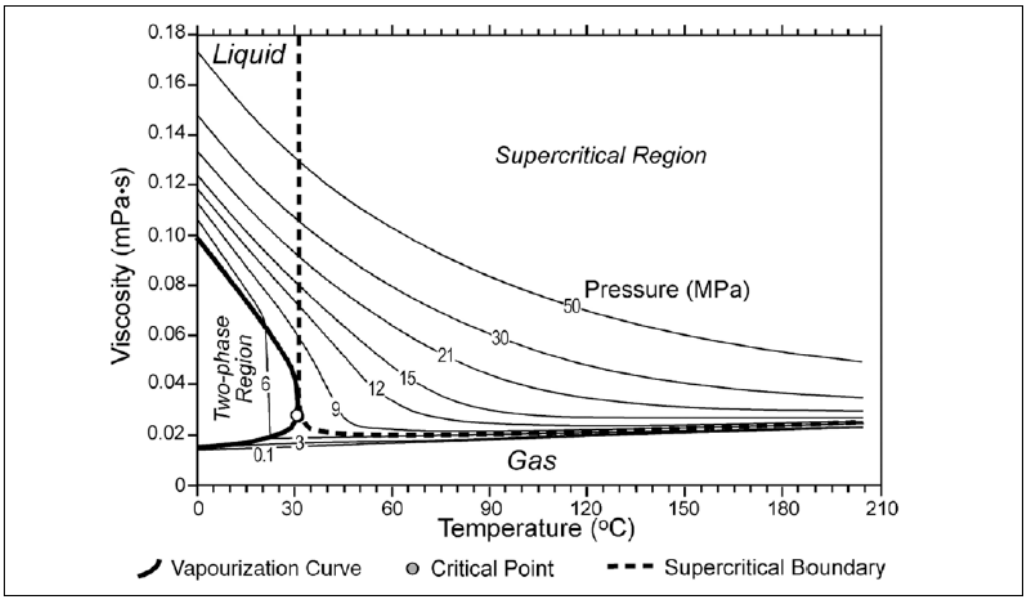

Figure 8 - CO_2 Viscosity vs temperature and pressure (Bachu, 2003)

2.2.1 CO_2 EOR Displacement Mechanisms

Two displacement mechanisms may occur during CO_2 injection: miscible and immiscible displacement. Reservoir pressure, temperature and oil composition affect the displacement type. For a specific reservoir, oil composition is constant before CO_2 injection and temperature is constant during CO_2 injection. There is a lowest pressure at which CO_2 and oil are miscible at constant composition and temperature, which is called the minimum miscibility pressure (MMP). Above MMP, displacement mechanism is miscible and below MMP, displacement mechanism is immiscible.

2.2.1.1 Immiscible CO_2 EOR

Immiscible displacement occurs when the reservoir pressure is below MMP. In immiscible displacement, CO_2 and oil will not be miscible and they will not form one phase. Therefore, recovery will be less than a miscible displacement. In immiscible flooding, there are four major mechanisms. First one is oil swelling;

CO_2 dissolves in oil and cause oil swelling. When trapped oil swells, it will come out of the pores. Also, increasing oil saturation with the swelling effect will increase oil relative permeability and so mobility. Second one is viscosity reduction of oil; when CO_2 dissolves in oil, oil viscosity decreases. With the decrease in oil viscosity, its mobility will increase (Mosavat and Torabi, 2014). Also, CO_2 will push the oil with the increasing pressure and oil recovery will increase (Remson, 2010). An empirical correlation proposed by National Petroleum Council was used to calculate the MMP (Ahmed, 2007). According to their study, if the reservoir pressure is below 27^o API, minimum MMP is 4000 psi and if the reservoir temperature is between 120 ^{o}F and 150 ^{o}F, 200 psi needs to be added to the minimum MMP. By using API gravity of 12.4^o and reservoir temperature of 122 ^{o}F, MMP was found as 4200 psi that is higher than the initial reservoir pressure. Therefore, miscibility fails for our reservoir.

2.2.1.2 Miscible CO_2 EOR

Multiple contact miscible displacement occurs when the pressure is higher than the MMP. Therefore, to design a multiple contact miscible displacement, the MMP needs to be known. Calculation of MMP is well studied (Benham et al., 1959; Michelsen, 1980; Metcalfe et al., 1973; Wang and Orr, 1998; Kuo, 1985; Wang and Orr, 1997; Luks et al., 1987; Noar and Flock, 1986; Johns et al., 1993; Thomas, 2008; Ahmed, 2007). In miscible CO_2 displacement, heavy oil components like C_5-C_{30} are extracted by CO_2 from oil, some of the CO_2 is dissolved in oil and miscibility occurs after multiple contacts (Taber et al., 1997). To achieve miscibility, medium-light or light oil must be in the reservoir because MMP of heavy oil is very high that cannot be achieved during CO_2 injection. According to Taber et al. (1997), miscibility check fails when API gravity of oil is less than 22 API. Highest oil recovery can be achieved by miscible CO_2 injection.

2.2.3 CO_2 Flooding Methods

In this section, CO_2 flooding methods are discussed; cyclic CO_2 injection, continuous CO_2 injection, water alternating gas injection, tapered water alternating gas injection and carbonated water injection.

2.2.3.1 Cyclic CO_2 Injection (Huff-N-Puff)

Cyclic CO_2 injection technique is a single well CO_2 injection method. In this method, CO_2 is injected from a production well (huff), and then the well is shut in to let the CO_2 soak into the formation (diffuse into the formation). After a while, well is put on production again (Figure 9). After well production decreases to minimum or a preset value, cycle starts again. During soaking period, CO_2 dissolves in oil, swells oil; reduces its viscosity and increases oil saturation and so relative permeability of oil (Wolcott et al., 1995). Slug size, soaking time, injection rate or pressure and number of cycles are design parameters of a cyclic CO_2 injection study. It was observed that oil recovery increases with the increasing slug size and longer soaking times (Bybee, 2007).

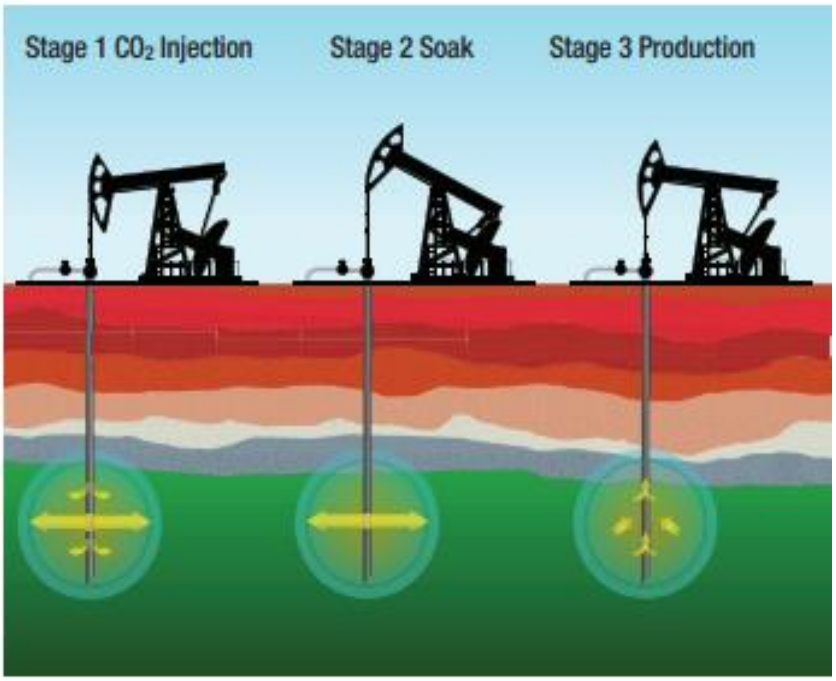

Figure 9 - Cyclic CO_2 injection method (Oil, 2016)

2.2.3.2 Continuous CO_2 Injection

In this technique, CO_2 is injected continuously into the reservoir. Injection rate or pressure and slug size are the design parameters for continuous CO_2 injection method. It was shown that oil recovery increases with increasing CO_2 slug size (Hadlow, 1992). Disadvantage of this methodology when compared with other CO_2 flooding techniques is that there is no mobility control in this method. Viscous fingering may occur during CO_2 injection due to low viscosity of CO_2 and adverse mobility ratio (Nasir and Chong, 2009).

2.2.3.3 Water Alternating Gas Injection (WAG)

In this technique, water and CO_2 is injected in cycles. The aim is to increase the efficiency of CO_2 flooding and sweep efficiency by reducing CO_2 channeling. The duty of water is to control the mobility to make the front more stable. The other advantage of using water is that it will flow into high permeable channels so that CO_2 may go into the low perm zones. It can be said that CO_2 tackles microscopic displacement and water deals with macroscopic displacement. Water-gas ratio (WAG ratio), slug size, injection rates or pressures, production rates and cycle timing are the design parameters that have great impact on the success of WAG (Chen et al., 2009).

2.2.3.4 Tapered Water Alternating Gas Injection

This technique is a modification of WAG method. In this technique, WAG ratio is increased or decreased based on the reservoir properties and economics. Project will be like water flooding with a high WAG ratio and project will be like gas flooding with a low WAG ratio. Bender and Yılmaz (2014) showed that in a heavy oil field where CO_2 breakthrough already occurred, increasing WAG ratio will be very effective.

2.2.3.5 Carbonated Water Injection

Carbonated water injection (CWI) or CO_2 enriched water injection is another CO_2 EOR method. In this method, CO_2 and water are injected simultaneously. They might be mixed at the surface or at the downhole. In this method, CO_2 dissolves in water so that mobility of CO_2 is decreased and sweep efficiency is improved (Sohrabi et al., 2009). When compared with continuous CO_2 injection and WAG, CO_2 breakthrough time will increase during CWI due to decreased mobility. CO_2 has higher solubility in oil than water. Therefore, CO_2 will be transferred into oil. CO_2 will swell the oil, reduce the viscosity of oil and increase recovery (Mosavat and Torabi 2014).

2.2.4 Screening Criteria for CO_2 EOR

As discussed before, there are two displacement mechanisms for CO_2 EOR. These are miscible and immiscible displacement. For a miscible displacement, reservoir pressure before injection or during injection needs to be higher than minimum miscibility pressure. However, there are some limitations for achieving MMP. One of these is formation fracture pressure; MMP needs to be lower than the formation fracture pressure to keep the CO_2 in the reservoir. The other one is project economics. Based on these, there are some screening criteria, which need to be reviewed together. Reservoir depth, API gravity, oil viscosity, oil composition, and oil saturation are some of the screening parameters for a successful CO_2 flooding project. Table 1 presents the screening criteria proposed by Taber et al. (1997).

Table 1 - Screening criteria for CO_2 EOR (Taber et al., 1997)

Technical Screening Guides		
	Recommended	Range of Current Projects
Crude Oil		
Gravity, °API	>22	27 to 44
Viscosity, cp	<10	0.3 to 6
Composition	High percentage of intermediate hydrocarbons (especially C_5 to C_{12})	
Reservoir		
Oil saturation, % PV	>20	15 to 70
Type of formation	Sandstone or carbonate and relatively thin unless dipping.	
Average permeability	Not critical if sufficient injection rates can be maintained.	
Depth and temperature	For miscible displacement, depth must be great enough to allow injection pressures greater than the MMP, which increases with temperature (see Fig. 7 of Ref. 1) and for heavier oils. Recommended depths for CO_2 floods of typical Permian Basin oils follow.	
	Oil Gravity, °API	Depth must be greater than (ft)
For CO_2-miscible flooding	>40	2,500
	32 to 39.9	2,800
	28 to 31.9	3,300
	22 to 27.9	4,000
	<22	Fails miscible, screen for immiscible*
For immiscible CO_2 flooding (lower oil recovery)	13 to 21.9	1,800
	<13	All oil reservoirs fail at any depth
At <1,800 ft, all reservoirs fail screening criteria for either miscible or immiscible flooding with supercritical CO_2.		

2.3 Co-Optimization of CO_2 EOR and Storage

As discussed in Section 2.1 and Section 2.2, the aim of CO_2 storage is to maximize the amount of CO_2 sequestered and the aim of the CO_2 EOR is to maximize the oil recovery. The aim of the co-optimization of CO_2 EOR and storage is to maximize the CO_2 storage and oil recovery. Oil recovered and CO_2 sequestered must be maximum when the reservoir is abandoned. CO_2 have been used to increase oil recovery since 1960's. Due to the effect of CO_2 on global warming, not only increasing oil recovery but also increasing the CO_2 storage is an important issue for today's world. In the literature, there are several studies about co-optimization of CO_2 EOR and storage (CCS) (Cakici, 2003; Kovscek, 2002; Kovscek and Cakici, 2004; Kovscek and Wang, 2004; Jahangiri and Zhang, 2012; Leach et al., 2011; Safarzadeh and Motahhari, 2014; Forooghi et al., 2009; Babadagli, 2006; Hitchon, 2013). However, there are only a few applications of co-optimization of CO_2 EOR and storage (CCS) (Hitchon, 2012; Feenstra et al., 2010; Hund and Greenberg, 2010; Bradbury and Wade, 2010; Ashworth et al., 2010). Weyburn oilfield is a good example for a CCS project due to the size of the project and data gathered for a long time. Weyburn CCS project is the first large field application and has been started in 2000 (Hitchon, 2013). A coal-gasification plant located in North Dakota is the source of the injected CO_2 (Mayer et al., 2013). Approximately 20 million tons of anthropogenic CO_2 has been stored in Weyburn (Hitchon, 2013). Optimal conditions for CCS are not same for each field so that more field applications need to be performed. Ghomian (2008), states that density of oil, reservoir capacity for storage, depth of the reservoir, thickness of the reservoir, oil and water in place are important factors that might affect the CCS projects. CCS is still in the development phase and needs development in technology and policy. To maximize the oil recovery and CO_2 storage, there is need to decide the CO_2 injection strategies and to optimize the operating parameters. Kovscek and Cakici (2004) showed that injecting water and CO_2 like a WAG project does not increase the amount of the CO_2 stored. According to their study, shutting in high amount of gas producing oil wells and closing injection wells whose bottom hole pressure become more than

the required pressure, are desired strategies for the co-optimization project. As can be seen from this discussion, well operating parameters impact the results and must be optimized in each case. In this study, producing gas oil ratios and injection rates are changed to optimize CO_2 storage and oil recovery.

2.4 Flue Gas

Flue gases are one of the major contributors to global warming due to their large CO_2 content. Flue gas is a mixture of gases which are produced during combustion of fuel; wood, coal, gas, oil etc. and during the production of the material. It can be produced by a power generator, oven or any other heat required process and released to atmosphere. Composition of a gas depends on the fuel used for combustion process but it mainly consists of nitrogen (N_2), carbon dioxide (CO_2), water vapor (H_2O), oxygen (O_2) and sulfur dioxide (SO_2). Figure 10 shows the global greenhouse emissions by gas (Pachauri and Meyer, 2014). Sulfur, nitrogen oxide (NO_x), carbon monoxide (CO), carbon dioxide and dust are some of the air polluting components that may occur in flue gases. In this study, flue gas produced from a cement factory was used. Cement is a widely used ingredient in construction industry and produced in almost all parts of the world. Cement is used to make concrete. Approximately 5% of the anthropogenic CO_2 emissions are released to the atmosphere by the cement industry (Arachchige, 2013). CO_2 is emitted during cement clinker production and during fuel combustion. For cement production (Figure 11), firstly raw material is prepared. Once the limestone quarry is mined, limestone and other naturally occurring minerals are transported from limestone quarry to the process area. Size of the raw material needs to be reduced and homogenized. As a result, raw material goes into main crusher to make rough ground material and then goes into a second crusher to produce fine ground material. After that, it is moved to grinding mill to produce finer material. After grinding, finer material goes into preheater, which generally works with recycled heat and then goes into kiln system. Material is heated to nearly 1500 °C in kiln system, where most of the energy (90%) is consumed (Lisa and Hanle, 2004). In this part, material gets the required heat to start the clinkering reactions (Nazmul,

2005) and calcinated to decompose the calcium carbonate ($CACO_3$) into calcium oxide (CaO) and CO_2 where most of the CO_2 is released (Cement Production, 2010). Then clinker is cooled to increase the cement quality by stopping the reactions and to protect the clinker handling equipment. Last part of the cement production process is finishing grinding mill where gypsum is added and mixed with the clinker during grinding. In the last part gypsum or some other minerals are added to get the required type of cement in terms of strength and setting time (Cement Production, 2010). After these steps, cement is stored, packed and shipped.

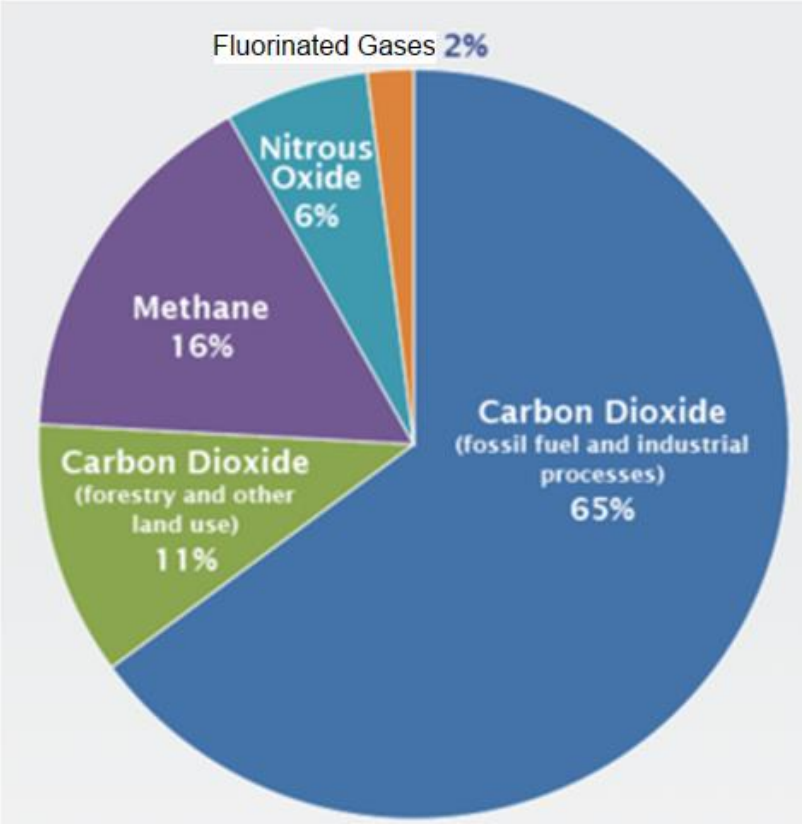

Figure 10- Global greenhouse emissions by gas (Pachauri and Meyer, 2014)

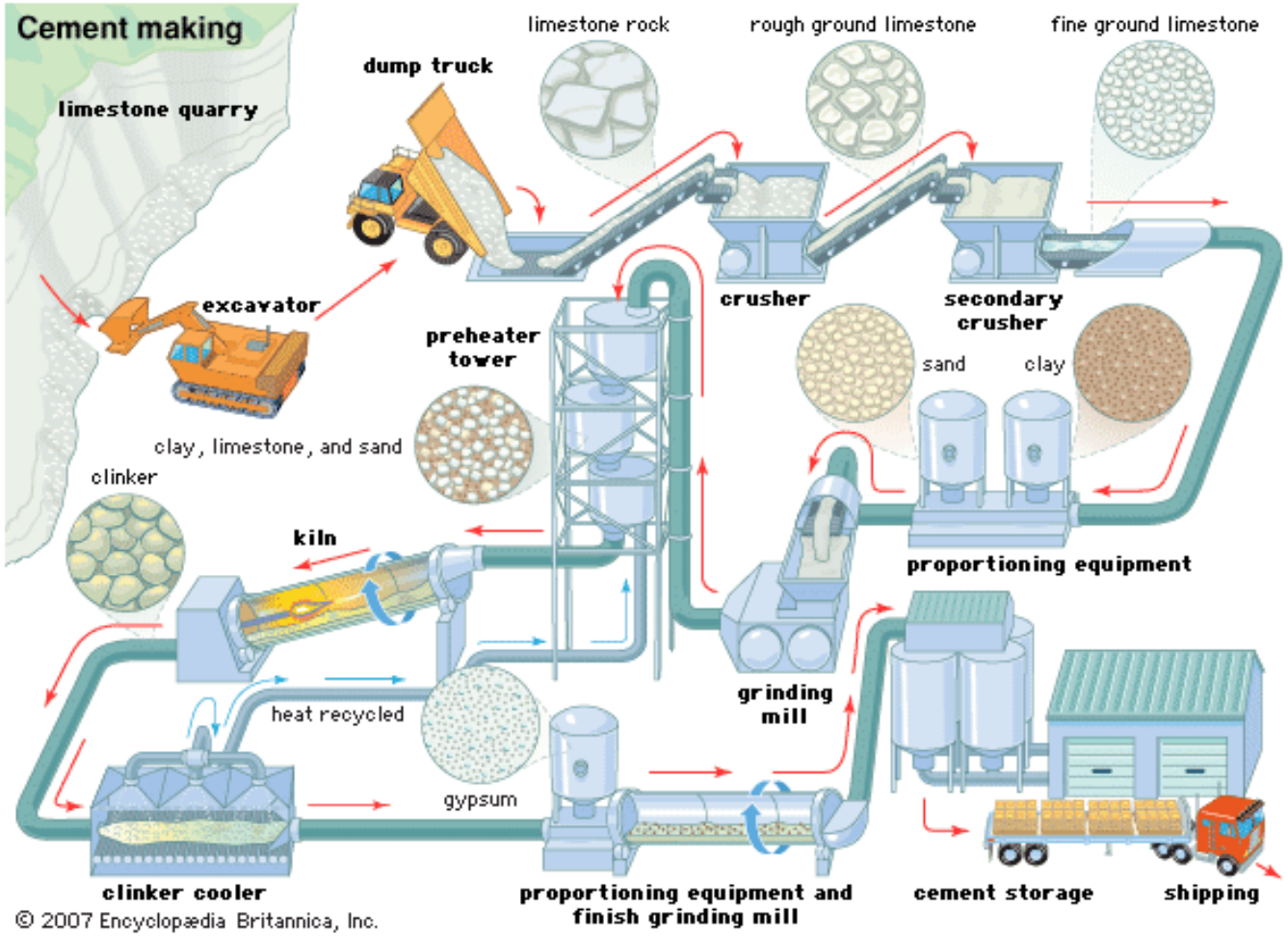

Figure 11 - Cement production process (Cement, 2016)

Emissions related with cement industry can be divided into two groups: CO_2 emissions and non-CO_2 ones. CO_2 emissions occur during the process of calcination (Eq. 2.1) and occur during the required energy production. During calcination, approximately 50% of the CO_2 is released. 40% of the CO_2 is released during fossil fuel combustion. 5% of the CO_2 is released during transportation and another 5% is released during electricity consumption (Mahasenan et al., 2005). According to Portland Cement Association (PCA), average CO_2 released during the production of Portland cement in USA is 0.927 kg of CO_2 per 1 kg of cement (Marceau et al., 2006). Whereas gross CO_2 emissions factor for China's cement is 0.883 kg of CO_2 per 1 kg of cement, 0.415 kg comes from calcining process and 0.467 kg comes from energy production (Shen et al., 2014). SO_x, NO_x, CO, N_2, O_2 and volatile organic compounds and dust might be released during cement production. Among these CO_2, NO_x, SO_x, CO and some of the volatile organic compounds are greenhouse gases. Amount of these emissions is based on cement type, cement production method and type of fuels used for the process. In this study, amount of CO_2 emissions is calculated by using clinker production data of the factory. Detailed information about the cement factory is given in Chapter 4.4 and flue gas stream composition and properties used for simulation are given in Table 9.

$$CaCO_3 + \text{heat} \longleftrightarrow CaO + CO_2 \quad (2.1)$$

Injection of flue gas containing mostly N_2 and CO_2 might increase oil recovery with energy provided by both and with the swelling and viscosity reduction effect of CO_2. In addition to these, if the project becomes miscible with increasing pressure, oil recovery will be higher. However, high percentage of N_2 in the flue gas will increase the MMP of the flue gas so that oil recovery will be less than miscible CO_2 injection. According to Huang (1997), CO_2 works better than flue gas for heavy oils at high pressures. Shokoya et al. (2005) states that with increase in CO_2 amount in flue gas may increase the oil recovery for the light oil. CO_2 EOR might have better oil recovery but capturing CO_2 from flue gas will increase the project costs. CO_2 capture from flue gas will cost $25-70 per tons of CO_2 but large quantities of flue gas are available for a lower cost (Dong and Huang, 2002).

CHAPTER 3

STATEMENT OF PROBLEM

There are many studies about CO_2 storage and EOR; however, only a few studies have been made on flue gas injection (Koch and Hutchinson, 1958; Fong et al., 1992; Huang, 1997; Zhang et al., 2006; Shokoya et al., 2005; Ossa et al., 2010). Majority of these studies focused on maximizing the oil recovery and did not deal with the CO_2 storage. In addition, these studies are experimental or conducted using synthetic reservoir models. The main aim of this research is to investigate the effects of immiscible CO_2 injection while maximizing CO_2 storage in a mature heavy oil carbonate reservoir located in south east Turkey. Three different nearby natural gas reservoirs with differing amounts of CO_2 (77.17%, 28.15% and 20.65%) and flue gas originating from a cement factory were considered as CO_2 sources. CO_2 can be sequestered by injecting raw flue gas that will decrease the CAPEX and OPEX of the project because there is no need to invest on capturing equipment. Transportation of CO_2 is another major expense. However, cement factory discussed in this study is close to oil field and there is a pipeline for transportation, which was built previously for another project. To make the flue gas injection project comparable, pure CO_2 injection, natural gas injection, and high CO_2 percentage natural gas injection from nearby natural gas reservoirs have been studied. Comparisons were made after conducting a detailed field-wide compositional simulation study. CO_2 storage was conducted by injecting flue gas and CO_2. Effects of the injected gas composition and various operating strategies such as producing gas oil ratio and CO_2 injection rate have been studied. These parameters were optimized by changing their values and effects on oil recovery and CO_2 storage were discussed. In addition to these, economic analysis was performed for each scenario.

CHAPTER 4

SOURCES AVAILABLE FOR STORAGE & EOR APPLICATION AND PVT TESTS

There are three different sources of CO_2 which can be used for CO_2 EOR and storage purposes. These are anthropogenic sources, hydrocarbon reservoirs containing CO_2 and natural CO_2 reservoirs. There are three natural CO_2 reservoirs around the oil field. All of them consist mostly of methane and CO_2 gases. These are named as gas source A, gas source B, and gas source C (Figure 12). Also, there is one industrial area close to the mature oil field. Industrial areas are one of the major contributors of carbon dioxide emissions. Flue gas produced from a cement factory located in this area, will be injected in the mature oil field. Tests given in this chapter were conducted by Turkish Petroleum Research Center.

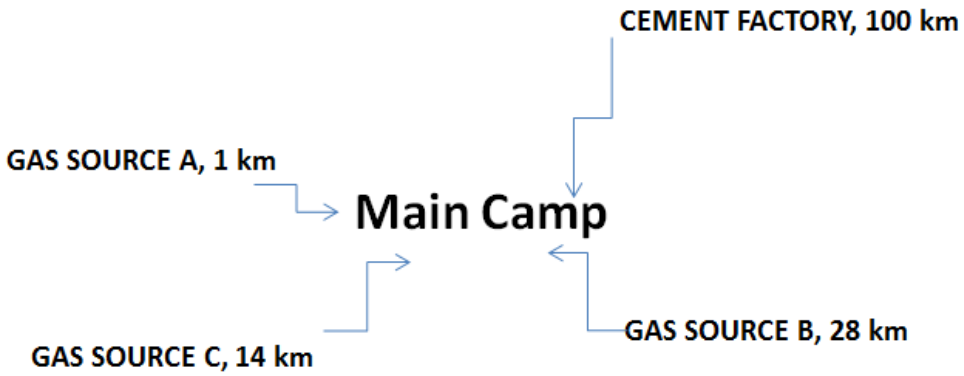

Figure 12 - Distance of the sources to the main camp

4.1 Gas Source A

Gas source A is a natural CO_2 reservoir. Reservoir lithology is dolomitic limestone. Field was discovered in 1977. Reservoir depth is 2250 m and water gas contact is -1730 m. Initial reservoir pressure is 3040 psi and reservoir temperature is 160 ^oF. Original gas in place is approximately 1.3 billion sm^3 with a recovery factor of 70 %. Field was developed with 7 wells and 200 million sm^3 of gas was produced between 2003 and 2012. Produced gas was used to apply CO_2 EOR. In 2012, it was decided to suspend the CO_2 EOR project due to lack of surface facilities. Source A consists of mostly CO_2. Mole percentage of CO_2 is 77 %. Table 2 represents the gas composition of source A. Table 3 shows source A reservoir gas properties. Table 4 presents source A reservoir gas PVT properties.

Table 2 - Source A reservoir gas composition (Bender and Yilmaz, 2014)

Composition	% Mol
N_2	2.69
CO_2	77.17
C_1	18.02
C_2	1.13
C_3	0.53
iC_4	0.1
nC_4	0.19
iC_5	0.08
nC_5	0.07
C_6	0.02

Table 3 - Source A reservoir gas properties (Demir, 2016)

Gas Properties	
P_{pc},psia	973
T_{pc}, ^{o}R	504
M_w, lb/lbmol	38
γ_g	1.33

Table 4 - Source A reservoir gas PVT properties (Demir, 2016)

PVT Properties				
p, psia	γ_g	Z	B_g, cf/scf	μ_g, cp
1750	1.2219	0.818	0.0078	0.0209
1500	1.2252	0.788	0.0087	0.0198
1250	1.2272	0.761	0.0101	0.0182
1000	1.2477	0.758	0.0125	0.0167
750	1.2881	0.825	0.0181	0.0163
500	1.322	0.878	0.0285	0.0162
250	1.4023	0.932	0.0589	0.0159
0	1.4497	1		0.015

4.2 Gas Source B

Gas source B is a natural gas reservoir with abundant CO_2. Reservoir lithology is dolomitic limestone. Field was discovered in 2010. Reservoir depth is 3500 m. Initial reservoir pressure is 3944 psi and reservoir temperature is 218 ^{o}F. Original gas in place of gas source B is approximately 200 million sm^3 with a recovery factor of 70 %. Field is currently under development. 1 million sm^3 of gas was produced

in 2010. Production was ended in 2010 due to decreased gas prices and lack of market. Gas source B consists mostly methane. Mole percentage of methane is 60 % and mole percentage of CO_2 is 28 %. Table 5 represents the gas composition of gas source B. Table 6 shows gas source B gas properties.

Table 5 - Gas source B gas composition (Demir, 2016)

Composition	% Mol
N_2	2.92
CO_2	28.15
H_2S	0.02
C_1	60.72
C_2	5.67
C_3	1.62
iC_4	0.33
nC_4	0.34
iC_5	0.14
nC_5	0.07
C_6	0.02

Table 6 - Gas source B gas properties (Demir, 2016)

Gas Properties	
P_{pc}, psia	775.8
T_{pc}, R	418
M_w, lb/lbmol	25.93
γ_g	0.898

4.3 Gas Source C

Gas source C is a natural gas reservoir with abundant CO_2. Reservoir lithology is dolomitic limestone. Field was discovered in 2015. Reservoir depth is 2500 m. Initial reservoir pressure is 3361 psi and reservoir temperature is 180 ^oF. Original gas in place of gas source C is approximately 70 million sm^3 with a recovery factor of 50 %. Field is currently under development. Current reserve is approximately 35 million sm^3. Gas source C consists of mostly methane. Mole percentage of methane is 63.11 % and mole percentage of CO_2 is 20.65 %. Table 7 represents the gas composition of gas source C. Table 8 shows gas source C gas properties.

Table 7 - Gas source C gas composition (Demir, 2016)

Composition	% Mol
N_2	7.62
CO_2	20.65
H_2S	0.01
C_1	63.11
C_2	5.37
C_3	1.77
iC_4	0.44
nC_4	0.51
iC_5	0.29
nC_5	0.17
C_6	0.06

Table 8 - Gas source C gas properties (Demir, 2016)

Gas Properties	
P_{pc},psia	736.2
T_{pc}, ^{o}R	399.7
M_w, lb/lbmol	24.684
γ_g	0.855

4.4 Cement Factory

Cement factory located approximately 100 km to the base camp started production in 1975. Company's facilities were reconstituted in 1980 to be used with natural gas and coal as an alternative fuel to oil after oil crisis of 1973 and 1979 (About Mardin Cement, 2016) . Cement factory's natural gas requirement had been supplied between 1982 and 2012 from a natural gas field connected to main camp. To transport the natural gas from the main camp to factory, 100 km long pipeline was constructed. In this study, the idea is to use the same pipeline for flue gas transportation to reduce the project costs. Instead of transporting natural gas from the camp to factory, flue gas will be transported from factory to main camp and then to the mature oil field compressor station. Pipeline between the main camp and the oil field compressor station is 10 km long. Note that cement factory is producing 2,400 tons of clinker per day. To calculate the CO_2 emitted during cement production, clinker emission factor needs to be determined. Clinker emission factor was calculated by using (Eq. 4.1) and fraction of lime in clinker is taken as 64.6 percent, which is IPCC default value (Gibbs et al., 2001). Therefore, clinker emission factor is calculated as 0.507 tons of CO_2 per tons of clinker (Gibbs et al., 2001). By using this clinker emission factor, CO_2 emission is calculated as 1,217 tons/day from calcining process and CO_2 emission from fuel combustion is calculated as 973.6 tons/day. Total possible gas flow rates are given in Table 9 for

different operating levels of cement factory. Flue gas composition used in this study given in Table 9 is taken from literature. It is assumed that NO_x, SO_2, O_2 and H_2O are removed before injecting into reservoir.

$$EF_{clinker} = \text{fraction CaO} \times (44.01 \text{ g/mole } CO_2 / 56.08 \text{ g/mole CaO}) \quad (4.1)$$

Table 9 - Flue gas stream gas composition and properties used for simulation (Nazmul, 2005)

Flue Gas Properties			
Operating Level	Low	Medium	High
CO_2, %	29.6	29.6	29.6
N_2, %	70.4	70.4	70.4
Total Gas Volume Flow, m^3/hr	134,000	201,000	268,000
Total Gas Mass Flow , kg/hr	171,312	256,968	342,624

4.5 Mature Oil Field PVT Tests

PVT properties of reservoir fluid and injected gases are necessary for simulation. To know the fluid behavior in the reservoir, in wellbore, at the surface and at the separator, fluid properties at different temperatures and pressures must be estimated. Also for EOR operations like CO_2 flooding requires detailed information about PVT tests applied with the mature oil fields oil and gas source. Table 10 represents the summary of PVT measurements.

Table 10 - PVT Report summary (Demir, 2016)

PVT Report Summary			
	Oil	Oil + Gas Source A Gas	
Oil Compressibility	4.813×10^{-6} (500-2000 psi)	6.14×10^{-6} (2000-3000 psi)	1/psig
Thermal Expansion	0.164		$1/^{o}F$
@P_{bi}			
Oil Density	0.947	0.916	gr/cc
B_o	1.041	1.215	rbbl/stb
GOR	10	393.6	scf/stb
Oil Viscosity	387.5	63.4	cp

4.5.1 Constant Composition Expansion

Constant composition expansion test, which is also known as flash vaporization test, was conducted in Turkish Petroleum Research Laboratories. Tests were conducted at reservoir temperature of 132 ^{o}F. First oil was put in a cell whose pressure is above initial reservoir pressure. Following this, pressure was gradually reduced at constant temperature. With the decrease in pressure, oil expanded and expanding volume was recorded. Measurements were done after phase equilibrium had been reached each time. Gas evolved below bubble point pressure from oil was not separated during measurements. Therefore, composition of the cell is known and constant during experiment. Bubble point pressure, bubble point density, thermal expansion of oil, isothermal compressibility of oil at pressures above bubble point and relative volume was measured. As mentioned, to prepare the cell,

it was heated to 132 ^{o}F and thermal expansion of oil was calculated from the volume expansion of the cell (Table 10). Table 11 shows one phase oil isothermal compressibility for oil. Table 12 presents relative volumes for oil, oil and gas mixture. Oil formation volume factors for different pressures above bubble point pressure were calculated by dividing total volume of the cell divided by volume of stock tank oil. Calculated Bo values above bubble point pressure are given in Table 13.

Table 11 - One phase oil isothermal compressibility (Demir, 2016)

One Phase Oil Isothermal Compressibility 1/psig × 10^{-6}	
Pressure, psig	Oil
2000	4.4085
1500	4.5314
1000	4.8867
800	4.8929
600	5.6955
500	5.9405
400	6.3928

Table 12 - Relative volume (Demir, 2016)

Relative Volume, $V_r=V/V_{pb}$			
Pressure, psig	Oil, V_r	Pressure, psig	Oil and Gas Mixture,V_r
3000	0.9851	3000	0.9939
2500	0.9875	2750	0.9954
2000	0.9898	2500	0.9969
1500	0.9919	2250	0.9985
1000	0.9943	2100	0.9993
800	0.9951	2050	0.9996
600	0.9962	2000	1
500	0.9968	1950	1.0044
400	0.9974	1900	1.0081
300	0.9981	1750	1.0233
200	0.9988	1500	1.0649
150	0.9991	1250	1.1352
100	0.9996	1000	1.2649
50	1	750	1.514
35	1.0004	500	2.0592

Table 13 - Bo, GOR, oil density (Demir, 2016)

Oil			
p, psig	B_o, rbbl/stb	GOR, scf/stb	Oil Density, gr/cc
3000	1.0250		0.9609
2500	1.0275		0.9585
2000	1.0299		0.9563
1500	1.0320		0.9543
1000	1.0346		0.9520
800	1.0355		0.9512
600	1.0366		0.9501
500	1.0372		0.9496
400	1.0378		0.9490
300	1.0385		0.9484
200	1.0392		0.9477
150	1.0396		0.9474
100	1.0401		0.9469
50	1.0405	10	0.9466
0	1.0273	0	0.9571

4.5.2 Differential Liberation Expansion (DLE)

Differential liberation test which is also known as differential vaporization test is applied to mimic the reservoir depletion process. Aim of this test is to generate PVT data below bubble point pressure. Test was conducted with oil and gas mixture. Tests were conducted at reservoir temperature of 132 ^{0}F. Oil was put in a cell where pressure was above bubble point pressure and pressure was gradually reduced at constant temperature. Measurements were conducted after phase equilibrium had been reached each time. Below bubble point pressure, gas evolved from oil was

separated after phase equilibrium had been reached at each pressure. Oil and gas volumes, densities, specific gravities, gas expansion and gas compressibility were measured at each pressure. Separated gas composition was measured by using a gas chromatograph. Measurements continued until atmospheric pressure is reached and at the end, temperature is decreased to 60 ^{0}F for last measurement only. Solution gas oil ratio, gas oil ratio and oil formation volume factors are then calculated.

Oil formation volume factor, oil and gas densities, GOR measured by differential liberation expansion test below bubble point pressure and oil formation volume factor, oil and gas densities measured by constant composition expansion test above bubble point pressure are given in Table 13. Table 14 shows oil gravity and density at standard conditions. Gas composition is given in Table 2. Table 3 shows gas properties and Table 4 presents specific gravity, Z, B_g and gas viscosity of gas. Figure 13 shows crude oil formation factor and viscosity - pressure relationship for heavy oil sample. Oil viscosity decreases until bubble point pressure (50 psig) and then increases due to release of the dissolved gas. Bubble point pressure increases until bubble point pressure (50 psig) due to swelling of oil and starts to decrease above bubble point pressure. Figure 14 shows oil formation factor, solution gas oil ratio and viscosity - pressure relationship when crude oil is combined with source gas A. As can be seen, oil viscosity at 2000 psig can be reduced from 559 cp to 63.37 cp by injecting source A gas. (Figure 13).

Table 14 - Oil gravity & density at standard conditions (Demir, 2016)

@ 60 ^{o}F Temperature and 1 atm Pressure	
	Oil
API Gravity	12.4
Density, gr/cc	0.9822

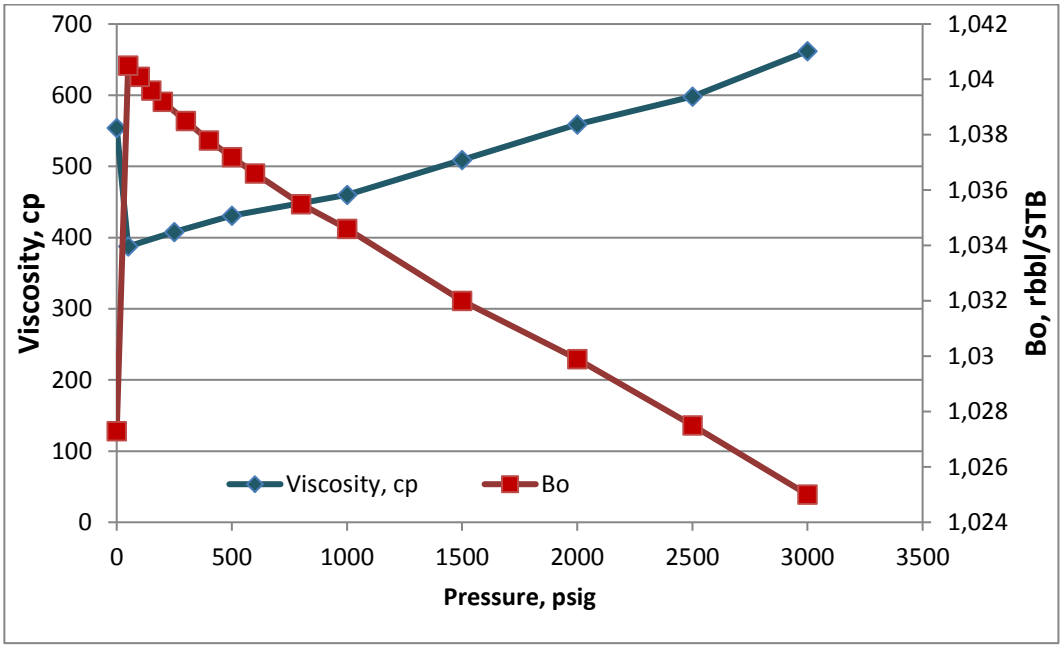

Figure 13 - Oil properties vs pressure (Bender and Yilmaz, 2014)

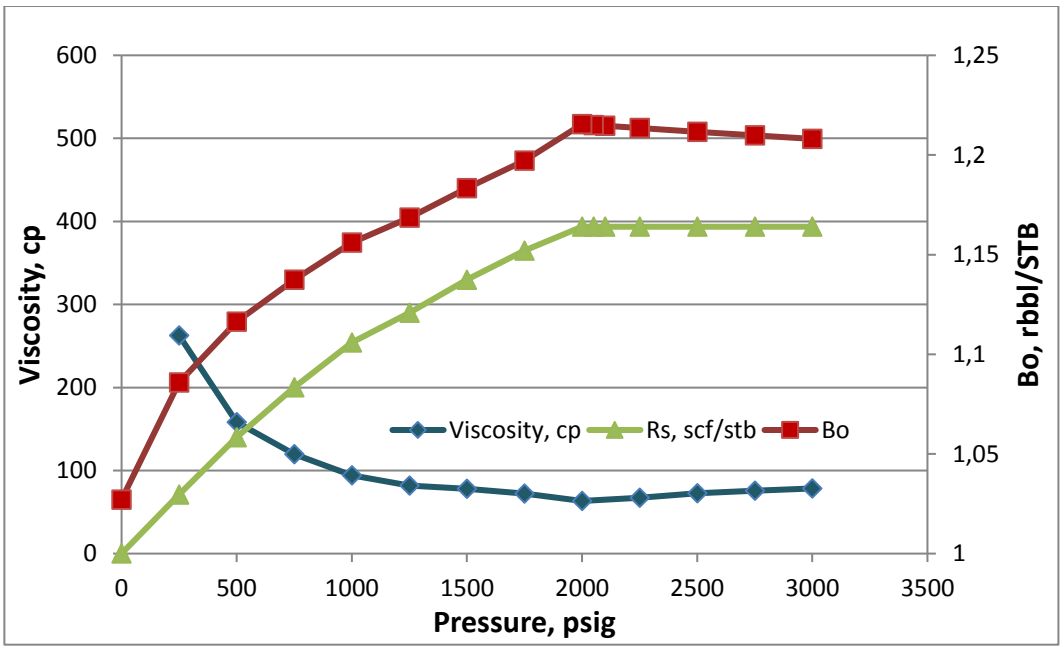

Figure 14 - Oil & Gas mixture properties vs pressure (Bender and Yilmaz, 2014)

4.5.3 Viscosity Measurement

Oil viscosity measurements were carried out by using a rolling-ball viscometer. Test was initiated at a pressure of 3000 psig and temperature of 132 ^{o}F. Then, pressure was decreased gradually. Measurements were conducted after phase equilibrium reached. Viscosities were measured for each pressure step above and below bubble point pressures. Evolved gas was separated below bubble point pressures and then oil and gas viscosities were measured. Viscosity measurements for oil and gas mixture are given in Table 15.

Table 15 - Viscosity measurements for oil and gas mixture (Demir, 2016)

	Oil	Oil and Gas Mixture
p, psig	Viscosity, cp	
3000	662	78.25
2750		75.74
2500	598	72.71
2250		67.18
2000	559	63.37
1750		72.3
1500	509	77.98
1250		81.92
1000	460	94.02
750		119.51
500	431	158.21
250	408	262.56
50	387.5	
0	554	562.75

CHAPTER 5

NUMERICAL MODELING AND HISTORY MATCHING

In this section, detailed information about the field production history, injection history, geologic description, rock and fluid properties, fluid characterization study, lumping scheme, equation of state tuning, model construction and history matching are given. Aim of this section is to build a dynamic model calibrated with historical production and pressure data to realistically simulate CO_2 injection. Eclipse 300 and Petrel software were used for simulations. Measured parameters such as porosity, permeability, relative permeability, capillary pressure data, and fluid PVT parameters were used in the reservoir model.

5.1 Field Data

Heavy oil carbonate reservoir located in South East Turkey was discovered in 1985 (Bender and Yilmaz, 2014). The reservoir commenced primary production in 1985 and it was developed with 41 wells (Figure 15). In this figure, green dots represent the production wells, blue dots represent the injection wells, and the area between the two red lines shows the production area. Moreover, the blue dashed lines show the faults, and the pink dashed curves show the surface elevation contours. Peak daily oil production reached to 300 sm^3/day in 1987 (Figure 16). There was a sharp decline after 1987 due to lack of pressure support, low API and high oil viscosity. Production plateau period had started in 1994 and continued until 2002. In order to remediate prodcution, continuous CO_2 injection was started in May 2003 by using 7 injection wells. The effect of the CO_2 injection on oil production was seen after 12 months of injection, also corresponding to breakthrough time of CO_2. It was observed that oil production increased as a result of CO_2 injection in the field.

Due to high producing gas oil ratios in the production wells and low sweep efficiencies, continuous CO_2 injection was converted to water alternating gas injection in 2007. More than 240 Msm^3 of additional oil was produced by CO_2 injection. 900 $sm^3$of CO_2 was injected to produce 1 sm^3 of oil. CO_2 flooding showed a great success in this heavy oil field. CO_2 kept up the required energy support for the production. CO_2 decreased the oil viscosity by swelling that also lead to increase in oil saturation so that oil relative permeability was increased. However, after stopping WAG injection in 2012 due to depletion of CO_2 reservoir, decline in oil production has started again. Details of the CO_2 reservoir are given in Section 4.1.

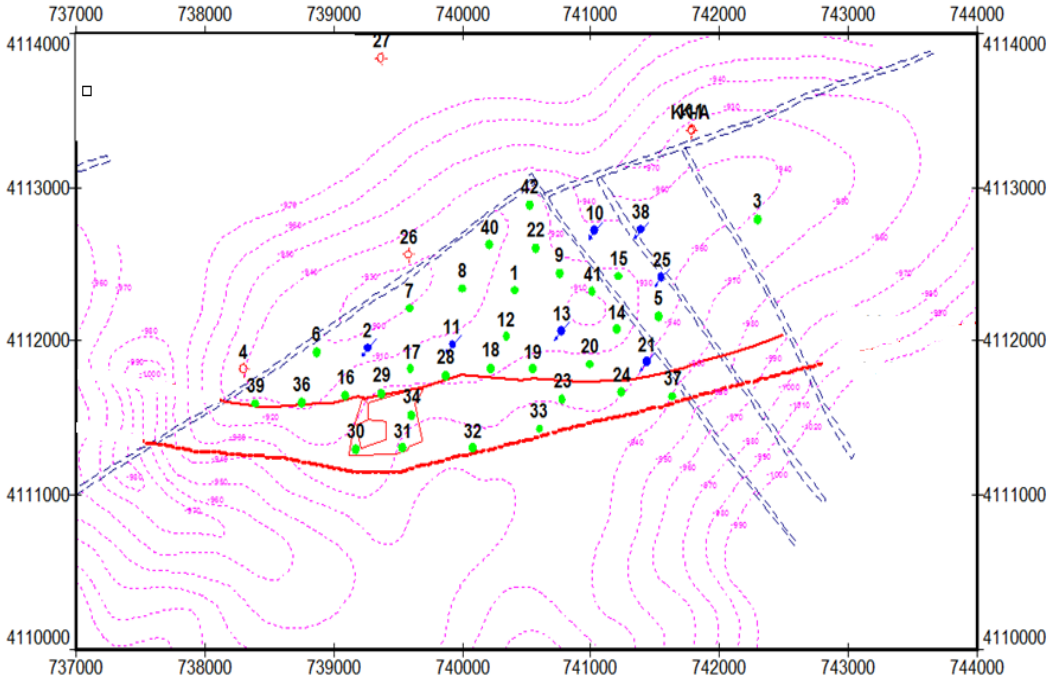

Figure 15- Field structure map (Bender and Yilmaz, 2014)

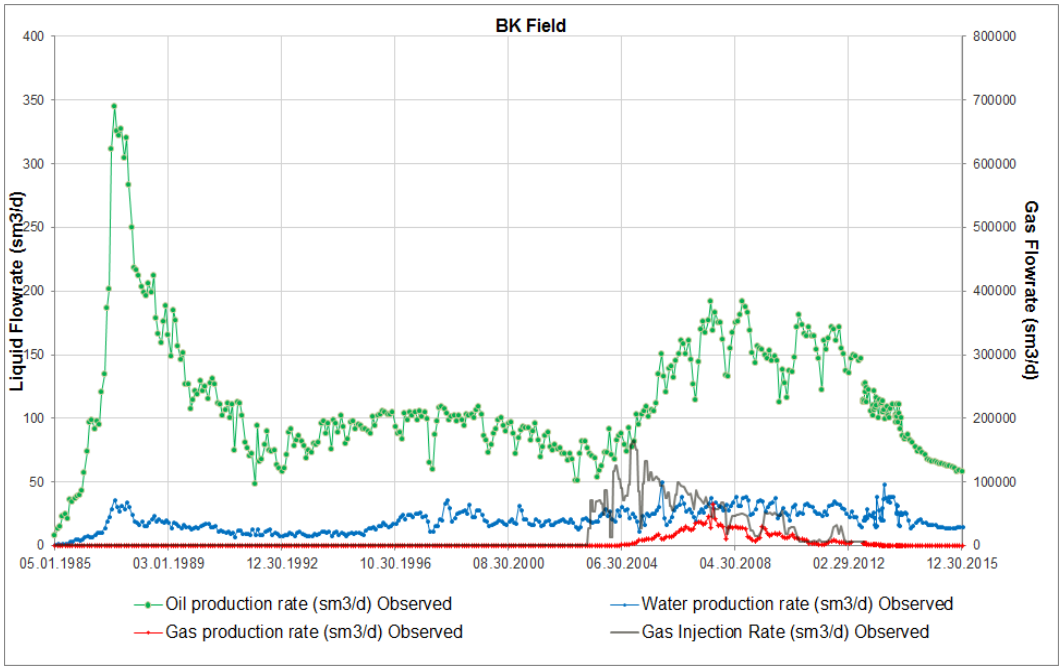

Figure 16 - Field production and injection history

5.2 Geologic Description

The heavy oil field is located in a tectonically active area dominated by WSW-ENE oriented faults, anticlinal features and southerly formation dips (Bender and Yilmaz, 2014). Southwest to northeast oriented sealing normal fault together with three orthogonal faults defines the northern and western boundaries of the reservoir. Crest of the anticline leans to this sealing fault and dips to the south. In addition to this fault there are three partially sealing northwest to southeast oriented strike slip partially sealing faults. Main production formation has an average thickness of 60 m. There are three facies at three different depths in the reservoir identified by core data, drill stem test results, Density-Neutron logs, and Gamma Ray logs. Figure 17 shows the petrographic and log characteristics of these facies. Bottom layer is 10% to 18% of porosity bearing wackestone with very low permeability. In contrast, the second layer has higher porosity (15% to 25%) and low permeability (Cobanoglu, 2001). Topmost facies is porosity (22% to 30%) bearing grainstone with the highest permeability where main production is taking place. Figure 18 presents a simple conceptual model of the reservoir where a cap rock lies above the production layers. Below this cap rock, aforementioned facies of the producing formation are

present. Below these layers there is a weak aquifer. Due to the low permeability of the bottom most facies, there is little energy support from this aquifer. Additional information about the geologic description of the field is reported elsewhere (Demiral et al., 1995).

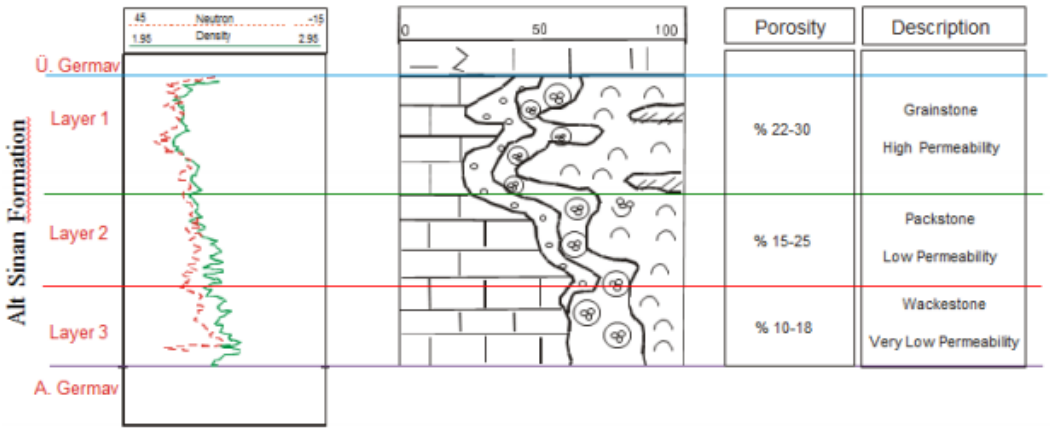

Figure 17 - Petrographic and log characteristics of the reservoir (Bender and Yilmaz, 2014)

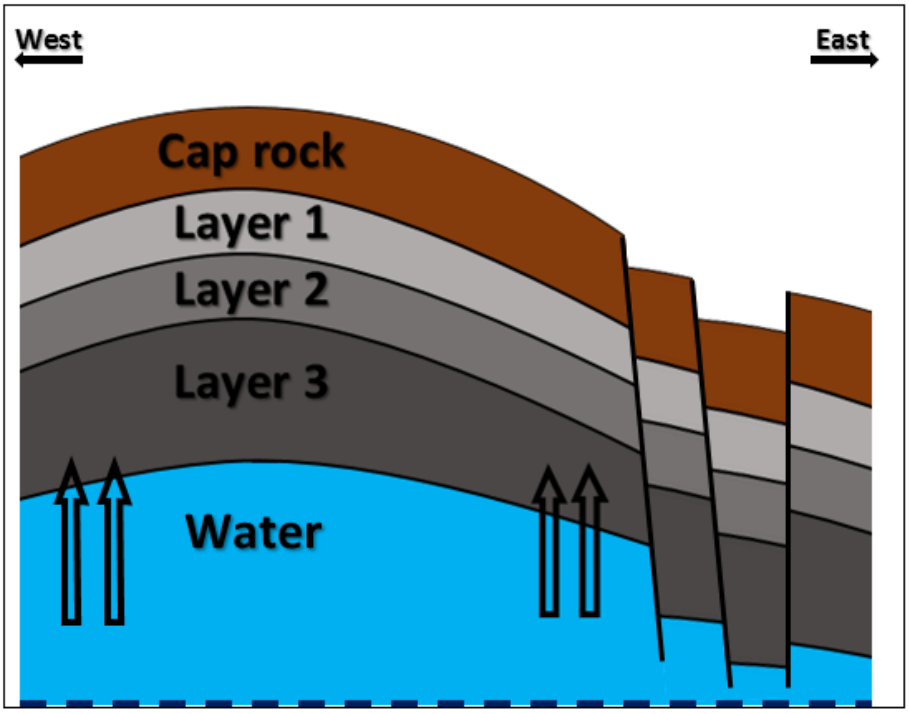

Figure 18 – Conceptual model of the reservoir

5.3 Rock and Fluid Properties

By using well logs and core data porosity distribution was obtained (Figure 19). The porosity distribution shows that porosity decreases as the depth increases. Porosity and permeability values determined from the core data and permeability values determined from drill stem tests were used to establish a relationship between porosity and permeability for each layer (Figure 20). Equations 5.1, 5.2, 5.3 and 5.4 represent the relationship for each of the aforementioned facies. As can be seen from Figure 17 and Figure 20, there is a large difference in permeability and porosity values of the topmost layer to those of other layers. In Figure 20, blue dots represent porosity and permeability values obtained from core analysis whereas red dots show permeability values calculated from drill stem tests. It can be seen that drill stem test permeability is higher than the core permeability because there are vugs and fissures in this field and it is hard to see these in core analysis. Therefore, slope of the line of the core data was used and that line was shifted to drill stem test data and then a relationship found between porosity and permeability values. Available special core analysis tests were used to construct relative permeability curves representing oil-water and gas-oil system (Figure 21). Leverett J-function was used to combine all capillary pressure measurements obtained from cores (Figure 22). Initial water saturation for each grid cell was calculated by using the constructed J-function. Similar plots were developed for layers 2 and 3.

$$Permeability = 0.0006 \times e^{41.595 \times Porosity} \quad (5.1)$$

$$Permeability = 1 \times 10^{-7} \times e^{85.438 \times Porosity} \quad (5.2)$$

$$Permeability = 4 \times 10^{-5} \times e^{51.05 \times Porosity} \quad (5.3)$$

$$Permeability = 0.0047 \times e^{21.175 \times Porosity} \quad (5.4)$$

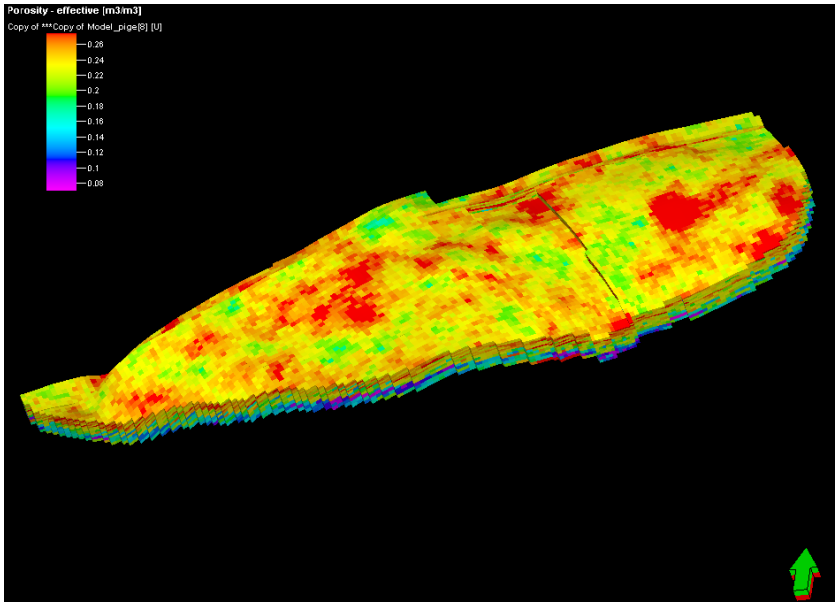

Figure 19 - Porosity distribution map (Bender and Yilmaz, 2014)

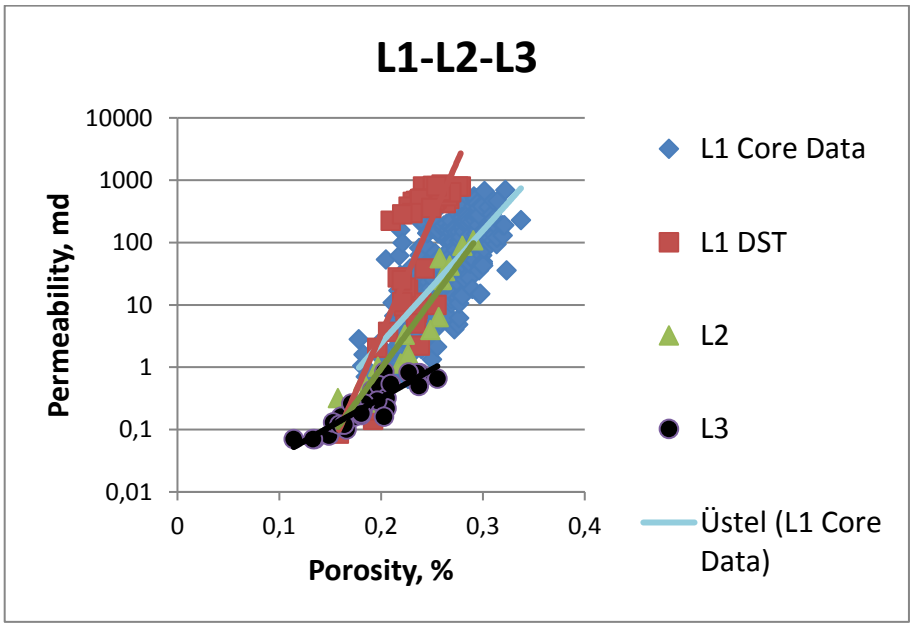

Figure 20 - Permeability and porosity relationship for Layers 1, 2, 3

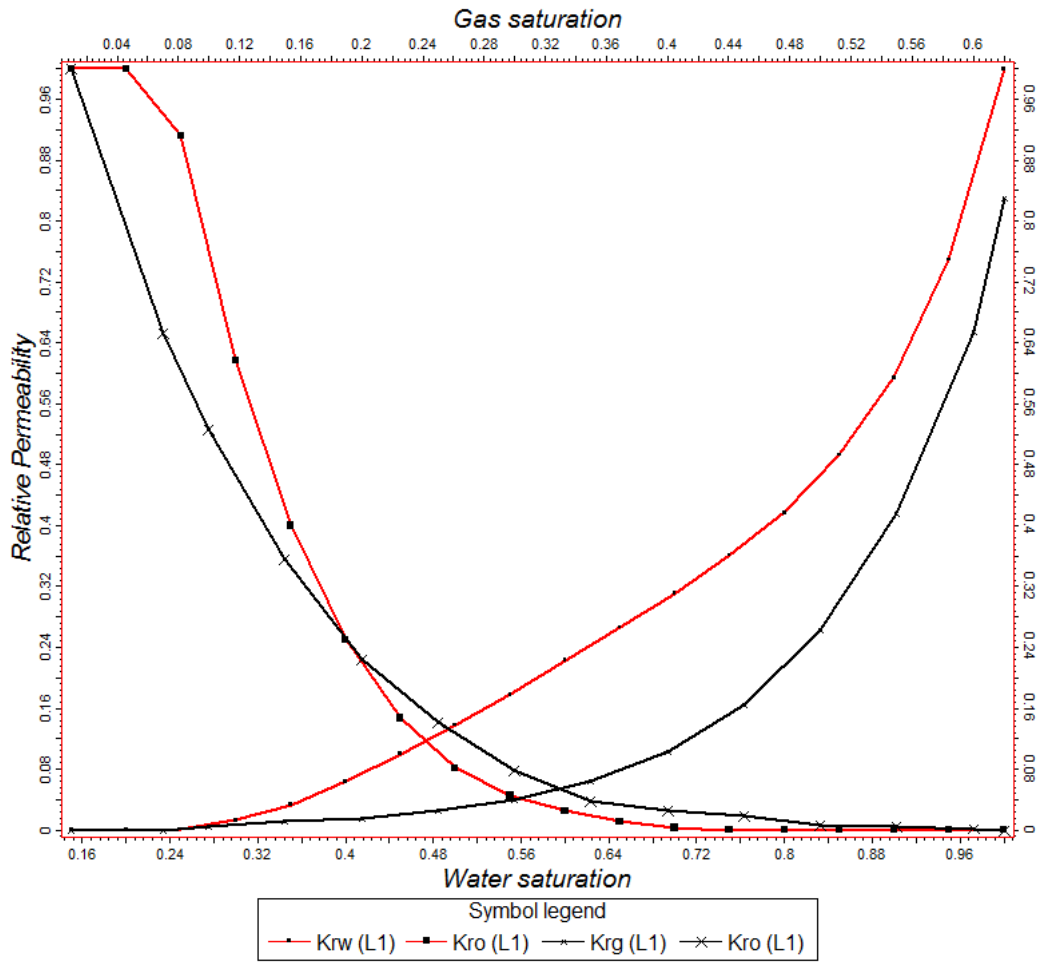

Figure 21 - Relative permeability vs water & gas saturation for Layer 1 (Bender and Yilmaz, 2014)

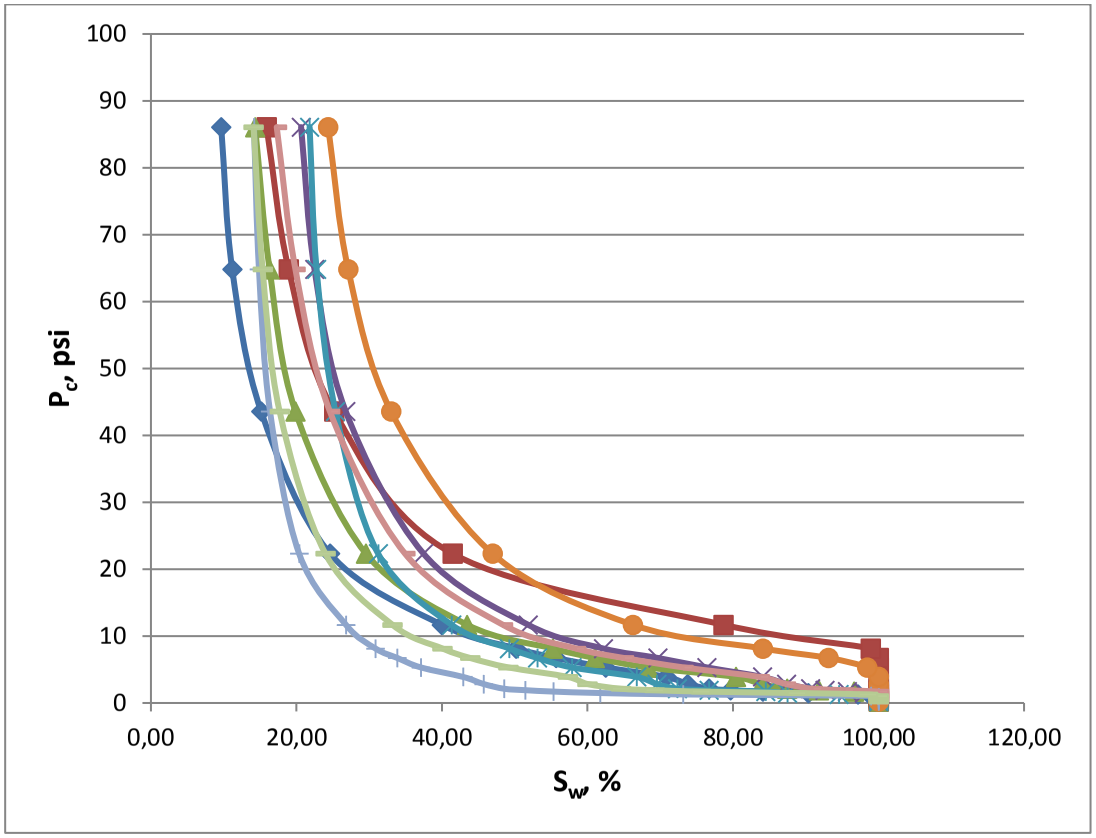

Figure 22 - Capillary pressure vs water saturation for Layer 1 (Bender and Yilmaz, 2014)

5.4 Fluid Characterization for Compositional Simulation

The main aim of this research is to investigate the effects of immiscible CO_2 injection while maximizing CO_2 storage in a mature heavy oil carbonate reservoir located in south east Turkey. Three different nearby natural gas reservoirs with differing amounts of CO_2 (77.17%, 28.15% and 20.65%) and flue gas originating from a cement factory were considered as CO_2 sources. In order to realistically simulate several possible mechanisms such as CO_2 swelling and viscosity reduction a 3D compositional simulation model was built after a detailed fluid characterization study. Compositional simulation requires an equation of state model (EOS), which describes the relationship between pressure, volume and temperature of a gas or liquid. Thermodynamic properties and the equilibrium states are calculated by an equation of state by using ECLIPSE PVTi software (Schlumberger, 2005). Number of phases and composition of each phase was determined by solving EOS model.

EOS needs to be matched with laboratory experiments before it can be used to realistically predict the injected CO_2 behavior in the reservoir. Properties of pure components are defined accurately. However, oil and gas reservoirs may also contain heavy fractions whose properties are usually not accurate (Ahmed and Meehan, 2010). Heavy fractions composed of aromatic, paraffinic, and naphthenic compounds are not well defined. In our study, these are C_{36+} fractions. Table 16 presents the molar composition of the produced oil. Compositional simulators solve N_{c+2} equations for each grid (Sclumberger, 2005). Since, running a compositional simulation with 36+ components (N_c) will be computationally expensive, there is need to lump the components to reduce the CPU time. To do all these changes in an accurate way, we need to stick to laboratory observations.

Table 16 - Molar compositions of oil (Demir, 2016)

Component	Mol%	Component	Mol%	Component	Mol%
H_2S	0.00001	C_{10}	13.359	C_{24}	0.45
CO_2	0.0003	C_{11}	10.36	C_{25}	0.12
N_2	0.0001	C_{12}	5.67	C_{26}	0.27
CH_4	1.0021	C_{13}	5.94	C_{27}	1.83
C_2	1.33	C_{14}	4.82	C_{28}	1.33
C_3	1.66	C_{15}	5.74	C_{29}	0.87
nC_4	2.54	C_{16}	1.57	C_{30}	0.14
iC_4	0.67	C_{17}	2.22	C_{31}	0.36
nC_5	0.05	C_{18}	2.3	C_{32}	0.31
iC_5	0.02	C_{19}	0.28	C_{33}	0.28
C_6	2.479	C_{20}	0.61	C_{34}	0.23
C_7	3.7506	C_{21}	1.11	C_{35}	0.22
C_8	11.71	C_{22}	0.67	C_{36+}	0.3
C_9	12.69	C_{23}	0.74		

To characterize the reservoir fluid, ECLIPSE PVTi was used (Schlumberger, 2005). Firstly, oil composition given in Table 16 is defined in PVTi. Default library was used to get physical properties of the components. Characterization of heavy plus components was carried out by using their corresponding molecular weights. There is minimum information about properties of heavy plus component so that it was used for tuning of equation of state. Properties of the components before regression and lumping are shown in Table 17. In the software, 3-Parameter Peng Robinson EOS which is a modified version of Soave Redlich Kwong EOS is used to calculate the phase behavior (Peng and Robinson, 1976).

Equation 5.5 presents the Peng Robinson EOS (Ahmed, 2000). In this equation, "V" is volume, "T" is temperature, "p" is pressure, and "R" is universal gas constant. Calculation of parameters "a" and "b" are given in Equation 5.6 and Equation 5.7 respectively. "T_c" and "P_c" are the critical temperature and critical pressure. In addition to these, equation of "α" is given in Equation 5.8. "m" given in Equation 5.9 was proposed by Peng and Robinson (1976) for heavier components and "ω" is the acentric factor (Ahmed, 2000). To match PVT experiments using the EOS an automatic nonlinear regression method embedded is Eclipse PVTi software was used. In order to match the saturation pressure acentric factor was adjusted. Volume parameters of components were then matched with the experimental data in such a way that "$P_c*V_c=Z_{crit}*R*T_c$" is satisfied for each component by adjusting Z factors ±10%. Viscosity of the components were matched similarly by Z_{crit} values. Detailed information about equation of state tuning is given in Section 5.6.

$$p = \frac{R \times T}{V - b} - \frac{a \times \alpha}{V \times (V + b) + b \times (V - b)} \tag{5.5}$$

$$a = 0.45724 \times \frac{R^2 \times T_c^2}{p_c} \tag{5.6}$$

$$b = 0.07780 \times \frac{R \times T_c}{p_c} \tag{5.7}$$

$$\alpha = (1 + m \times (1 - \sqrt{T})^2 \tag{5.8}$$

$$m = 0.379642 + 1.48503 \times \omega - 0.1644 \times \omega^2 + 0.016667 \times \omega^3 \tag{5.9}$$

Table 17 - Properties of components before regression and lumping

Components	Mol. Weight	Crit. Pres., psia	Crit. Temp., °F	Omega A	Omega B	V Crit., ft^3 /lb-mole	Z Crit.	Ref. Temp., °F
C_1	16.04	667.8	-116.59	0.4572	0.0778	1.57	0.2847	-258.6
C_2	30.07	708.3	90.104	0.4572	0.0778	2.371	0.2846	-130.3
C_3	44.09	615.8	205.97	0.4572	0.0778	3.204	0.2762	-43.87
IC_4	58.12	529.1	274.91	0.4572	0.0778	4.213	0.2827	67.73
NC_4	58.12	550.7	305.69	0.4572	0.0778	4.085	0.2739	67.73
IC_5	72.15	491.6	369.05	0.4572	0.0778	4.934	0.2727	67.73
NC_5	72.15	488.8	385.61	0.4572	0.0778	4.982	0.2684	67.73
C_6	84	436.6	453.83	0.4572	0.0778	5.623	0.2504	60.53
C_7	96	426.2	526.73	0.4572	0.0778	6.279	0.2528	60.53
C_8	107	417.7	575.33	0.4572	0.0778	6.936	0.2608	60.53
C_9	121	381.5	625.73	0.4572	0.0778	7.753	0.2539	60.53
C_{10}	134	350.9	667.13	0.4572	0.0778	8.554	0.2483	60.53
C_{11}	147	323.5	706.73	0.4572	0.0778	9.403	0.243	60.53
C_{12}	161	301.7	742.73	0.4572	0.0778	10.2	0.2386	60.53
C_{13}	175	284.2	776.93	0.4572	0.0778	10.94	0.2343	60.53
C_{14}	190	269.8	811.13	0.4572	0.0778	11.69	0.2314	60.53
C_{15}	206	255.3	843.53	0.4572	0.0778	12.48	0.2278	60.53
C_{16}	222	240.7	872.33	0.4572	0.0778	13.31	0.2242	60.53
C_{17}	237	230.6	899.33	0.4572	0.0778	14	0.2214	60.53
C_{18}	251	221.9	920.93	0.4572	0.0778	14.63	0.2191	60.53
C_{19}	263	214.7	940.73	0.4572	0.0778	15.2	0.2172	60.53
C_{20}	275	208	962.33	0.4572	0.0778	15.92	0.217	60.53
C_{21}	291	202.8	982.13	0.4572	0.0778	16.5	0.2163	60.53
C_{22}	305	195.5	1001.9	0.4572	0.0778	17.17	0.214	60.53
C_{23}	318	191.1	1019.9	0.4572	0.0778	17.72	0.2132	60.53
C_{24}	331	185.2	1037.9	0.4572	0.0778	18.31	0.211	60.53
C_{25}	345	179.3	1055.9	0.4572	0.0778	19	0.2094	60.53
C_{26}	359	174.9	1070.3	0.4572	0.0778	19.53	0.208	60.53
C_{27}	374	170.5	1086.5	0.4572	0.0778	20.07	0.2062	60.53
C_{28}	388	166.1	1100.9	0.4572	0.0778	20.65	0.2047	60.53
C_{29}	402	163.1	1113.5	0.4572	0.0778	21.1	0.2038	60.53
C_{30}	416	160.2	1127.9	0.4572	0.0778	21.69	0.2039	60.53
C_{31}	430	144.6	1142.3	0.4572	0.0778	22.19	0.1866	60.53
C_{32}	444	139.9	1156.7	0.4572	0.0778	22.71	0.1832	60.53
C_{33}	458	136.1	1169.3	0.4572	0.0778	23.18	0.1804	60.53
C_{34}	472	131.7	1180.1	0.4572	0.0778	23.69	0.1773	60.53
C_{35}	486	128.9	1190.9	0.4572	0.0778	24.08	0.1752	60.53
C_{36}	500	124.9	1203.5	0.4572	0.0778	24.6	0.1722	60.53

5.5 Lumping Scheme

As discussed above, number of components (39), needs to be reduced by lumping to decrease the simulation time. Lumping is grouping of the components into pseudo components. There are many possibilities for lumping process. For example, if we want to reduce the number of components to 7, there are 2,760,681 lumping possibilities. Therefore, a lumping scheme needs to be used.

To appropriately simulate CO_2 injection, there is need to define CO_2, N_2, H_2S and CH_4 as pure components. Therefore, they will not be lumped with other components. It is quite common to lump C_2-C_3 and C_4-C_6 based on their similar molecular weights (Khan et al., 1992). For C_7+, it is decided to use two pseudo components and Whitson's method was used to decide these groups (Whitson, 1983). According to Whitson (1983), C_{n+} fractions can be lumped to multi carbon number groups (MCN) that can be found by Equation 5.10. Equation 5.11 was used to obtain the molecular weights separating each MCN group. Until now, apart from the already 6 components, C_7 to C_{36} will be lumped into two groups so that N_g is 2. From Equation 5.11, molecular weight separating MCN group is found as 219. Therefore, C_7 to C_{15} are grouped into one lumped parameter and C_{16} to C_{36} grouped to another. As a result, final components are CO_2, N_2, H_2S, C_1, $C_{2\text{-}3}$, $C_{4\text{-}6}$, $C_{7\text{-}16}$, $C_{16\text{-}36}$. Table 18 shows properties of components after lumping. Injected gas stream must be lumped with the same lumped components of the oil. Table 19 shows properties of injected gas stream components after lumping.

$$N_g = \text{Int}[1 + 3.3 \log_{10}(N - n)] \quad (5.10)$$

N_g= number of MCN groups (which is taken as 2 in our study)
N= number of carbon atoms of the last component which is 36 for our case
n= number of carbon atoms of the plus fraction which is 7 for our case

$$M_I = M_n(\exp((1/N_g)\ln(M_N/M_n)))^I \text{ which is equal to } M_I = M_n*(M_N/M_n)^{1/Ng} \quad (5.11)$$

M_N= molecular weight of the last component which is M_{36}=500 for our case

M_n= molecular weight of the + component which is M_7=96 for our case

Table 18 - Properties of components after lumping

Components	Mol	Mol Weight	Crit Pres	Crit Temp	Omega A	Omega B	V Crit	Z Crit (Visc)	Ref Temp
	%		(psia)	(°F)			(ft^3 /lb-mole)		(°F)
CO_2	0.0003	28.01	492.3	-232.5	0.4572	0.078	1.4417	0.29	-319
H_2S	0.00001	34.08	1296	212.8	0.4572	0.078	1.5698	0.28	-75.2
N_2	0.0001	34.08	1296	212.8	0.4572	0.078	1.5698	0.28	-75.2
C_{1+}	1.0021	16.04	667.8	-116.6	0.4572	0.078	1.5698	0.28	-259
C_{2+}	2.9963	37.86	656.9	154.4	0.4572	0.078	2.8332	0.28	-82.3
C_{4+}	5.7621	69.41	498.4	366.7	0.4572	0.078	4.771	0.27	64.64
C_{7+}	75.568	143.7	342.7	685.6	0.4572	0.078	9.0816	0.25	60.53
C_{18+}	14.671	327.1	190.3	1020	0.4572	0.078	17.939	0.21	60.53

Table 19 - Properties of injected gas stream components after lumping

Gas Source A-Lumped											
Comp.	% Mol	Mol Weight	Crit Pres	Crit Temp	Omega A	Omega B	V Crit	Z Crit	Boil Temp	Ref Dens	Ref Temp
			(bar)	(°K)			(m^3/kg-mole)		(°K)	(kg/m^3)	(°K)
N_2	2.69	28.013	33.94	126.2	0.4572	0.07779	0.09	0.291	77.4	804	78.1
H_2S	0.11	34.076	89.36	373.6	0.4572	0.07779	0.098	0.281	213.5	993	213.6
CO_2	77.06	44.01	73.86	304.7	0.4572	0.07779	0.094	0.274	194.7	777	293
C_1	18.02	16.043	46.04	190.6	0.4572	0.07779	0.098	0.284	111.6	425	111.7
C_{2+}	1.66	34.548	46.80	325.9	0.4572	0.07779	0.1646	0.284	199.4	558.8	198.3
C_{4+}	0.46	63.823	35.94	437.9	0.4572	0.07779	0.2786	0.275	283.5	593.1	292.8
Gas Source B-Lumped											
	% Mol	Mol Weight	Crit Pres	Crit Temp	Omega A	Omega B	V Crit	Z Crit	Boil Temp	Ref Dens	Ref Temp
			(bar)	(°K)			(m^3/kg-mole)		(°K)	(kg/m^3)	(°K)
N_2	2.92	28.013	33.94	126.2	0.4572	0.07779	0.09	0.291	77.4	804	78.1
H_2S	0.02	34.076	89.36	373.6	0.4572	0.07779	0.098	0.281	213.5	993	213.6
CO_2	28.15	44.01	73.86	304.7	0.4572	0.07779	0.094	0.274	194.7	777	293
C_1	60.72	16.043	46.04	190.6	0.4572	0.07779	0.098	0.284	111.6	425	111.7
C_{2+}	7.29	33.187	47.42	319.7	0.4572	0.07779	0.1595	0.284	194.9	555.5	193.6
C_{4+}	0.9	61.972	36.28	429.6	0.4574	0.07779	0.2726	0.276	277.1	583.3	292.9
Gas Source C-Lumped											
	% Mol	Mol Weight	Crit Pres	Crit Temp	Omega A	Omega B	V Crit	Z Crit	Boil Temp	Ref Dens	Ref Temp
			(bar)	(°K)			(m^3/kg-mole)		(°K)	(kg/m^3)	(°K)
N_2	7.62	28.013	33.94	126.2	0.4572	0.07779	0.09	0.291	77.4	804	78.1
H_2S	0.01	34.076	89.36	373.6	0.4572	0.07779	0.098	0.281	213.5	993	213.6
CO_2	20.65	44.01	73.86	304.7	0.4572	0.07779	0.094	0.274	194.7	777	293
C_1	63.11	16.043	46.04	190.6	0.4572	0.07779	0.098	0.284	111.6	425	111.7
C_{2+}	7.14	33.547	47.25	321.3	0.4572	0.07779	0.1608	0.284	196.1	556.4	194.9
C_{4+}	1.47	63.57	35.90	435.5	0.4572	0.07779	0.2782	0.275	281.7	590.2	292.8

5.6 Equation of State Tuning

EOS models are built based on empirical correlations, which may not perfectly match with specific cases so that there are some uncertainties from the beginning. Other uncertainties come to the play when heavy fractions are split, lumped and some of their properties are found by using mixing rules. Therefore, there is need to tune EOS by either trial and error procedure or by an automatic nonlinear regression (Ahmed, 2007). In this study, automatic nonlinear regression method was used to match EOS results with PVT lab data. Available PVT experiments for our case are, saturation pressure (P_b), constant composition expansion (CCE), and differential liberation expansion test (DLE), zero flash test and viscosity measurements, that are discussed in the previous chapter. For tuning, Coats and Smart Approach (1986), Whitson and Brule Approach (2000), Christensen Approach (1999), Ali and Al-Banbi Approach (2015), Aguilar and McCain Approach (2002), and Al-Meshari and McCain Approach (2005) can be used. Al-Meshari and McCain Approach (2005), which is the most accurate one was modified and used for tuning. Uncertainties in the properties of the plus fraction are the main problem while predicting volumetric behavior and thermodynamic properties by EOS. Small changes in the properties of plus fraction may have a big effect on PVT properties (Ahmed, 2007). Therefore, tuning was started by a property of a plus fraction. First, saturation pressure was matched by tuning the acentric factor of C_{18+}. Following that, volume shift parameters of all components were used for the regression of the volumetric data of CCE and DLE. Volume shift parameters were also tuned to match liquid density. Finally, viscosity was matched by tuning Zcrit, which is the ratio of molar volume of gas to the molar volume of ideal gas at critical temperature and pressure. Decreasing relative volume behavior (Figure 23) and decreasing formation volume factor with the pressure that is above the bubble point pressure is matched. As can be seen both the lumped model and the measured oil viscosity (Figure 27) and oil density (Figure 24) are decreasing until bubble point pressure and then increasing thereafter (Figure 27). There was a reasonable match for most parameters except for the gas oil ratio (Figure 25). It

was thought that might be a mechanical problem related to opening or closing the sampler, which may lead to releasing of gas.

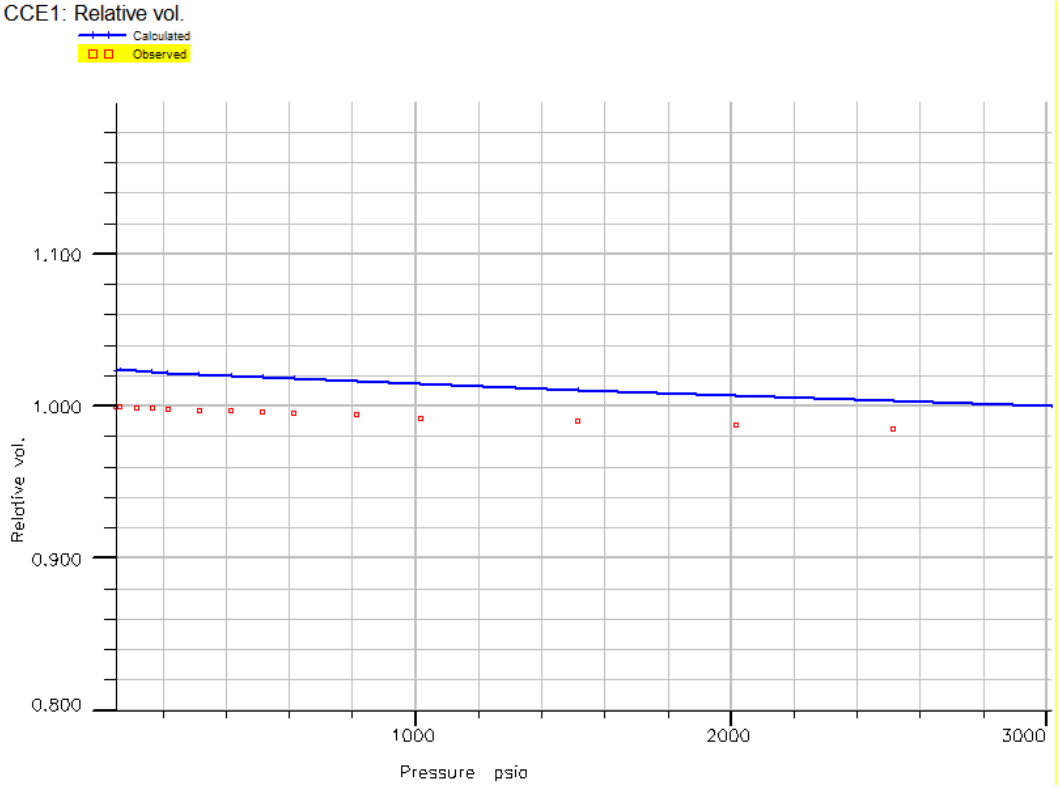

Figure 23 - Relative volumes from CCE experiment vs calculated

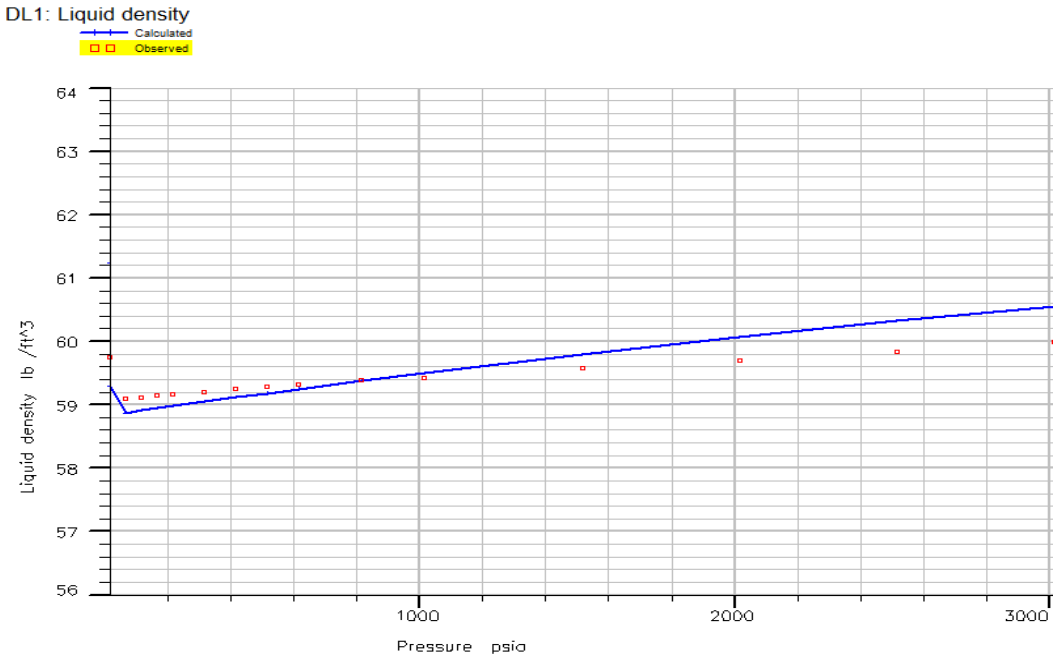

Figure 24 - Liquid density from DLE experiment vs calculated

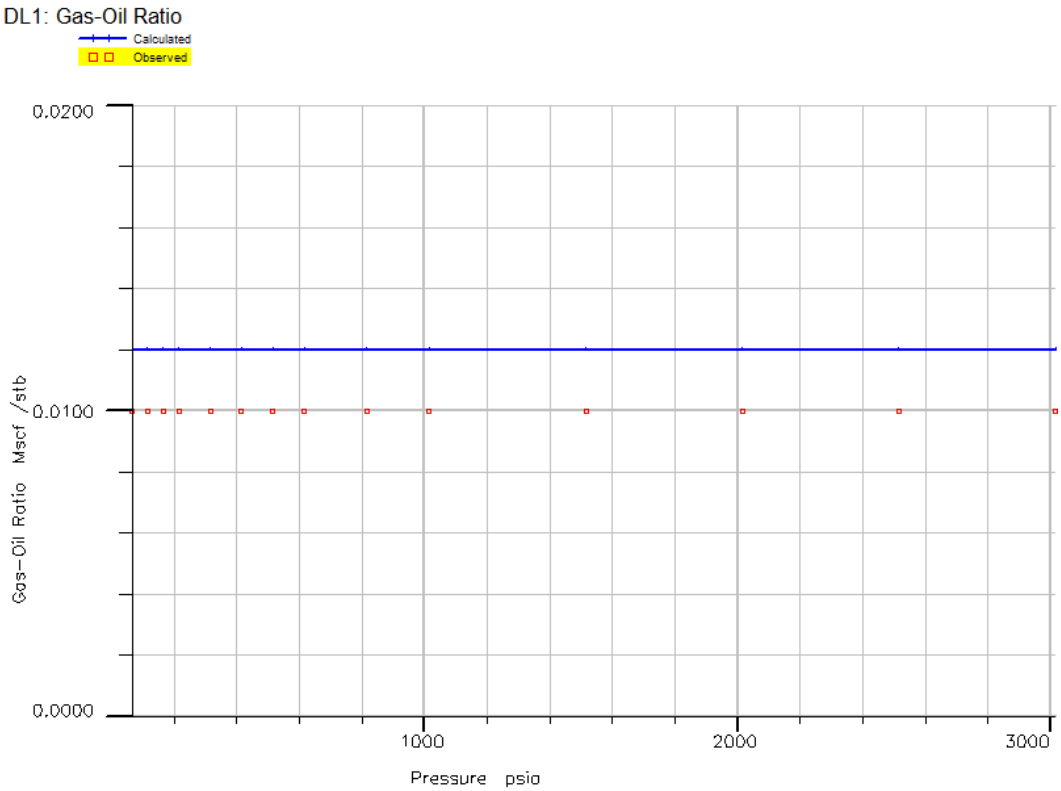

Figure 25 - GOR from DLE experiment vs calculated

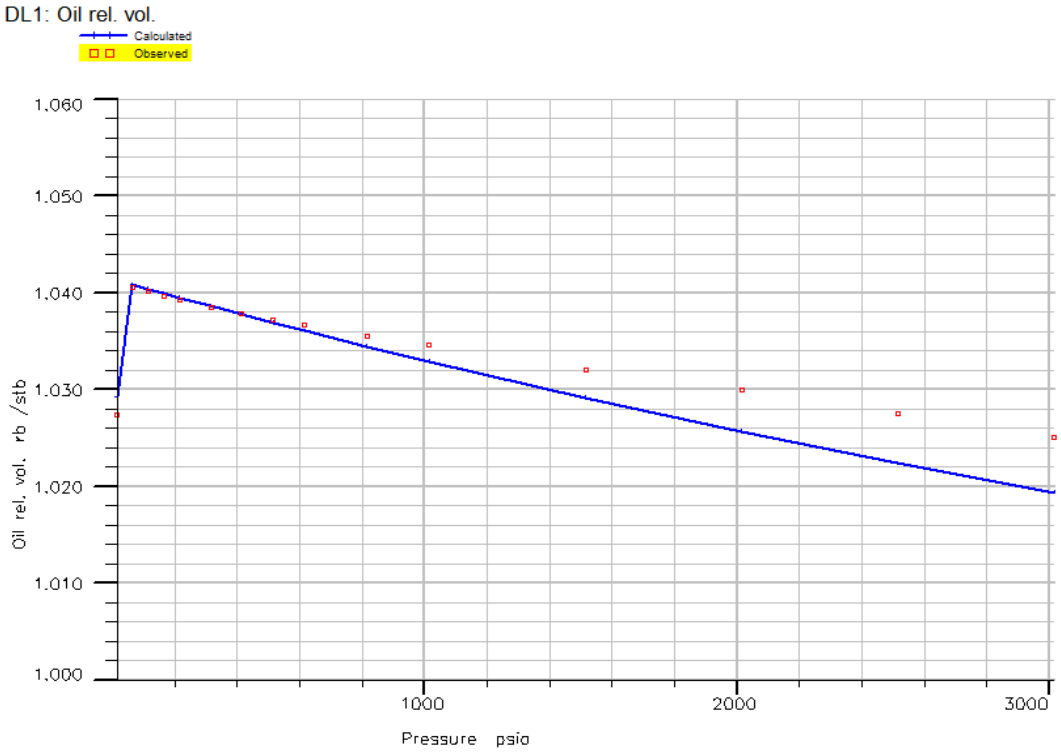

Figure 26 - B_o from DLE experiment vs calculated

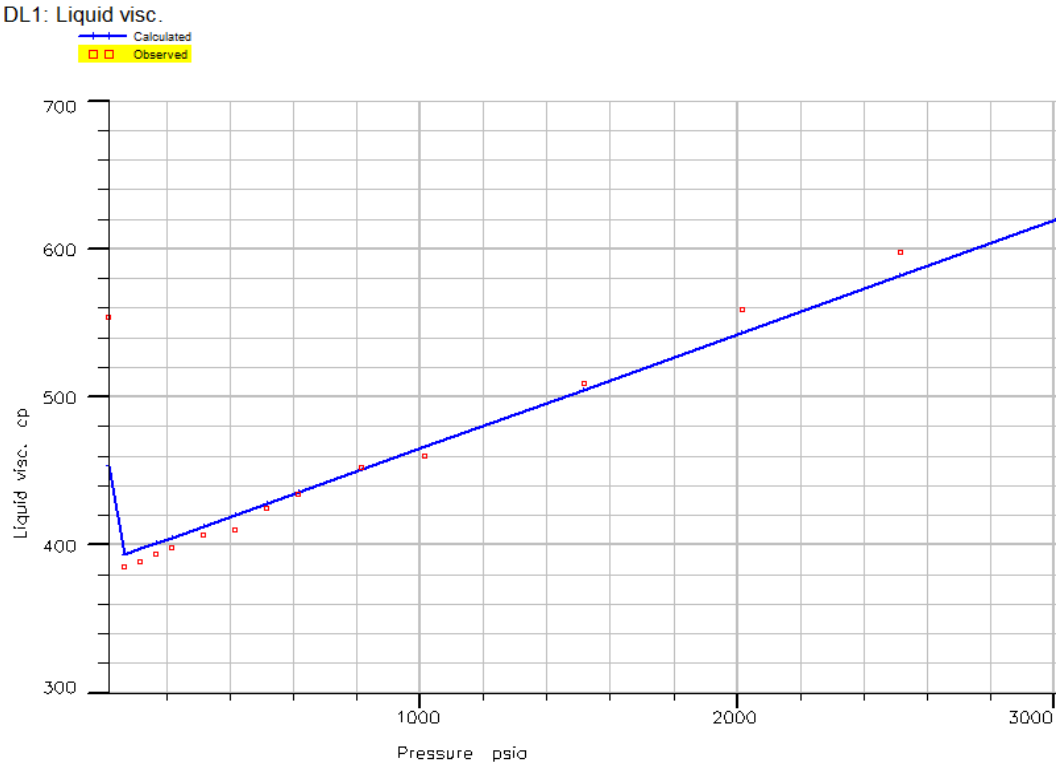

Figure 27 - Viscosity from viscosity experiment vs calculated

5.7 Model Construction and History Matching

In this study, a previously developed geological model was used (Bender and Yilmaz, 2014). This geological model consists of 106704 grid blocks, 54 in the y direction, 152 in the x direction and 13 in the z direction corresponding to an area of 13.3 km^2 (Bender, 2013). Grid block size is 50 m in the x direction, 50 m in the y direction. In the z direction, grid block size is between 3 to 8 m. Model gross pore volume is 162 million m^3. Model properties are given in Table 20. A three dimensional compositional reservoir simulation model was constructed by using Schlumberger's Eclipse 300 and Petrel software.

Table 20 - Summary of the reservoir model properties (Bender and Yilmaz, 2014)

Parameters	Values	Units
Number of cells in the x direction	152	
Number of cells in the y direction	54	
Number of cells in the z direction	13	
Number of Gridblocks	106704	
x gridblock size	50	m
y gridblock size	50	m
z gridblock size	13	m
Total Pore Volume	162×10^6	m^3

History matching is a critical step to calibrate the model, which will be used to predict the reservoir performance. History match part covers 30 years of production and 10 years of injection periods. Production and injection periods are divided into 4 parts. These are primary production period, continuous gas injection period and water alternating gas injection periods and decline period after CO_2 flooding projects. Our strategy was tuning and matching during primary production period and then checking the others. History matching parameter selection is a crucial step to achieve correct predictions. In this study, matching parameters were decided based on the uncertainty. Uncertainty level of matching parameters is well discussed by Mattax and Dalton (1990). According to their study, aquifer connectivity, permeability anisotropy, high conductivity streaks, relative permeability functions, rock compressibility are some of the uncertain parameters and these parameters were used in our study. Firstly, reservoir pressure was matched by using reservoir volume as a control mode. Build up tests and static gradient data were used to match. No areal change was made during reservoir pressure matching period. To match the reservoir pressure, aquifer connectivity was decreased and total compressibility was tuned. Aquifer connectivity was

chosen to match the reservoir pressure because it has the highest uncertainty among other data. Therefore, history matching initiated by using aquifer connectivity. Fault transmissibility is another uncertain parameter due to limited data. To match the pressures of the regions close to the faults, fault transmissibility were tuned. As discussed in Section 5.3, drill stem test permeability is higher than the core permeability because there are vugs and fissures in this field and it is hard to see these in core analysis. Therefore, there is uncertainty in global permeability. To match the well pressures global horizontal permeability was increased. Cumulative oil, water, gas productions and breakthrough times were then matched by using oil rate as a control mode. To match the water and gas productions, vertical permeability to horizontal permeability ratio was decreased. Also, relative permeability data (endpoints) were tuned to match the water cuts and breakthrough times. Figure 28 shows the history match of the field oil-water-gas production rate, and pressure. Finally, individual well behaviors which are oil, water, gas productions, water cuts, gas oil ratios and log-derived saturations were matched by sticking to initial match. In this part global k_h, k_v/k_h ratio, fault transmissibility and endpoints were tuned. Only parameter that is changed regionally is Leveret J Function. As mentioned before, initial saturation distribution was conducted by using Leveret J Function. Match was performed by comparing the initial water saturations in well grids and log derived saturations from old and new wells. During the history match period for wells, knowledge of the completion data is very important to calibrate the model correctly. When engineer could not match the data, changing the properties around the well may not be realistic and correct. In this study, we experienced a situation, which can be a good example for that. Figure 29 presents the history match of oil and water productions for two wells. First, one matched perfectly but water rate could not be matched for the second one. When we checked the completion data, it was seen that there was a casing problem in this well and water was coming from the surface. As a result this well was not included in the matches.

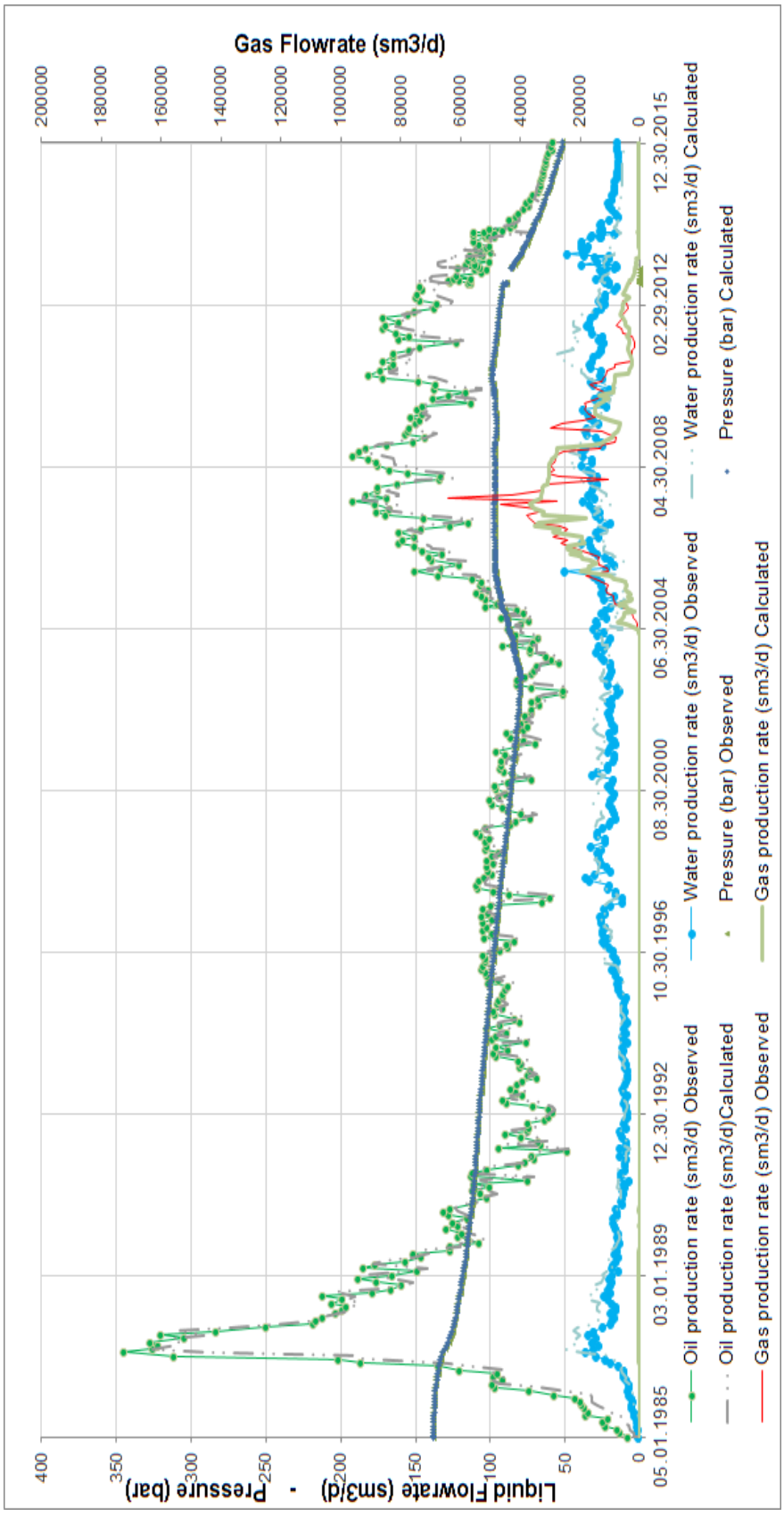

Figure 28 - History match of the field oil water gas production rate and pressure

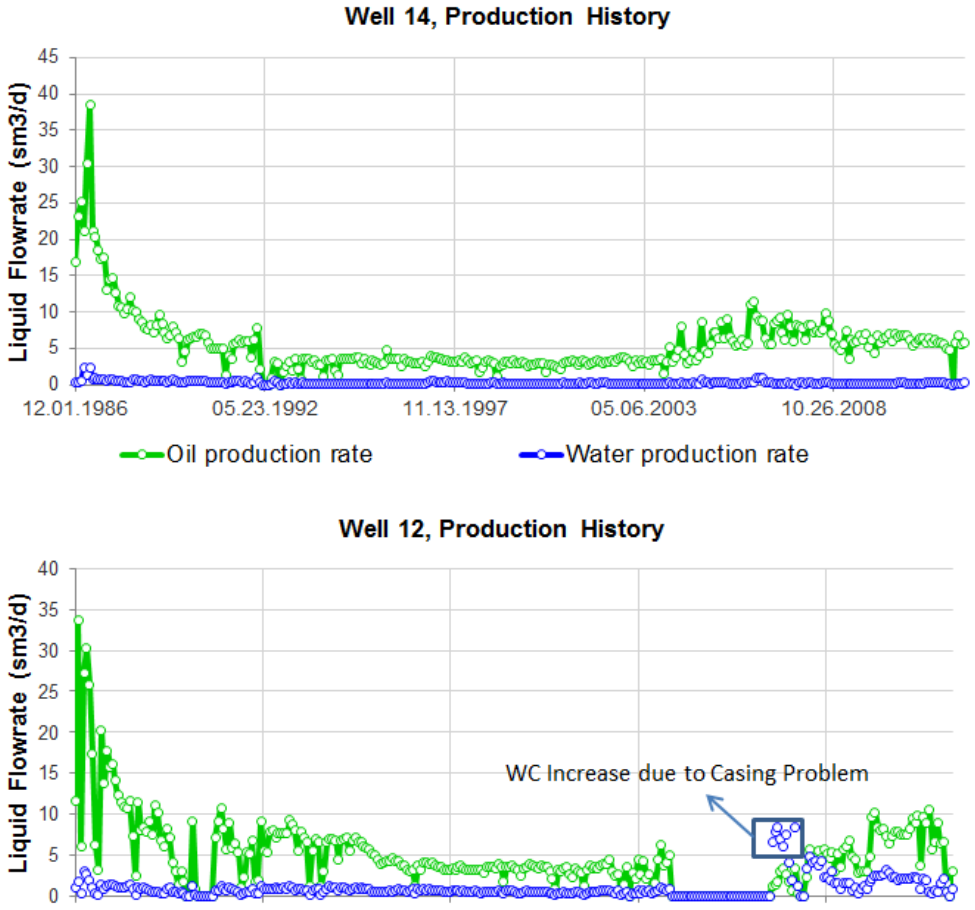

Figure 29 - History match for Well #14 and Well #12

Quality of history match was checked by well by well and was also checked by using Equation 5.12 which enables us to quickly check the whole field for all time steps for different parameters. This is also useful to show the quality of the match in one graph instead of many graphs. In this equation, "S" is the simulated value, "O" is the observed value, "σ" is the normalization parameter, "N" is the number of points and "M" is the match value, which shows the quality of the match (Schlumberger, 2013). The normalizing parameter is chosen such that "M" values calculated by this equation are graded from 1 (good) to 5 (poor) each value corresponding to 10% increments. Any raw match value below 10% is graded as 1. All raw values above 50% are graded 5. The interval in between is divided into three equally sized intervals, graded between 2 and 4. Values are assigned to different colors. Figure 30 shows history match analysis of oil production rate, oil production cumulative, water cut and pressure. In this figure, green dots represent a good match (i.e. $M \leq 1$), yellow dots represent a reasonable match (i.e. $1 < M \leq 4$), and red dots represents a bad match (i.e. $M > 4$). It can be observed that each well's oil production rate, oil production cumulative, water cut and pressure had been matched less than 10% except for well #38 and well #3. A high permeability fault crosses Well #38 that results in decreased oil production and increased water cut in less than a month. This well was shut in after a month due to high water cut and then used for injection. Well #3 is located in an area with a high uncertainty. Excess water feeding this well could not be modeled resulting in a poor match.

$$M = \sqrt{\frac{1}{N}\sum_{i=1}^{N}\left(\frac{Si-Oi}{\sigma}\right)^2} \tag{5.12}$$

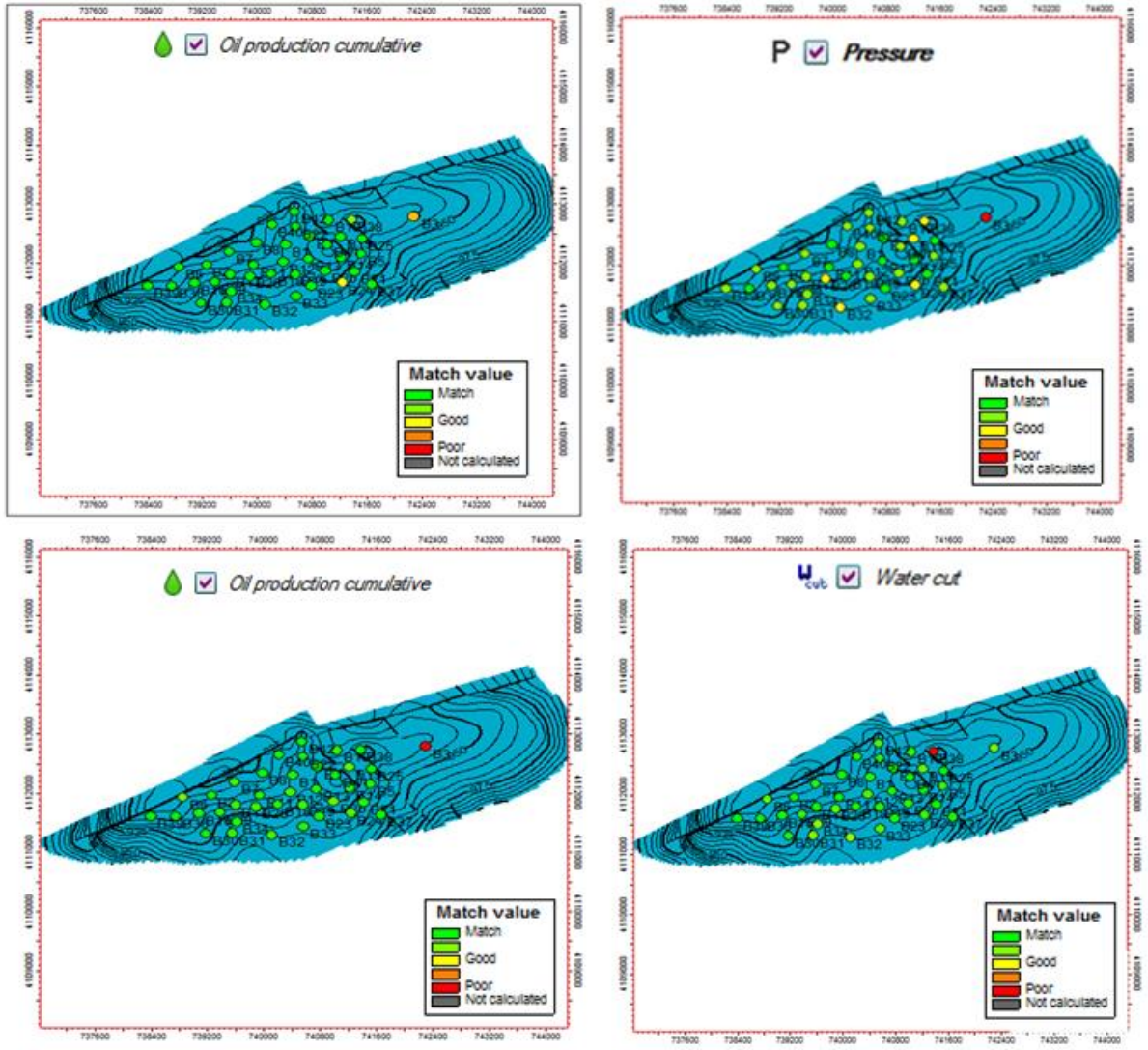

Figure 30 - History match analysis of oil production rate, oil production cumulative, water cut & pressure

CHAPTER 6

OPTIMIZATION OF GAS INJECTION AND OIL RECOVERY

In this chapter, CO_2 injection methodologies are discussed and compared. Effect of changing injected CO_2 amount on CO_2 storage, oil recovery and economics were investigated by optimizing produced gas oil ratios and injection rates. Optimization of produced gas oil ratios and injection rates are essential to maximize the amount of CO_2 storage and oil recovery. Sensitivity of these parameters and their effects were discussed in this chapter.

6.1 Flue Gas Injection

Primary objective of this section is to maximize the amount of flue gas storage and secondary objective is to increase the oil recovery while maximizing the flue gas storage. To achieve these goals, history matched compositional simulation model was used for numerical predictions. Three different scenarios were built to understand the effect of the CO_2 solubility, effect of different gas oil ratio constraints, and effect of different injection rates on CO_2 storage and oil recovery. All simulation runs were started from 01.01.2016 and field production predictions for 100 years had been carried out under operational constraints. For all cases, maximum water cut for production wells was set as 100 % and minimum oil production for each production well was set as 0 stb/day to be able to continue the storage project in the absence of oil production. For injection wells, maximum bottom hole pressure was restrained as 131 bar that is 7 bars less than the initial reservoir pressure. Firstly, base case (do nothing case) was run for 100 years without any flue gas injection for comparison purposes. Field production was started with 31 production wells (Figure 15). Oil production continued for 29 years

until 2045. Figure 31 shows oil production cumulative, oil flow rate, average field pressure, water production rate vs date for the base case. Additional oil recovery and cumulative oil recovery were estimated as 89,965 sm^3 and 1,339,721 sm^3 corresponding to a recovery factor of 5.7 %.

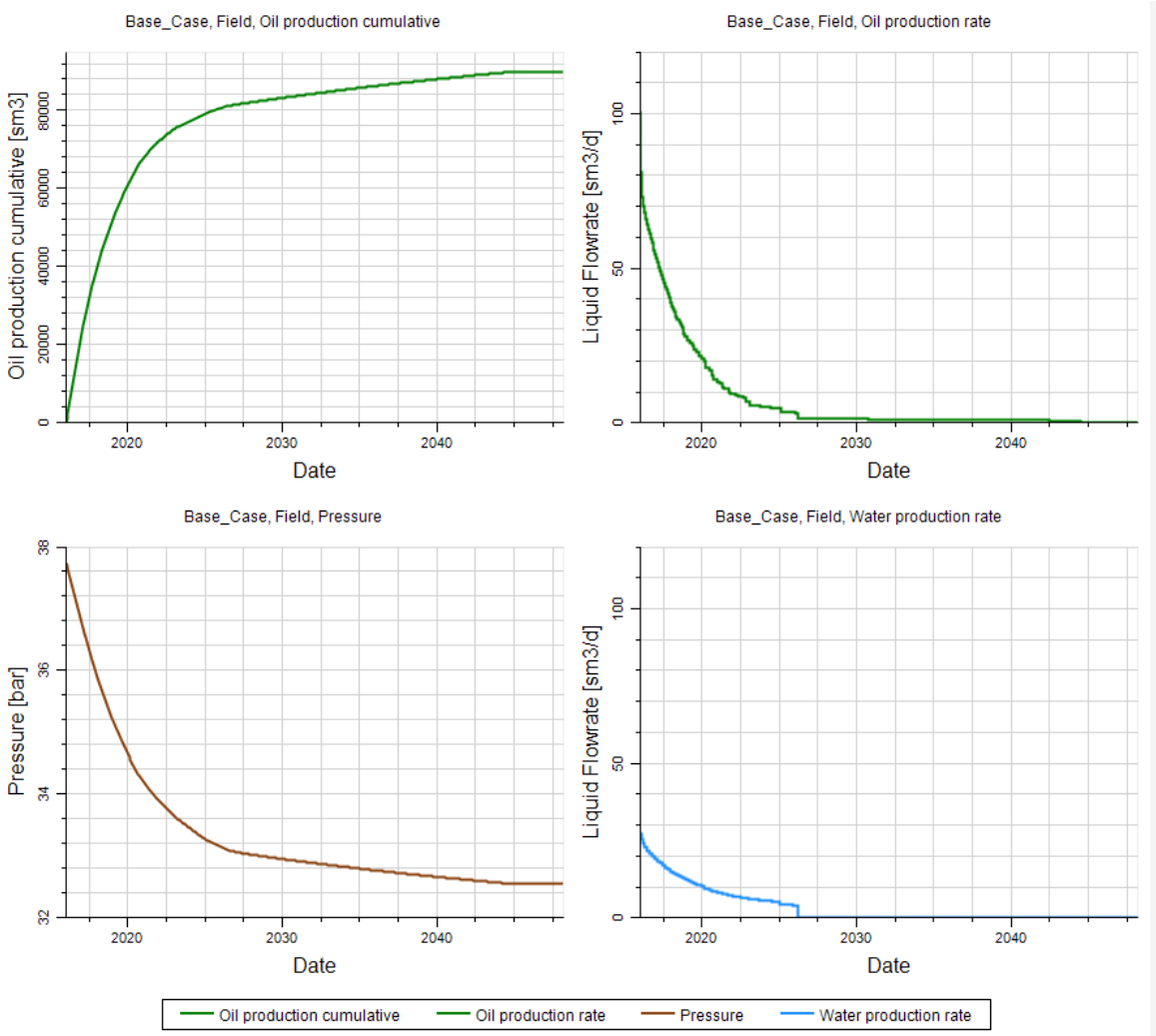

Figure 31 - Field cumulative oil production, oil rate, pressure and water production rate for the base case

6.1.1 Effect of CO_2 Solubility

In this scenario, effect of CO_2 solubility in three phases on CO_2 storage and oil recovery was studied. Equilibration method was used to calculate CO_2 partitioning between oil and gas (Schlumberger, 2011). Oil and gas densities and fugacity were modeled by using 3-Parameter Peng Robinson EOS. Due to lack of CO_2 solubility data in water, CO_2 solubility was determined by using solubility data from the literature (Chang et al., 1996). First run was simulated without enabling the CO_2 solubility and second run was studied enabling the CO_2 solubility in three phases. For both of the runs, GOR constraint was set as 1000 sm^3/sm^3 and daily field gas injection was set as 50,000 sm^3/day that is shown as "GOR-1000-Inj-50000" in Table 21. Flue gas injection was started in 01.01.2016 and continued for 100 years. Figure 32 shows cumulative oil production, gas in place, and CO_2 dissolved in aqueous phase for CO_2 solubility case. As can be seen from this figure cumulative oil production and gas in place are very close to each other and gas in aqueous phase is very low for CO_2 solubility case. For CO_2 solubility case, cumulative flue gas storage is 1,105 $MMsm^3$, total CO_2 storage is 268.29 $MMsm^3$, 47 $MMsm^3$ of CO_2 is dissolved in oil, 19.86 $MMsm^3$ of CO_2 is dissolved in water and recovery factor is 10.09%. For without CO_2 solubility case, cumulative flue gas storage is 1,087 $MMsm^3$, total CO_2 storage is 262.52 $MMsm^3$ and recovery factor is 10.06%. As can be seen from Figure 32, both results are very close to each other. Reservoir pressure is always below the minimum miscibility pressure resulting in immiscible gas injection in all cases. For immiscible gas injections, effect of CO_2 solubility is very low when compared to miscible gas injections. Yet another reason is that there is no active aquifer or water injection for both cases where effect of CO_2 solubility in water is important. For the scenarios discussed in other sections CO_2 solubility option was enabled for more accurate results. Table 21 shows summary of the results for both of the cases.

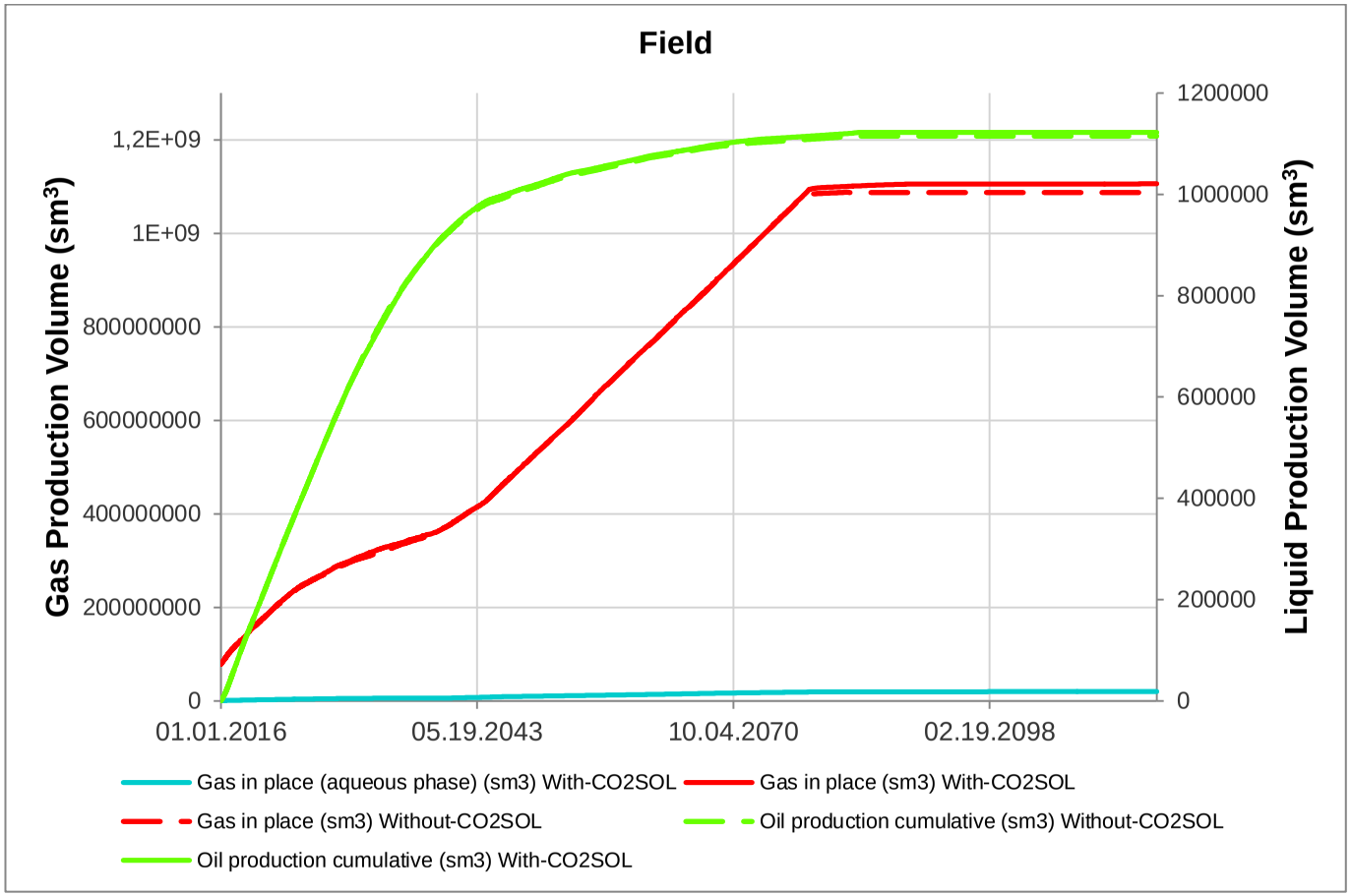

Figure 32 - Cumulative oil production, gas in place and CO_2 dissolved in aqueous phase with and without CO_2SOL

Table 21 - Summary of simulation results

Case Name	Injected Gas	CO_2SOL	Flue Gas In Place, $MMsm^3$	CO_2 In Res, $MMsm^3$	CO_2 In Aqueous Phase, $MMsm^3$	Additional Cumulative Oil Production, sm^3	Cumulative Oil Production, sm^3	RF, %
Base Case	-	-	0.00	0.00	0.00	89,965	1,339,721	5.70
GOR-1-Inj-50000	Flue Gas	✓	642.18	190.08	10.09	715	1,250,471	5.32
GOR-500-Inj-50000	Flue Gas	✓	968.86	221.60	17.14	813,576	2,063,332	8.78
GOR-1000-Inj-50000	Flue Gas	✓	1105.92	268.29	19.86	1,122,280	2,372,036	10.09
GOR-1000-Inj-50000	Flue Gas	-	1087.26	262.52	Not Applicable	1,115,088	2,364,844	10.06
GOR-2000-Inj-50000	Flue Gas	✓	980.22	210.34	18.20	1,001,712	2,251,468	9.58
GOR-1000-Inj-40000	Flue Gas	✓	1088.17	260.32	18.79	1,177,198	2,426,954	10.33
GOR-1000-Inj-75000	Flue Gas	✓	905.61	213.11	15.75	740,067	1,989,823	8.47
GOR-1000-Inj-100000	Flue Gas	✓	853.16	197.28	14.26	615,412	1,865,168	7.94
GOR-1000-Inj-150000	Flue Gas	✓	843.19	195.86	14.71	598,006	1,847,763	7.86
CO_2 Injection GOR-1000-Inj-50000	CO_2	✓	-	1627.60	80.87	1,568,318	2,818,074	12.00

6.1.2 Effect of GOR

For storage objective, one of the most important factors affecting amount of gas sequestered is produced GOR constraint. Different GOR constraints (1, 500, 1000, and 2000 sm^3/sm^3) were used in production wells to see the effects of GOR constraint on storage and recovery. When the simulated GOR reached the set GOR value in each well, perforations responsible for this increase was shut down. For all cases, daily field gas injection rate was set as 50,000 sm^3/day and CO_2 solubility option was enabled in all scenarios. Figure 33 shows gas in place, CO_2 dissolved in aqueous phase, cumulative oil production, and average reservoir pressure for each scenario. For GOR-1 case, there was almost no oil production because gas breakthrough occurred quickly in already CO_2 flooded oil field. As the wells were closed due to GOR-1 constraint, reservoir pressure increased quickly. As a result, amount of gas storage did not increase after 24 years (Figure 33). After this case, GOR constraint was increased. When GOR-1000 case was run it gave the maximum gas storage and oil recovery among the values discussed here. Totally, 1.1 billion sm^3 of flue gas stored and oil recovery factor increased from 5.7% to 10.09% for GOR-1000 case. Following that, GOR-2000 was tried but did not give good results in terms of gas storage and oil production. As can be seen from Figure 33, reservoir pressure reached to the maximum value in 44 years that lead to decrease in storage and recovery. Pressure had started to decrease after 10 years of injection for GOR-1000 and GOR-2000 cases due to increased GOR ratio that lead to better sweep efficiency (Figure 33). Gas production control plays a crucial role not only for gas storage but also for oil recovery. There are two reasons for that. First, GOR management contributes to better sweep efficiency. Second, oil production decreases after gas breakthrough due to high mobility of gas. Results show that there is an optimum value for GOR which maximize the amount of gas storage. Also, maximum oil recovery was achieved by the optimum GOR which maximized gas storage. Detailed results for each case are given in Table 21. Table 21 presents results for all scenarios, the number written after "GOR" represents GOR value and the number written after "Inj" represents daily injection rate.

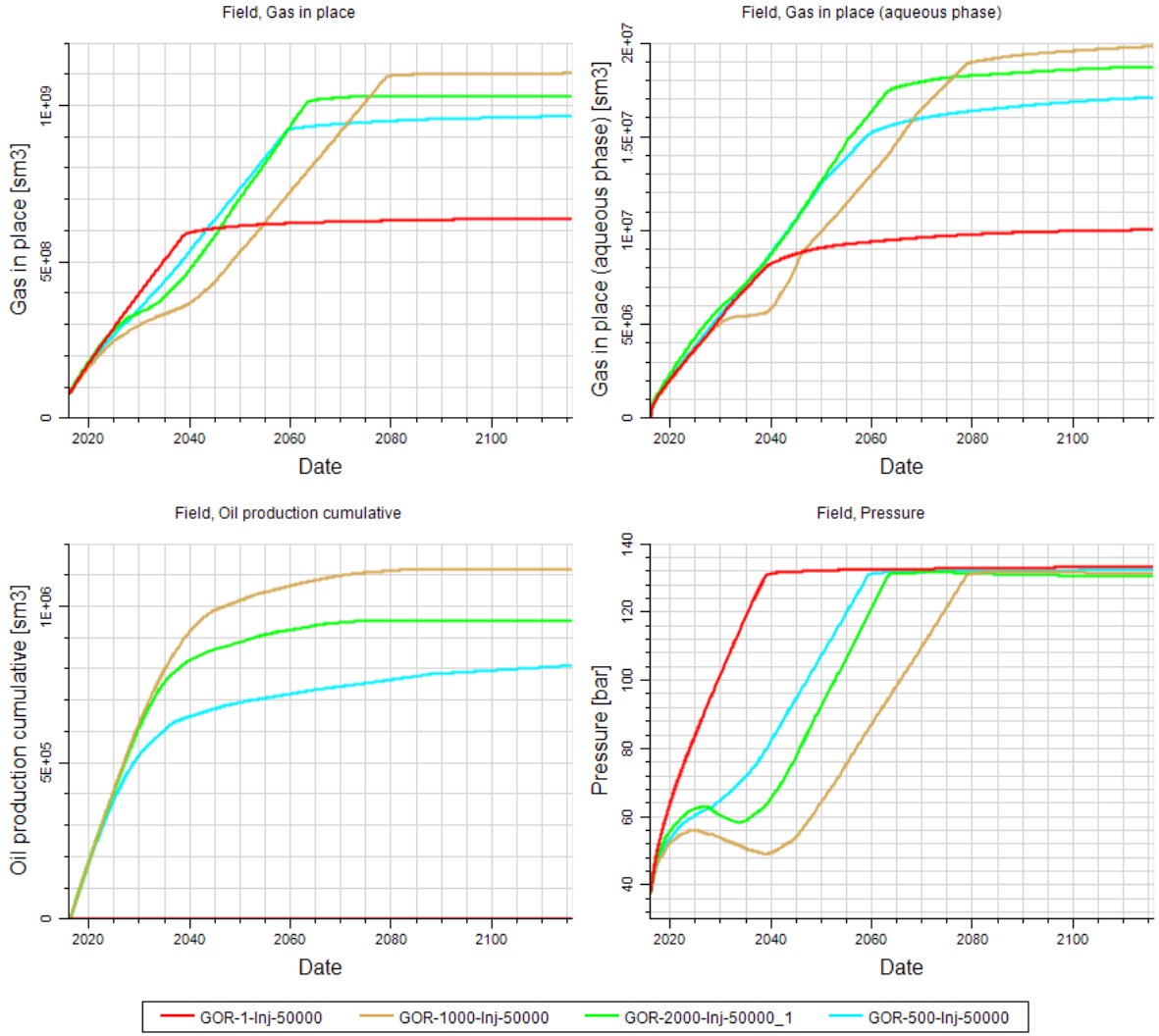

Figure 33 - Gas in place and CO_2 dissolved in aqueous phase, cumulative oil production and average reservoir pressure for the GOR Case

6.1.3 Effect of Injection Rates

Optimization of injection rates is absolutely necessary to maximize the storage capacity of the reservoir and to increase the oil recovery. Five different injection rates (40,000, 50,000, 75,000, 100,000, and 150,000 sm^3/day) were used to study sensitivity of injection rates to production and storage. For all cases, GOR constraint was set as 1000 sm^3/sm^3 and CO_2 solubility option was enabled. Simulation time, 100 years, was adjusted to determine the maximum storage capacity of the reservoir before exceeding the regulated pressure for all cases. Injection rate for each well was constrained by the bottom hole pressure of 131 bars which is 95% of the initial reservoir pressure. Maximum flue gas storage of 1.10 billion sm^3 and additional oil recovery of 1.12 MMbbl was achieved by 50,000 sm^3 of daily flue gas injection and maximum additional oil recovery of 1.17 MMbbl was reached by 40,000 sm^3 of daily flue gas injection (Table 21). CO_2 storage capacity and oil recovery decreased with higher injection rates. As can be seen from Figure 34, higher injection rates caused quick pressure buildup in the reservoir so that CO_2 storage capacity was limited by decreased injectivity. Increase in pressure was quick and continuous for higher injection rates; 75,000, 100,000, and 150,000 sm^3/day. However, pressure increased, decreased and then increased for lower injection rates; 40,000, 50,000 sm^3/day because reservoir oil production continued with high daily rates that leads to decrease in reservoir pressure. Also, high oil recoveries were achieved at early times with high gas injection rates but after that oil recoveries decreased due to increase in reservoir pressure. In addition to these, high gas injection rates resulted in early gas breakthrough that increased the gas oil ratios and reduced the oil recovery in long term. Figure 35 shows the amount of flue gas storage vs recovery factor for all cases.

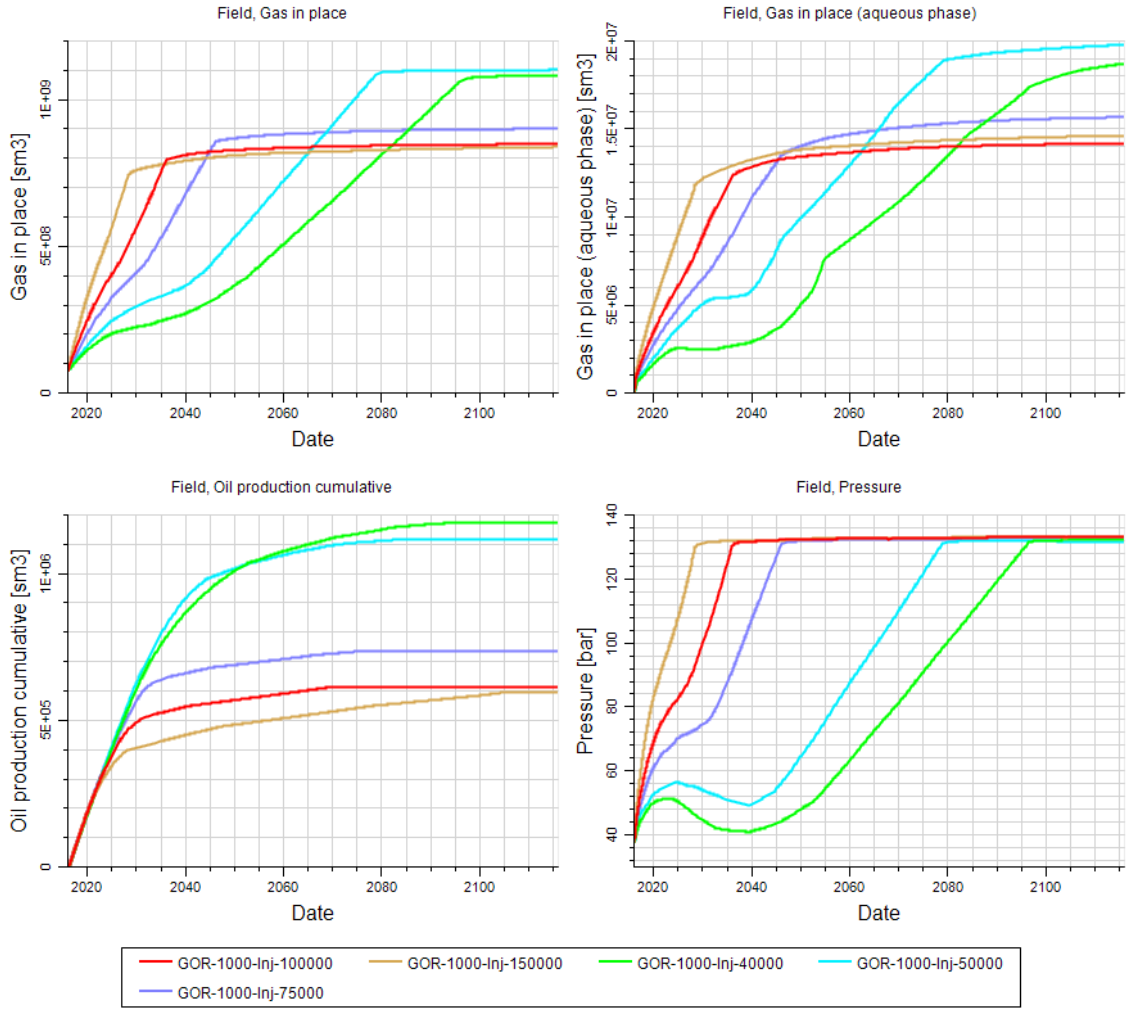

Figure 34 - Gas in place and CO_2 Dissolved in aqueous phase, cumulative oil production and average reservoir pressure for the injection rate case

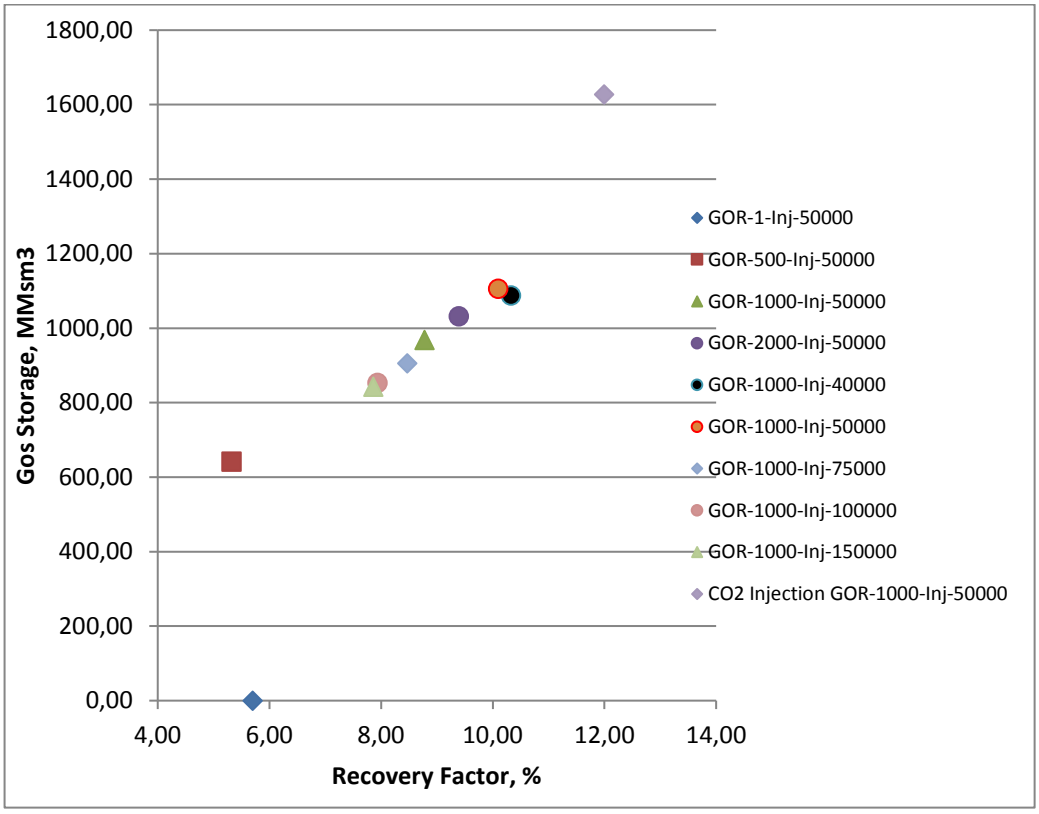

Figure 35 - Amount of flue gas storage vs recovery factor

6.2 Pure CO_2 Injection

In this section, pure CO_2 injection for storage and EOR purposes is discussed. History matched compositional simulation model was used for numerical predictions. All simulation runs were started from 01.01.2016. Field production predictions for 100 years had been performed under operational constraints. Maximum water cut for production wells was set as 100% and minimum oil production for each production well was set as 0 stb/day to be able to continue the storage project in the absence of oil production. For injection wells, maximum P_{bh} was restrained as 131 bar that was 7 bar less than the initial reservoir pressure.

6.2.1 CO_2 Storage

Equilibration method was used to calculate CO_2 partitioning between oil and gas (Schlumberger, 2011). Oil and gas densities and fugacity were modeled by using 3-Parameter Peng Robinson EOS. Due to lack of CO_2 solubility data in water, CO_2 solubility was determined by using solubility data from literature (Chang et al ., 1996). GOR was set as 1000 sm^3/sm^3 and daily field gas injection was set as 50,000 sm^3/day. CO_2 injection was started in 01.01.2016 and continued for 100 years. Gas storage and oil recovery continued to increase after 100 years. Totally, 1.63 billion sm^3 of CO_2 was stored, 342 $MMsm^3$ of CO_2 was dissolved in oil and 80 $MMsm^3$ of CO_2 was dissolved in water. Additional oil production was 1.57 $MMsm^3$. Figure 36 shows cumulative oil production, gas in place, and CO_2 dissolved in aqueous phase for CO_2 injection case. As can be seen from Figure 36, reservoir pressure did not reach to its maximum value. As a result, oil recovery and CO_2 storage increased continuously. Therefore, it can be said that CO_2 storage project can continue more than 100 years, if the injected gas is CO_2. After 2024, reservoir pressure started to decrease because produced volume was larger than injected volume. Around 2040, reservoir pressure started to increase again due to decrease in oil production rates that can be seen from the decrease in the slope of the oil production cumulative part of the Figure 36. 1040 sm^3 of CO_2 was injected to produce 1 sm^3 of oil. CO_2 injection enhances the oil recovery by viscosity reduction and swelling effects. Storage project had a positive effect on oil recovery that increased the oil recovery factor from 5.7 % to 12% and also increased the field's life. It was determined that the discussed field is a good candidate for CO_2 storage. Totally 1.63 billion sm^3 of CO_2 could be sequestered in this field. Figure 35 presents change of CO_2 gas storage with recovery factor. As can be seen from this figure, CO_2 injection case steps out of the line due to its favorable properties when compared with flue gas injection. During the storage project, most of the CO_2 was trapped by structural and stratigraphic trapping mechanism. Only 25.98% of the sequestered CO_2 was trapped by solubility trapping mechanism.

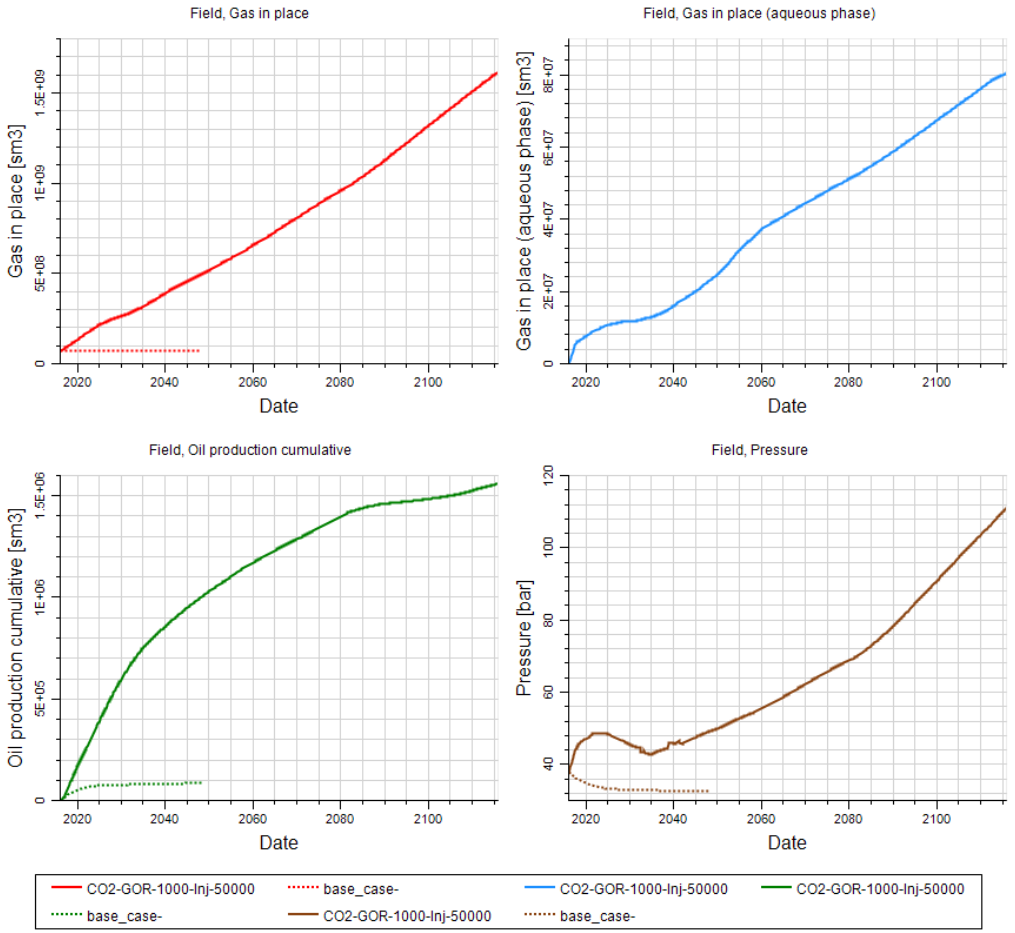

Figure 36 - Cumulative oil production, gas in place, CO_2 dissolved in aqueous phase and pressure for the CO_2 storage case

6.2.2 CO_2 EOR

To optimize the CO_2 flooding project, different operating parameters were studied; producing well gas oil ratio (GOR) constraint and injection rates. Firstly, injection rates were optimized to maximize the oil recovery. For all cases, producing GOR constraint was set as 1000 sm^3/sm^3. Injection rate for each well was regulated by the bottom hole pressure constraint of 131 bars, which was 95% of the initial reservoir pressure. Studied injection rates were 50,000, 100,000 and 200,000 sm^3/day. Maximum oil recovery was achieved by 50,000 sm^3/day of CO_2 injection. It was found that higher injection rates resulted in lower oil recoveries due to quick breakthrough, quick pressure build up and lower sweep efficiency. Producing GOR is one of the most important factors affecting oil recovery. Three different GOR constraints were set for production wells; 1, 1000, and 4000 sm^3/sm^3. Daily gas injection rate was set as 50,000 sm^3/day for all cases. Higher GOR constraint decreased the oil recovery due to high mobility of gas. Maximum oil recovery was achieved by 50,000 sm^3/day of CO_2 injection and 1000 sm^3/sm^3 GOR (Figure 37). Additional oil production was 1.56 $MMsm^3$ and recovery factor increased from 5.7 % to 12 %. 1040 sm^3 of CO_2 was injected to produce 1 sm^3 of oil. Totally, 1.63 billion sm^3 of CO_2 was stored.

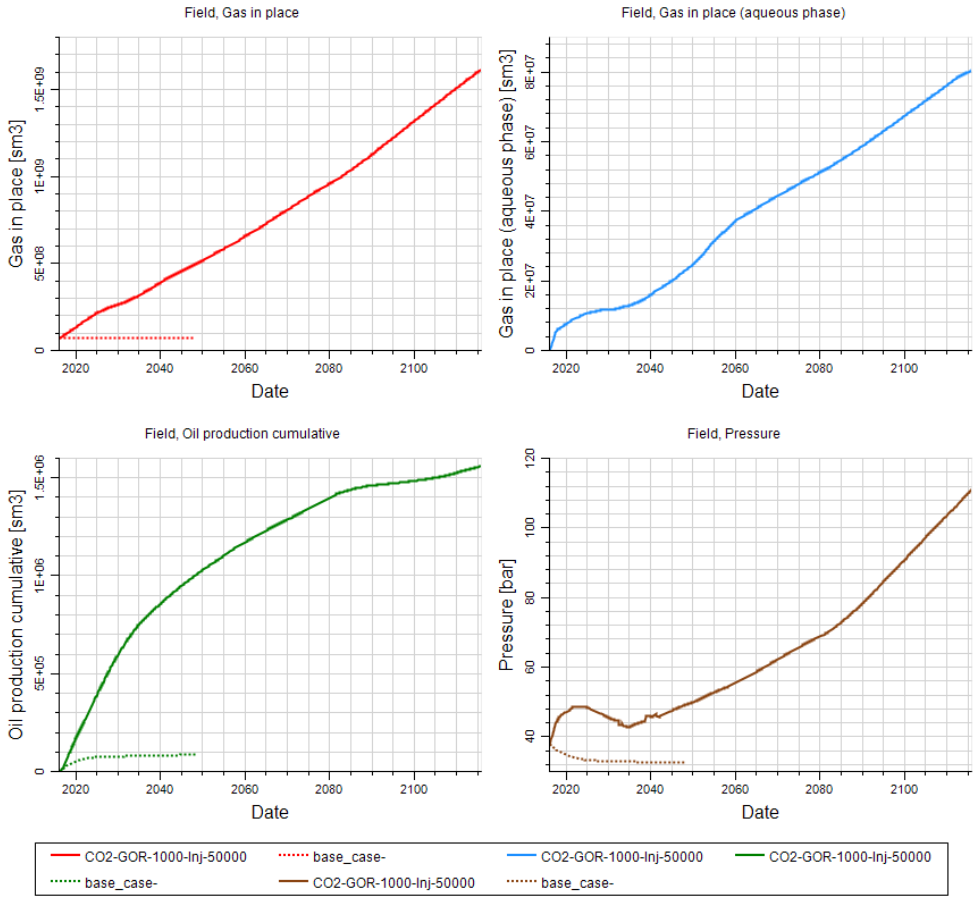

Figure 37 - Cumulative oil production, gas in place, CO_2 dissolved in aqueous phase and pressure for the CO_2 EOR case

6.3 Natural Gas Injection for EOR

As discussed in Chapter 4, there are three gas reservoirs around the mature oil field and all of them consists mostly methane and CO_2. In this section, injections of gases produced from these fields were simulated by using the aforementioned 3D compositional model. Main aim of this part is to find the effect of these gases on oil recovery and probable lifetime of these gas reservoirs.

All simulation runs were started from 01.01.2016 and field production predictions had been carried out until depleting the gas source. For all cases, maximum water cut for production wells was set as 95 % and minimum oil production for each production well was set as 1 stb/day. For injection wells, maximum bottom hole pressure was restrained as 131 bar that is 7 bar less than the initial reservoir pressure. Field production was started with 31 production wells. Daily gas injection rate was set as 50,000 sm^3/day for all cases and producing GOR constraint was set as 1000 sm^3/sm^3. It has been found that gas from Source A can feed the oil reservoir for 45 years, whereas gas source B can survive for 5 years and gas source C can last for 2 years. It was decided that it is not necessary to invest on the transportation of gas from gas source B and gas source C due to limited amount of OGIP and limited project time. Figure 38 shows cumulative oil productions for each case. It has been found that highest recovery was obtained by injecting gas source A's gas which has the highest CO_2 percentage. Additional oil recovery and cumulative oil recovery was estimated as 691,508 sm^3 and 1,941,264 respectively with a recovery factor of 8.8 % for gas source A case.

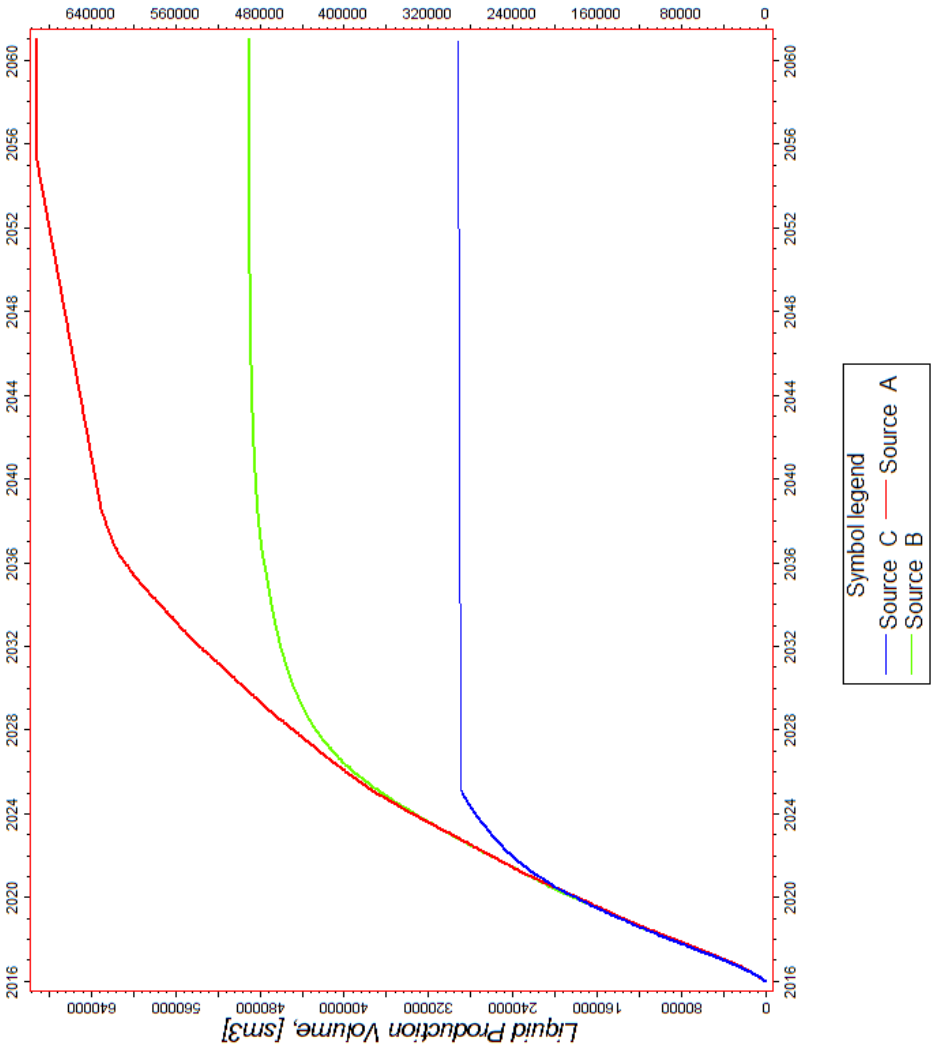

Figure 38 - Cumulative oil production vs time

6.4 A Discussion on Gas Saturation Distributions

In this section, CO_2 saturation distributions from 2002 to 2116 are discussed for continuous CO_2 flooding case. At the end of this section continuous CO_2 flooding case, flue gas injection case, and Source A gas injection cases are compared by evaluating gas saturation distributions at the end of each project.

Figure 39 presents the CO_2 saturation distributions for the CO_2 injection project applied between 2003 and 2012. As discussed before, continuous CO_2 injection project was started in 2003 by using 7 injection wells and had been continued until 2007. As can be seen from Figure 39, CO_2 saturation increased around the injection wells after 4 years of continuous CO_2 injection. Due to high gas oil ratios in the production wells and low sweep efficiencies, continuous CO_2 injection was converted to water alternating gas injection in 2007. After the start of the water alternating gas injection project in 2007, CO_2 saturation started to decrease due to decreased CO_2 injection from injection wells as well as due to increase in CO_2 productions from production wells. In addition to these, CO_2 injection decreased during WAG project because of injectivity problems. CO_2 injectivity of injection wells decreased while moving from water to CO_2 injection. Water blocked high permeable paths of CO_2 around the injection wells. On the other hand, CO_2 production from production wells increased due to the mobility contrast between oil and CO_2. Most of the produced CO_2 was from the continuous CO_2 injection project. In 2012, CO_2 injection project was stopped. After 2012, CO_2 saturation in the field decreased quickly due to high mobility contrast between CO_2 and oil. Last part of Figure 39 presents the CO_2 saturation distribution after 4 years of stopping the project.

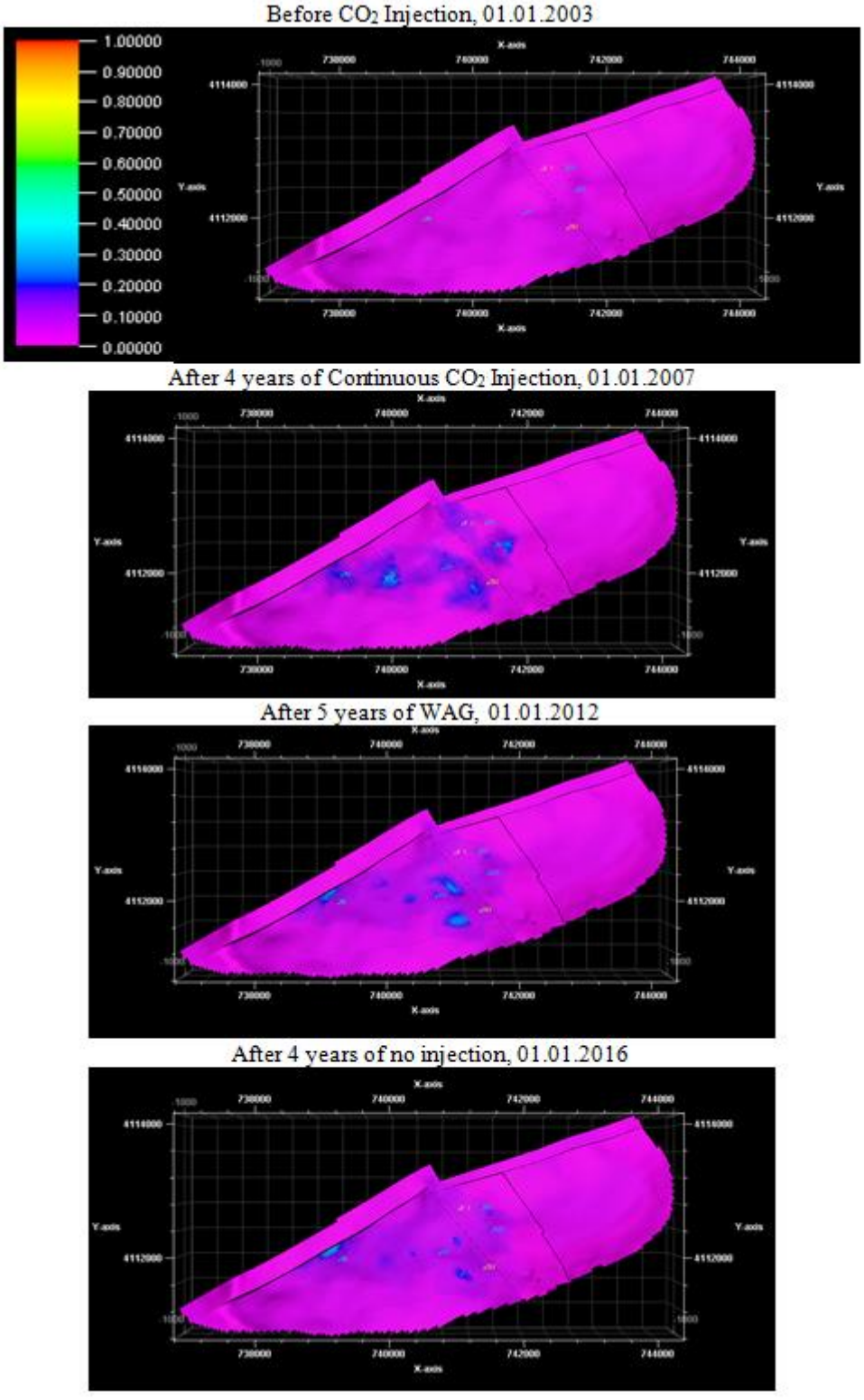

Figure 39 - 3D view of CO_2 saturation distribution from 2003 to 2016 (Real case)

Figure 40 and Figure 41 show the CO_2 saturation distributions for the CO_2 injection case (GOR: 1000 sm^3/sm^3, Injection Rate: 50,000 sm^3/d) from 2021 to 2116. After 5 years of continuous injection CO_2 started to move. Saturation of CO_2 increased quickly in the zone that is showed by a circle in the first part of Figure 40. This part of the reservoir is surrounded by permeable faults which have higher permeability than other parts. Increase in CO_2 saturation had continued to increase in this zone until 01.01.2081 (65 years). After 65 years, CO_2 saturation started to decrease in this area due to high permeability connection between production and injection wellss (Figure 41). There was both lateral and vertical migration of CO_2 but only one of them was dominant. Figure 42 presents the cross sectional view of CO_2 saturation distribution at the end of the CO_2 injection project (01.01.2116). As can be seen from this figure, there was an upward migration of CO_2 such that CO_2 plume moved to upper layers and accumulated at the top layer due to buoyancy of CO_2. In this reservoir, buoyancy force is large because of immiscible conditions and high density difference between the heavy oil and CO_2. Outcome of the upward migration was decrease in oil recovery. Only a small portion of oil could be displaced and produced from the bottom layers. It can be said that structural trapping is a very important trapping mechanism in this reservoir because of the buoyance forces. There has to be a good seal at the top of the reservoir to protect the CO_2 migration to the surface. Figure 43 shows gas saturation distribution of pure CO_2 flooding case, flue gas injection case, and Source A gas injection case at the end of each project. Injected gas moved to shallower sections of the reservoir in all cases. Source A gas moved to a smaller area when compared to that of flue gas injection and CO_2 injection due to limited amount of gas injection and shorter project time. Gas saturation distributions were higher for CO_2 flooding case when compared to flue gas injection case where less gas was injected. CO_2 has some favorable properties; oil swelling, viscosity reduction and increased injectivity. With the increase in pressure, more CO_2 dissolves in oil and oil recovery increases. Injectivity increases with increase in oil production and dissolution of CO_2. Therefore, CO_2 was injected more, occupied a larger area, and contacted with more oil.

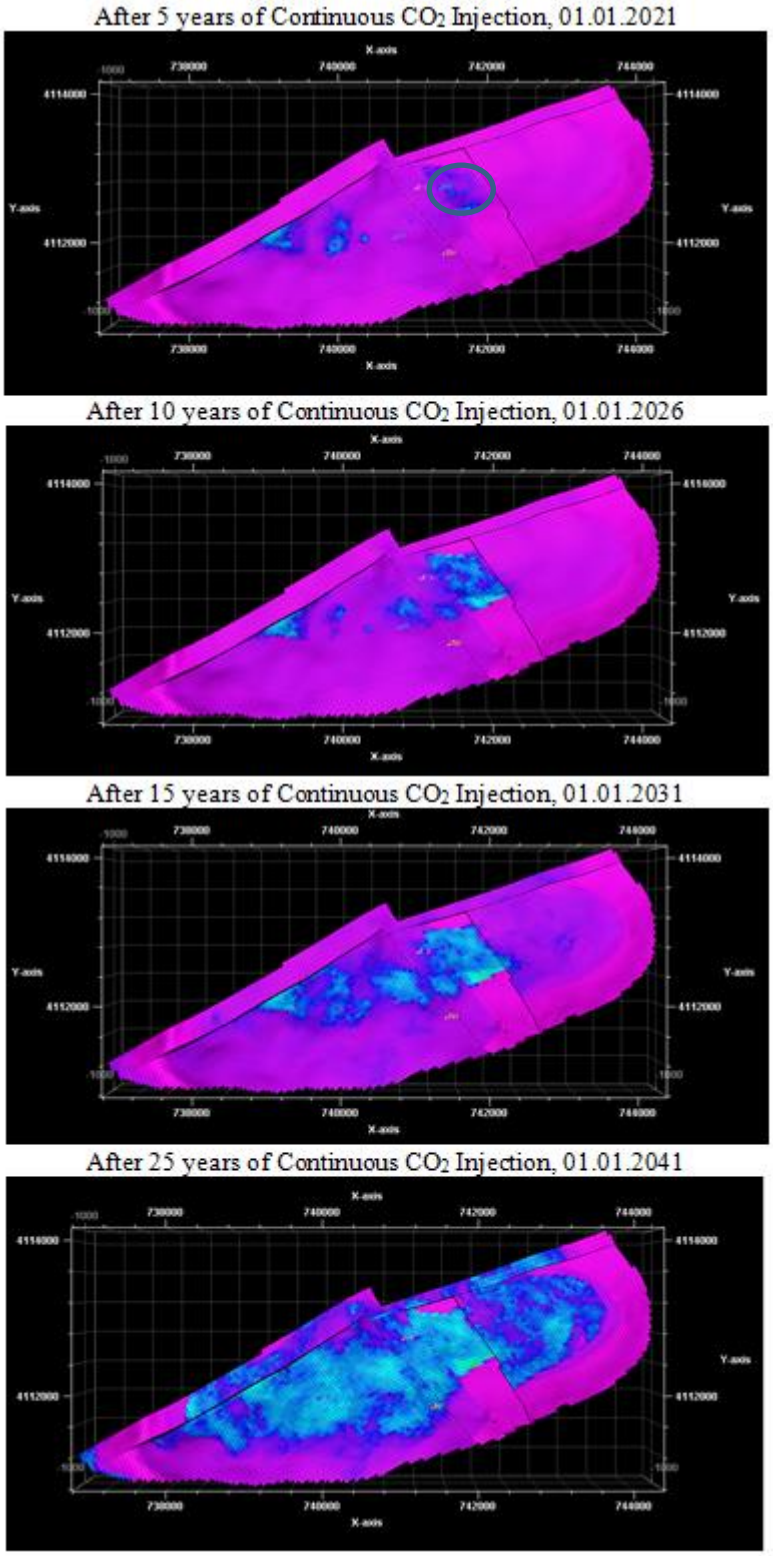

Figure 40 - 3D view of CO_2 saturation distribution from 2021 to 2041 (Continuous CO_2 injection case)

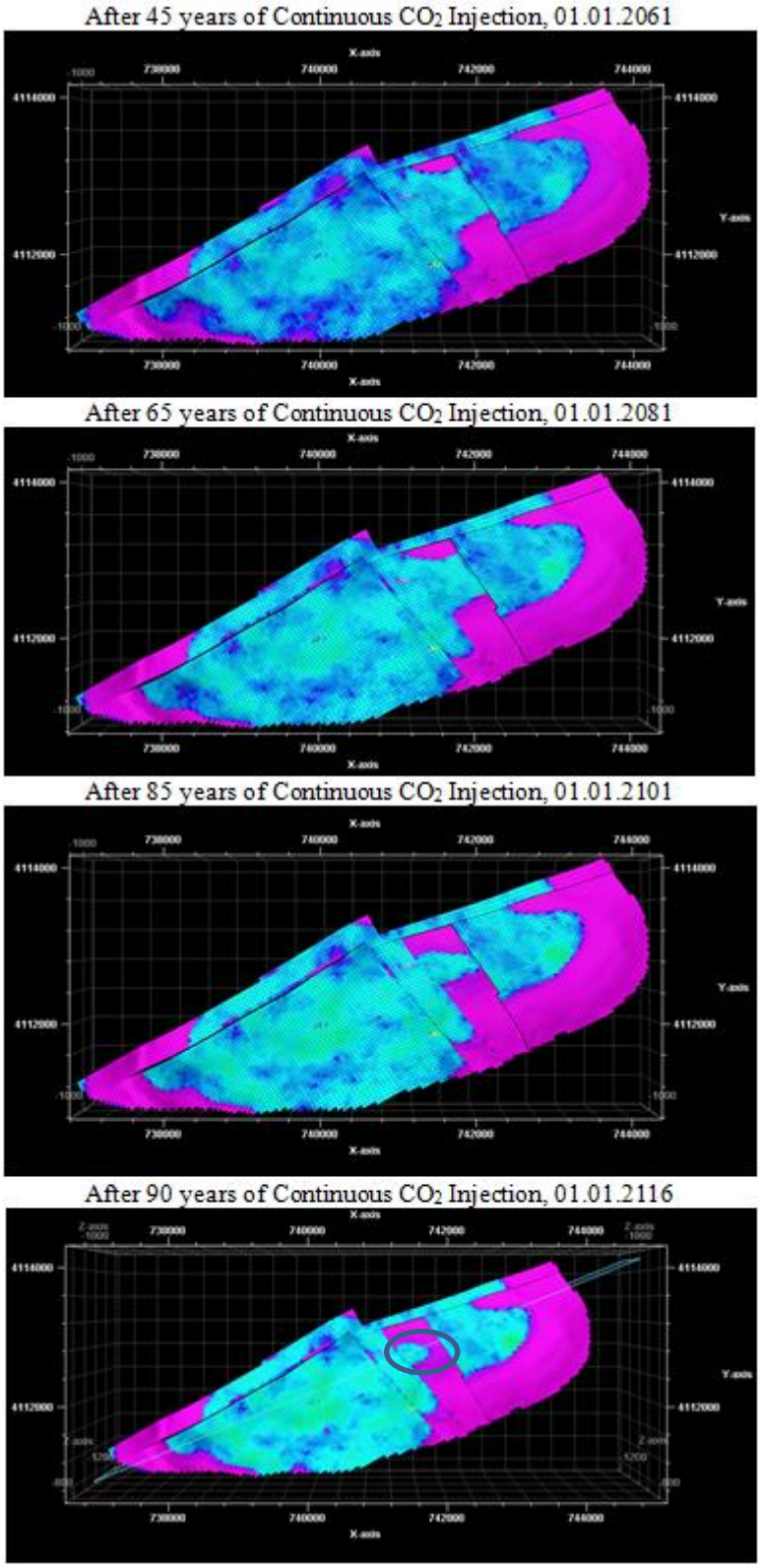

Figure 41 - 3D view of CO_2 saturation distribution from 2061 to 2116 (Continuous CO_2 injection case)

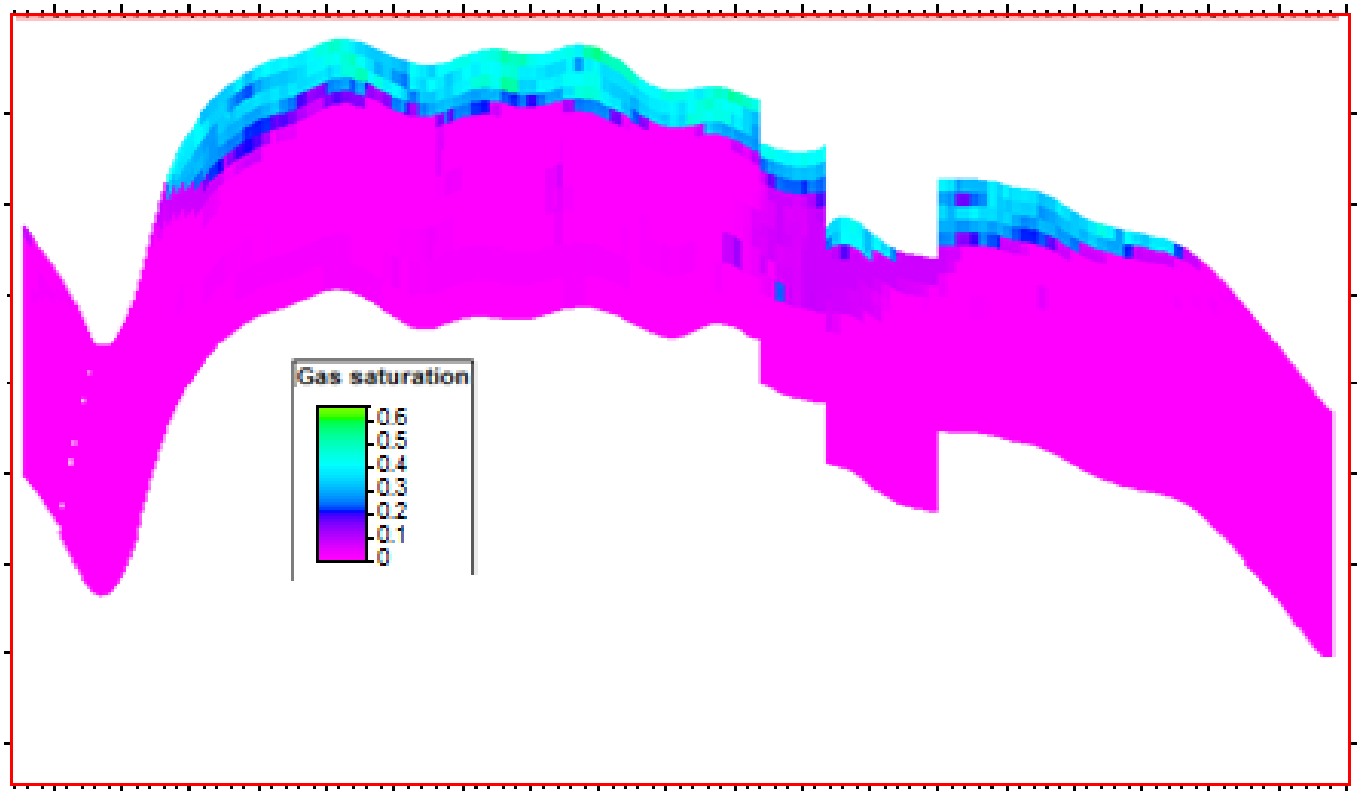

Figure 42 - Cross sectional view of CO_2 saturation distribution, 01.01.2116 (Continuous CO_2 injection case)

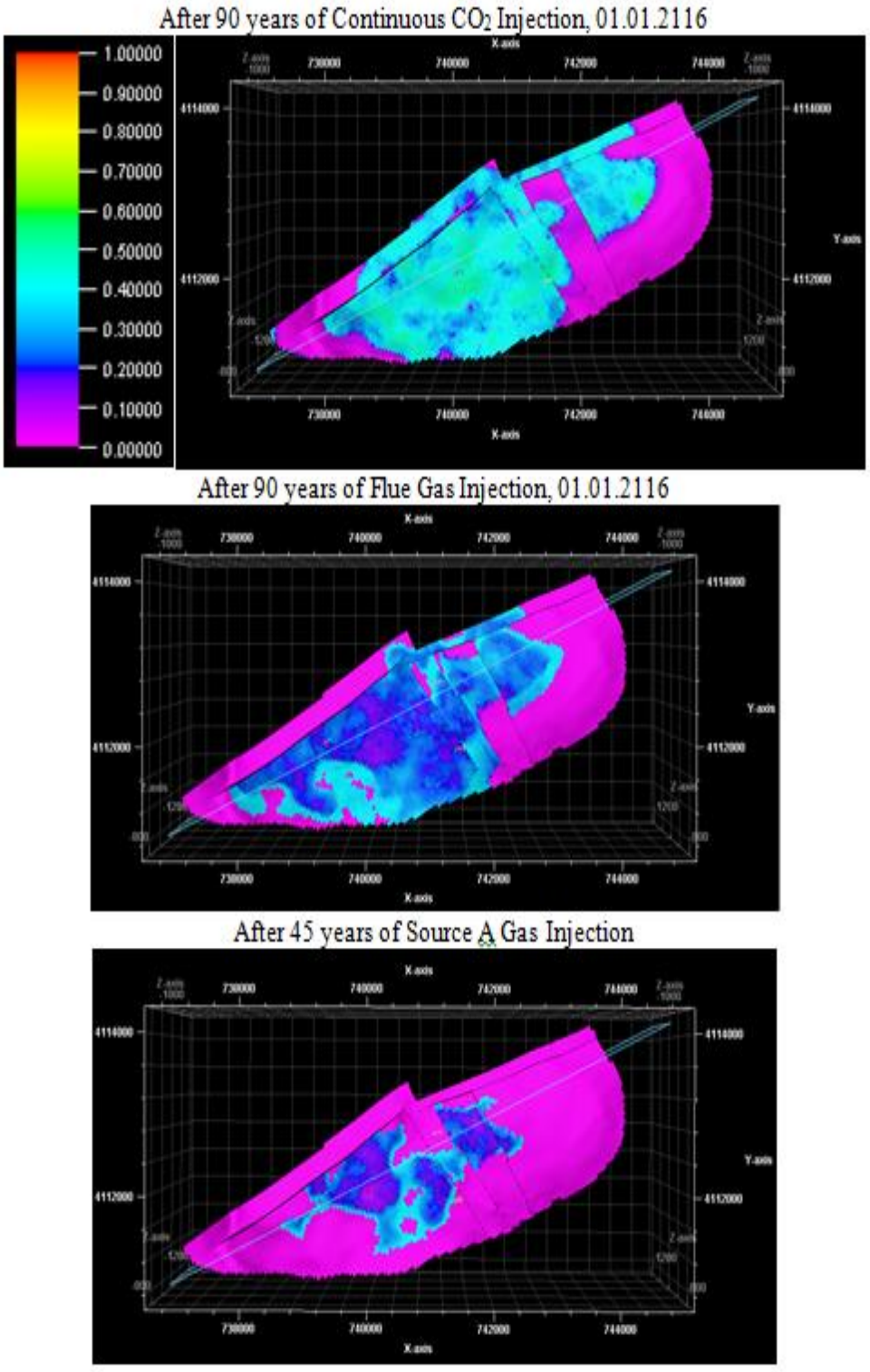

Figure 43 - 3D view of gas saturation distributions for CO_2 injection case, flue gas injection case and Source A gas injection case, 01.01.2116

6.5 Economic Investigation of Flue Gas Injection, CO_2 Injection and Natural Gas Injection

Economic model used in this study is built based on the requirements of the project. During the development of the storage or EOR project, there is a need for economic evaluation before making the final decision. For CO_2 storage and EOR projects, there are many factors that may affect the project economics. Complexity of these projects can be simplified by using objective functions. In this study, amount of CO_2 storage and net present value (NPV) are the objective functions. Our aim is to maximize the amount of CO_2 storage, and maximize the NPV of the project. Built economic model was used to calculate the NPV of the project for different scenarios. An Excel code was written to perform the economic analysis. During the construction of the model, Bender's (2011) and Ghomian's (2008) economic models were modified based on the project requirements and used. Data from the simulator is used as input in the economic model; these are; time, oil production, water production, CO_2 production and injection rates (Table 22). Table 23 shows the economic inputs used for the base case (Bender, 2011). Capital investment cost was not used for the base case and CO_2 price was used for only pure CO_2 injection case. Table 24 presents economic model outputs which were calculated by using input data from the simulator, economic inputs, and excel sheet.

Table 22 - Economic model input data from the simulator

	Units	Symbol
Time	day	t
Oil Production Rate	sm^3/d	Opro
Water Production Rate	sm^3/d	Wpro
CO_2 Injection Rate	sm^3/d	Ginj
CO_2 Production Rate	sm^3/d	Gpro
Water Injection Rate	sm^3/d	Winj

Table 23 - Economic inputs

Capital Investment (Compressor+Workover)	MM$	30
Oil Price	$/sm^3	314.491
Oil Price Inflation (Increase)	fraction/yr	0.100
Royalty	fraction	0.125
CO_2 Price	$/ton	10
Op Cost Inflation	frac/yr	0.014
Recycle and Injection Cost for CO_2	$/sm^3	0.011
Lift Cost	$/sm^3	1.250
Discount rate	frac/yr	0.120
Government Tax Rate	frac	0.200
CO_2 Credit +	$/ton	0.000
Recycle and Injection Cost for Water	$/sm^3	0.620

Table 24 - Economic model outputs

Year	yr
Oil Revenue	MM$/yr
CO_2 Purchase Cost	MM$/yr
Gas + Water Recycle & Operation Cost	MM$/yr
Lift Cost	MM$/yr
Income Before Tax	MM$/yr
Cumulative NCF before Tax	MM$
Depreciation	MM$/yr
CO_2 Credit +	MM$/yr
Government Income Tax	MM$/yr
Income After Tax	MM$/yr
Cumulative NCF after Tax	MM$
Discounted NCF After Tax	MM$
Cum Discounted NCF After Tax	MM$

Calculation algorithm to determine the net present value of the project is given below;

- Oil Revenue (MM$/yr)=

$$\frac{\text{Oil Production}(sm^3/\text{day}) * 365.25\,(\text{day}/\text{yr}) * \text{Oil Price}(\$/sm^3)}{10^6}$$

$$*(1\text{-Royalty}) * \frac{\left((\text{Oil Price Inflation} + 1)^t\right)}{10^6}$$

- CO_2 Purchase Cost (MM$/yr)=

$$\frac{Max\left((CO_2 Inj(sm^3/day) - CO_2\ \text{Pro}(sm^3/\text{day})),0\right) * 365.25 * CO_2\ \text{Price}(\$/sm^3)}{10^6}$$

- Gas and Water Recycling, Injection, and Operational Cost (MM$/yr)=

$$\left(\frac{\left(CO_2\ \text{Pro}(sm^3/\text{day}) * \text{Recycle Cost}^{CO_2}(\$/sm^3) + (CO_2 Inj(sm^3/\text{day})\right)}{10^6}\right.$$

$$\frac{\left(-CO_2\ \text{Pro}(sm^3/\text{day})\right) * CO_2 Inj\ Cost(\$/sm^3)\right)}{10^6}$$

$$\left. + \frac{\text{Water Pro}(sm^3/\text{day}) * \text{Recycle Cost}^{Water}(\$/sm^3)}{10^6}\right)$$

$$*\left((\text{Operational Cost Inflation}+1)^t\right)$$

- Lift Cost (MM$/yr)=

$$\frac{\left(\text{Oil Pro}(sm^3/\text{day}) + \text{Water Pro}(sm^3/\text{day})\right) * 365.25}{10^6}$$

$$*\text{Lift Cost}(\$/sm^3) * \frac{\left((\text{Operational Cost Inflation}+1)^t\right)}{10^6}$$

- Income Before Tax (Taxable Income), (MM$/yr)=

  $$\text{Oil Revenue(MM\$/yr)}-\text{CO}_2\text{ Purchase Cost(MM\$/yr)}-$$
  $$\text{(Gas + Water Recycle \& Operation Cost)(MM\$/yr)} - \text{Lift Cost(MM\$/yr)}$$

- Cumulative Net Cash Flow (NCF) Before Tax, (MM$)=

  -First Calculation;

  =Income Before Tax (MM$/yr)*t(yr)-Total Investments (MM$)

  -Other Calculations (at time= t_i);

  =Income Before Tax (MM$/yr)*($t_i$(yr)-$t_{i-1}$(yr))+ NCF Before Tax_{i-1}

- Depreciation (MM$/yr)=

  $$\text{Capital Investment(mm\$)*Max}((0.3094 - (t(yr) - 0.5)*0.0476),0)$$

- CO_2 Credit + (MM$/yr)=

  (CO_2Inj (sm^3/day)-CO_2Pro (sm^3/day))*365.25*CO_2 Credit ($/$sm^3$)*$10^{-6}$

- Government Income Tax (MM$/yr)=

  (Income Before Tax (MM$/yr)-Depreciation(MM$/yr)+ CO_2 Credit(MM$/yr))* Goverment Tax Rate

- Income After Tax(MM$/yr)=

  Income Before Tax (MM$/yr)-Government Income Tax (MM$)+$CO_2$ Credit(MM$/yr)

- Cumulative NCF After Tax (MM$)=

  -First Calculation;

  =Income After Tax (MM$/yr)*t(yr)-Total Investments (MM$)

  -Other Calculations (at time= t_i);

  =Income After Tax (MM$/yr)*($t_i$(yr)-$t_{i-1}$(yr))+ Cumulative NCF Before Tax_{i-1}

- Discounted NCF After Tax (MM$)=

-First Calculation;

$$= \frac{\text{Cumulative NCF After Tax (MM\$)}}{(1+\text{Discount Rate})^{t=0}}$$

-Other Calculations (at time= t_i);

$$\frac{\text{Cumulative NCF After Tax (MM\$)}_{t=i} - \text{Cumulative NCF After Tax (MM\$)}_{t=i-1}}{(1+\text{Discount Rate})^{ti}}$$

- Cumulative Discounted NCF After Tax (MM$)=

  -First Calculation = Discounted NCF After Tax (MM$)$_{t=0}$

  -Other Calculations (at time= t_i);

  =Discounted NCF After Tax (MM$)$_{t=i}$ + Discounted NCF After Tax (MM$)$_{t=i-1}$

Simulation results obtained from the simulator were imported to the code written and NPV for each case was calculated. Table 25 shows the results for each case. It has been found that highest profit can be achieved by pure CO_2 injection GOR-1000-Inj-50000 case. In addition, highest amount of CO_2 was stored with that case.

Table 25 - Economic analysis results

NPV, MM$	Case Name	Injected Gas
18.29	Base Case	-
-25.31	GOR-1-Inj-50000	Flue Gas
111.71	GOR-500-Inj-50000	Flue Gas
164.69	GOR-1000-Inj-50000	Flue Gas
163.92	GOR-1000-Inj-50000 (without CO_2SOL)	Flue Gas
141.63	GOR-2000-Inj-50000	Flue Gas
167.36	GOR-1000-Inj-40000	Flue Gas
107.98	GOR-1000-Inj-75000	Flue Gas
86.39	GOR-1000-Inj-100000	Flue Gas
73.92	GOR-1000-Inj-150000	Flue Gas
197.71	CO_2 Injection GOR-1000-Inj-50000	CO_2
98.00	Source A Gas Injection	CO_2+C_1

CHAPTER 7

CONCLUSIONS

Different gas injection scenarios in a mature oil field were studied using a history matched compositional numerical model. Due to the availability of nearby flue gas source (cement factory) and a pipeline for gas transportation, which was built to transport natural gas from the oil field to cement factory, there is a huge opportunity to decrease project costs. The results of the full-field compositional simulation have been used for an examination of the raw flue gas injection, CO_2 injection, natural gas injection, operating parameters and CO_2 solubility. Maximum CO_2 storage and oil recovery can be achieved by pure CO_2 flooding due to solubility trapping mechanism, which becomes dominant with increased CO_2 concentration and pressure. CO_2 flooding and flue gas flooding give same oil recovery for a certain time or until a certain reservoir pressure. After that, effects of CO_2 on oil increase its effectiveness. These effects are oil swelling, viscosity reduction and interfacial tension reduction due to increased CO_2 solubility. In addition, effect of CO_2 solubility becomes very important after a threshold time. CO_2 dissolved in aqueous phase increases continuously corresponding to high amount of CO_2 storage. Influence of CO_2 solubility during immiscible flue gas injection is low but it is very important during pure CO_2 injection. For mature oil reservoirs, pressurizing the reservoir with the flue gas and then injecting CO_2 might give better oil recoveries. In this way, N_2 in flue gas will provide energy to push the oil and CO_2 will dissolve in oil. In addition to these, it has been observed that water production decreases during pressurization by gas injection. Pressure of the oil production layer increases and becomes more than the underlying layer's, which is the source of the water. Highest oil recovery and gas storage can be achieved with optimized operating constraints targeting the sweep efficiency. With an increase in sweep efficiency,

reservoir gas storage capacity and oil recovery will increase. Lower GOR values as limiting criteria on production wells lead to quick pressure increase that decreases the project life, oil recovery and amount of CO_2 storage. On the other hand, higher GOR values give rise to gas production that in turn decrease oil recovery and gas storage with increased gas mobility and decreased sweep efficiency. High gas injection rates cause reduced injectivity due to quick pressure buildup that leads to early gas breakthrough. Both of these may cause reduction of both oil recovery and storage.

A comparative study was conducted to examine the efficiency of flue gas injection compared to CO_2 injection for simultaneous EOR and storage purposes. Results showed that;

1. Pure CO_2 injection leads to higher oil recovery and CO_2 storage, if injection continued for at least 25 years. Before this threshold injection time, flue gas injection and pure CO_2 injection resulted in comparable oil recoveries.
2. Amount of flue gas storage was determined as 1.1 billion sm^3 and 268 $MMsm^3$ of this gas was CO_2. 47 $MMsm^3$ of CO_2 was dissolved in oil and 19 MM sm^3 of CO_2 was dissolved in aqeous phase. Additional cumulative oil production was calculated as 1.12 $MMsm^3$ with a recovery factor of 10.09%. 1000 sm3 of flue gas was injected to produce 1 sm^3 of oil. NPV of the project was found as $141.63 MM.
3. Totally 1.63 billion sm^3 of CO_2 was sequestered and 1.57 $MMsm^3$ of oil was produced with continuous pure CO_2 flooding. 342 $MMsm^3$ of CO_2 was dissolved in oil and 80 MM sm^3 of CO_2 was dissolved in aqeous phase.1040 sm^3 of CO_2 was injected to produce 1 sm^3 of oil. NPV of the project was found as $197.71 MM.
4. It was observed that most of the CO_2 was trapped by structural and stratigraphic trapping mechanism. 26% of the sequestered CO_2 was trapped by solubility trapping mechanism for pure CO_2 injection case.

5. Pressurizing the reservoir with flue gas injection followed by pure CO_2 injection may improve the project economics. However, pure CO_2 injection is the right strategy to maximize the CO_2 storage.
6. Limiting the production wells with lower GOR constraint, caused the wells shut in due to quick breakthrough and reservoir pressure increased quickly which lead to diminished storage and oil recovery. Also, higher GOR values were resulted in low storage and recovery due to high gas mobility when compared with oil. Management of GOR values contributed to better sweep efficiency and better pressure management.
7. Injection rates need to be optimized to maximize the flue gas storage. Quick pressure buildup occurred with higher injection rates so that gas storage was reduced due to decreased injectivity. With higher injection rates, higher oil recoveries achieved at early times of the project.
8. In this reservoir, buoyancy force is large because of the immiscible conditions and high density difference between oil and CO_2. Outcome of the upward migration was decrease in oil recovery. Only a small portion of oil could be displaced and produced from the bottom layers. It can be said that structural trapping is a very important trapping mechanism in this reservoir because of buoyancy.
9. It was decided that not to invest on the transportation of gas from gas source B and gas source C due to limited gas in place and shorter project time. Gas source B can only support the reservoir for 5 years and gas source C can support the reservoir for 2 years.

CHAPTER 8

RECOMMENDATIONS AND FUTURE WORK

Even though a comprehensive study on CO_2 sequestration and EOR was conducted, there are some factors that were not considered. For example, mineral trapping, which takes long times from hundreds to thousands of years, was neglected. Modeling the mineral trapping during CO_2 storage requires additional laboratory tests and might be time consuming while working on full field simulations. Since our aim was to maximize both storage and recovery, a water injection scenario was not included. Water alternating gas injection methodology might be studied to increase recovery. Required number of additional wells, well locations, and well configurations might be optimized by maximizing storage and NPV. To add these factors, experimental design and response surface method can be used that will decrease the number of simulations.

REFERENCES

About Mardin Cement (2016). Retrieved from http://www.mardincimento.com.tr/en/aboutus/about-mardin-cement

Aguilar, R.A and McCain, W.D. (2002) "An Efficient Tuning Strategy to Calibrate Cubib EOS for Compositional Simulation", SPE 77382, SPE Annual Technical Conference and Exhibition, 29 September-2 October, San Antonio, Texas, USA.

Ahmed, T. (2000). Reservoir Engineering Handbook Second Edition. Houston, TX, Gulf Publishing Company

Ahmed, T. (2007). Equations of State and PVT Analysis. Houston, TX, Gulf Publishing Company

Ahmed, T. H., and Meehan, D. N. (2010). A Practical Approach for Calculating EOS. SPE-132455, SPE Russian Oil and Gas Conference and Exhibition, 26-28 October, Moscow, Russia.

Ali, M. T., and El-Banbi, A. H. (2015). EOS Tuning – Comparison between Several Valid Approaches and New Recommendations. SPE-175877, SPE North Africa Technical Conference and Exhibition, 14-16 September, Cairo, Egypt.

Al-Meshari, A. A., and McCain, W. D. (2005). New Strategic Method to Tune Equation-of-State for Compositional Simulation. SPE-106332, SPE Technical Symposium of Saudi Arabia Section, 14-16 May, Dharan, Saudi Arabia

Arachchige, U.S.P.R., Kawan, D., Tokheim, L. A., and Melaaen, M.C. (2013). Model Development for CO_2 Capture in the Cement Industry, International Journal of Modeling and Optimization; Volume 3, 535-540.

Ashworth, P., Rodriguez, S., Miller, A., (2010) Case Study of the CO_2CRC Otway Project, EP 103387, CSIRO Report, Pullenvale, Australia.

Babadagli, T. (2006) Optimization of CO_2 injection for sequestration/enhanced oil recovery and current status in Canada. In Lombardi S, Altunina LK, Beaubien SE, editors. Advances in the Geological Storage of Carbon Dioxide, Dordrecht: Springer; 261-270.

Bachu, S. and Adams, J.J., (2003) Sequestration of CO_2 in geological media in response to climate change: Capacity of deep saline aquifers to sequester CO_2 in solution. Energy Conversion and Management 44, 3151-3175.

Bachu, S. (2003). Screening and ranking sedimentary basins for sequestration of CO_2 in geological media in response to climate change. Environmental Geology, 44, 277−289.

Bachu, S., Bonijoly, D., Bradshaw, J., Burruss, R., Holloway, S., Christensen, N.P. and Mathiassen, O.M. (2007). CO_2 storage capacity estimation: Methodology and gaps International Journal of Greenhouse Gas Control, Vol. 1(4), 430 – 443.

Bender, S. (2011). Co-optimization of CO_2 Sequestration and Enhanced Oil Recovery and Co-optimization of CO_2 Sequestration and Methane Recovery in Geopressured Aquifers. MS thesis, University of Texas at Austin, Austin, Texas.

Bender, S., and Yilmaz, M. (2014). Full-Field Simulation and Optimization Study of Mature IWAG Injection in a Heavy Oil Carbonate Reservoir, SPE-169117, SPE Improved Oil Recovery Symposium, 12-16 April, Tulsa, Oklahoma, USA.

Bender, S., (2013). Simulation and Optimization of IWAG Injection in the Batı Kozluca Heavy Oil Field, ACI 3rd Optimising Enhanced Oil Recovery Conference, 26-28 November Doha, Qatar.

Benham, A.L., Dowden, W.E., and Kunzman, W.J., (1959). "Miscible fluid displacement — prediction of miscibility". Trans. AIME 216, 388–398.

Bradbury, J., Wade, S., (2010). Case study of the Carson CCS project. Prepared for CSIRO on Behalf of the Global CCS Institute: International Comparison of Public Outreach Practices Associated with Large Scale CCS Projects.

Bybee, K. (2007). Screening Criteria for Carbon Dioxide Huff "n" Puff Operations. Journal of Petroleum Technology, Vol. 59, No.01, 55-59.

Cakici, M. D. (2003). Co-optimization of oil recovery and carbon dioxide storage. M.Sc. Thesis, Stanford University.

Cement Production (2010). Retrieved from http://www.iea-etsap.org/web/E-TechDS/PDF/I03_cement_June%202010_GS-gct.pdf.

Chang, Y.-B., Coats, B. K., and Nolen, J. S. (1996). A Compositional Model for CO_2 Floods Including CO_2 Solubility in Water. SPE-35164, Permian Basin Oil and Gas Recovery Conference, 27-29 March, Midland, Texas.

Chen, S., Li, H., Yang, D., and Tontiwachwuthikul, P. (2009). Optimal Parametric Design for Water- Alternating-Gas (WAG) Process in a CO_2 Miscible

Flooding Reservoir. Journal of Canadian Petroleum Technology, Vol. 49, No. 10, 75-82.

Christensen, P.L. (1999) Regression to experimental PVT data, J. Can. Petroleum Technol. 38, 1-9.

CO_2 Capture Project (2008). Retrieved from http://www.co2captureproject.org/pdfs/3_basic_methods_gas_separation.pdf.

Coats, K.H., Smart, G.T. (1986) "Application of a Regression-Based EOS PVT Program to Laboratory Data", SPE Reservoir Engineering Journal, Vol. 1, No. 03, 277-299.

Cobanoglu, M. (2001). A Numerical Study to Evaluate the Use of WAG as an EOR Method for Oil Production Improvement at B. Kozluca Field, Turkey. Paper SPE-72127, SPE Asia Pacific Improved Oil Recovery Conference, 6-9 October, Kuala Lumpur, Malaysia.

Demir, M. (2016). Personal communication.

Demiral, B., Akın, S. and Okandan, E. (1995). "Characterization of a Carbonate Reservoir Using Computerized Tomography". Report PAL, Petroleum Research Center, METU, Ankara, Turkey.

Dong, M., and Huang, S. (2002). Flue Gas Injection for Heavy Oil Recovery. Petroleum Society of Canada, Vol. 41, No. 09, 44-50.

Eclipse Technical Description Version 2011.1 (2011), Schlumberger.

Encyclopædia Britannica Online, s. v. "cement". (2016). Retrieved from http://global.britannica.com/technology/cement-building-material.

Feenstra, C.F.J., Mikunda, T., Brunsting, D., (2010) What Happened in Barendrecht? Case Study on the Planned Onshore Carbon Dioxide Storage in Barendrecht, Report, The Netherlands, Energy Research Centre of the Netherlands, Petten, The Netherlands.

Fong, W. S., Tang, R. W., Emanuel, A. S., Sabat, P. J., and Lambertz, D. A. (1992). EOR for California Diatomites: CO_2, Flue Gas and Water Corefloods, and Computer Simulations. SPE-24039, SPE Western Regional Meeting, 30 March-1 April, Bakersfield, California.

Forooghi, A., Hamouda, A., Eilertsen, T. (2009) Co-optimization of CO_2 EOR and Sequestration in a North Sea chalk reservoir. SPE 125550, SPE/EAGE Reservoir Characterization and Simulation Conference, 19-21 October, Abu Dhabi, UAE.

Gale, J., Freund, P. (2001) Coal-bed methane enhancement with CO_2 sequestration worldwide potential. Environmental Geosciences, Vol. 8, 210–217.

Ghomian, Y. (2008). Reservoir Simulation Studies for Coupled CO_2 Sequestration and Enhanced Oil Recovery. Ph.D. dissertation, The University of Texas at Austin, Austin, Texas.

Gibbs, M. J., Soyka, P., Conneely, D., Kruger, D. (2001). CO_2 Emissions From Cement Production. IPCC Report: 175–82

Hadlow, R.E. (1992) Update of Industry Experience With CO_2 Injection, SPE-24928, SPE Annual Technical Conference and Exhibition, 4-7 October, Washington, D.C.

Hitchon, B. (2013) Best Practices for Validating CO_2 Geological Storage– Observations and Guidance from the IEAGHG Weyburn-Midale CO_2 Monitoring and Storage Project Geoscience, Geoscience Publishing, Sherwood Park, AB, Canada.

Huang, S. S. (1997). Comparative Effectiveness of CO_2, Produced Gas, and Flue Gas for Enhanced Heavy Oil Recovery. SPE-37558, International Thermal Operations and Heavy Oil Symposium, 10-12 February, Bakersfield, California

Hund, G., Greenberg, S., (2010). FutureGen case study. Report prepared for CSIRO on Behalf of the Global CCS Institute: International Comparison of Public Outreach Practices Associated with Large Scale CCS Projects.

Jahangiri, H. R., Zhang, D. (2012) Ensemble based co-optimization of carbon dioxide sequestration and enhanced oil recovery Int. J. Greenh. Gas Control, 8, 22–33.

Jessen, K., Kovscek, A. R., and Orr, F. M. (2005). Increasing CO_2 storage in oil recovery. Energy Conversion Management, 46(2), 293-311.

John, C. J., Maciasz, G., and Harder, B. J. (1998). Gulf Coast Geopressured-Geothermal Program Summary Report Compilation Executive Summary; DOE/ID/13366--T1-Vol.3.

Johns, R.T., Dindoruk, B., Orr F.M.Jr., (1993). Analytical theory of combined condensingrvaporizing gas drives, SPE Adv. Tech. Ser. 3,7–16.

Juanes, R., Spiteri, E. J., Orr, Jr, F. M. and Blunt, M. J. (2006). Impact of relative permeability hysteresis on geological CO_2 storage. Water Resources Research 42 (W12418), pp. 1–13.

Khan, S. A., Pope, G. A., and Sepehrnoori, K. (1992). Fluid Characterization of Three-Phase CO_2/Oil Mixtures. SPE-24130, SPE/DOE Enhanced Oil Recovery Symposium, 22-24 April, Tulsa, Oklahoma

Knopse, B., and Walleser L. (2004). Flue gas analysis in industry: Practical guide for Emission and Process Measurements 2nd ed. Retrieved from http://www.testo350.com/downloads/Flue_Gas_in_Industry_0981_2773.pdf.

Koch, H. A., and Hutchinson, C. A. (1958). Miscible Displacements of Reservoir Oil Using Flue Gas. Petroleum Transactions, AIME, Volume 213, 1958, pages 7-10.

Kovscek, A. R. (2002). Screening criteria for CO_2 storage in oil reservoirs. Petroleum Science and Technology; 20(7&8):841–66.

Kovscek, A. R., Cakici, M. D. (2004). Geologic storage of carbon dioxide and enhanced oil recovery. II: Cooptimization of storage and recovery. Energy Conversion and Management; 46 (11): 1941-1956.

Kovscek, A. R., Wang Y. (2004) Geologic storage of carbon dioxide and enhanced oil recovery. I. Uncertainty quantification employing a streamline based proxy for reservoir flow simulation. Energy Conversion and Management; 46: 1920-1940.

Kuo, S.S., (1985). Prediction of miscibility for the enriched gas drive process. SPE 14152, SPE Ann. Tech. Conf., Las Vegas, NV.

Law, D.H-S., and Bachu, S., (1996) "Hydro Geological and Numerical Analysis of CO_2 Disposal in Deep Aquifers in the Alberta Sedimentary Basin," Energy Conversion Management, Vol. 37, p. 1167–1174.

Leach, A., Mason, C.F., Veld, K. (2011), Co-optimization of enhanced oil recovery and carbon sequestration, Resource and Energy Economics., 33, 893–912.

Lisa, J., Hanle, U. S. (2004) CO_2 Emissions Profile of the U.S. Cement Industry Environmental Protection Agency Report, 1200 Pennsylvania Ave, NW. Washington DC 20460 Kamala R. Jayaraman and Joshua S. Smith ICF Consulting, 9300 Lee Highway, Fairfax, VA 22031

Lower, S. (2016). Changes of State. Retrieved from chemwiki.ucdavis.edu/Textbook_Maps/General_Chemistry_Textbook_Map/Changes_of_State.

Luks, K.D., Turek, E.A., Baker, L.E., (1987). Calculation of minimum miscibility pressure. SPE Reservoir Eng., 501–506, Nov.

Mahasenan, N., Dahowski, R. T., Davidson, C. L. (2005) "The role of carbon dioxide capture and storage in reducing emissions from cement plants in North America". Greenhouse Gas Control Technologies, Vol. 01, 901-909.

Marceau, M. L., Nisbet, M. A., VanGeem, M. G. (2006) Life Cycle Inventory of Portland Cement Manufacture, SN2095b, Portland Cement Association Report, Skokie, IL, 69 pages.

Mattax, C.C. and Dalton, R.L. (1990). Reservoir Simulation, Vol. 13. Richardson, Texas, USA: Monograph Series, SPE.

Mayer, B., Shevalier, M., Nightingale, M., Kwon, J. S., Johnson, G., Raistrick, M., Hutcheon, I., Perkins, E. (2013) Tracing the movement and the fate of injected CO_2 at the IEA GHG Weyburn-Midale CO_2Monitoring and Storage Project (Saskatchewan, Canada) using carbon isotope ratios, International Journal of Greenhouse Gas Control, Vol. 16, 177–184.

Metcalfe, R.S., Fussell, D.D., Shelton, J.L., (1973). A multicell equilibrium separation method for the study of multiple contact miscibility in rich gas drives. Society of Petroleum Engineering Journal, 3, 147–155.

Metz, B., Davidson, O., Coninck, H.C., Loos, M., Meyer L.A. (2005) Special Report on Carbon Dioxide Capture and Storage. Intergovernmental Panel on Climate Change. IPCC Chapter 5, 195–276.

Michael. L. G. (2014). Carbon Dioxide Enhanced Oil Recovery Industrial CO_2 Supply Crucial For EOR. Retrieved from http://www.aogr.com/magazine/editors-choice/industrial-co2-supply-crucial-for-eor.

Michelsen, M.L. (1980). Calculation of phase envelopes and critical points for multicomponent mixtures, Fluid Phase Equilibria, 4, 1–10.

Mosavat, N., Torabi, F. (2014). Application of CO_2-Saturated Water Flooding as a Prospective Safe CO_2 Storage Strategy. Elsevier. Energy Procedia 63 (2014) 5408 – 5419.

Mosavat, N., Torabi, F., (2014). Application of CO_2-Saturated Water Flooding as a Prospective Safe CO_2 Storage Strategy. Elsevier. Energy Procedia 63, 5408 – 5419.

Nasir, F., Chong, Y. Y. (2009). The Effect of Different Carbon Dioxide Injection Modes on Oil Recovery, International Journal of Engineering and Technology Vol: 9 No: 10, 54-60.

Nazmul, H. S. M., (2005) Techno-Economic study of CO_2 capture process for cement plants, Master thesis, University of Waterloo, Ontario, Canada.

Nghiem, L., Shrivastava, V., Kohse, B., Hassam, M., and Yang, C. (2010). Simulation and Optimization of Trapping Processes for CO_2 Storage in Saline Aquifers. Journal of Canadian Petroleum Technology, Vol. 49, No: 08, 15-22

Nouar, A., Flock, D.L. (1986). Prediction of the minimum miscibility pressures of a vaporizing gas drive. SPE Reservoir Engineering, Vol. 03, No. 01, 182-198

Ohga, K. (2003). "Fundamental tets on Carbon Dioxide Sequestration into Coal Seams" Greenhouse Gas Control Technologies, Vol. 1, J. Elsevier,Amsterdam 531-537.

Oil (2016). Retrieved from http://www.praxair.com/~/media/North%20America/US/Documents/Specification%20Sheets%20and%20Brochures/Industries/Oil%20and%20Gas/P403984%20Huff%20n%20Puff.pdf.

Oldenburg, C.M., Unger, A.J.A., Hepple, R.P., and Jordan, P.D., (2002). On leakage and seepage from geological carbon sequestration sites: Lawrence Berkeley National Laboratory, Report, Berkeley, California, U.S. Department of Energy.

Orr, F. M. (2004). Storage of Carbon Dioxide in Geologic Formations. Journal of Petroleum Technology 56, no. 9, 90−97.

Ossa. R., J. E., Bejarano, A., Flórez, A., and Santos, N. (2010). Experimental Evaluation of the Flue-Gas Injection of Barrancabermeja Refinery as EOR Method. SPE-139715, SPE International Conference on CO2 Capture, Storage, and Utilization, 10-12 November, New Orleans, Louisiana, USA.

Parson, E.A. and Keith, D.W. (1998). “Fossil Fuels Without CO_2 Emissions” Science, Vol. 282, No. 5391, 1053-1054.

Peng, D. Y., and Robinson, D. B. (1976). "A New Two-Constant Equation of State". Industrial and Engineering Chemistry: Fundamentals, Vol. 15, No.01, 59-64

Petrel Reservoir Engineering Course Book (2013). Houston, TX, Schlumberger, 1-532.

Pruess, K., Xu, T., Apps, J., and Garcia, J. (2003). Numerical Modeling of Aquifer Disposal of CO_2. SPE Journal 8, 49-60.

R.K. Pachauri and L.A. Meyer (2014). Climate Change 2014: Synthesis Report. Contribution of Working Groups I, II and III to the Fifth Assessment Report of the Intergovernmental Panel on Climate Change. IPCC, Geneva, Switzerland, 151.

Remson, D. (2010). "Storing CO_2 and Producing Domestic Crude Oil with Next Generation CO_2-EOR Technology: An Update", Report prepared for U.S. National Energy Technology Laboratory, DOE/NETL-2010/1417.

Ripepi, N. (2009). Carbon Dioxide Storage in Coal Seams with Enhanced Coalbed Methane Recovery: Geologic Evaluation, Capacity Assessment and Field Validation of the Central Appalachian Basin. PhD Thesis, Virginia Polytechnic Institute and State University, Blacksburg, Virginia.

Safarzadeh, M. A., Motahhari, S. M. (2014). Co-optimization of carbon dioxide storage and enhanced oil recovery in oil reservoirs using a multi-objective genetic algorithm (NSGA-II), Pet. Sci., 11 (2014), pp. 460–468.

Schlumberger (2005). An Introduction to PVT Analysis and Compositional Simulation, PVTI and Eclipse 300, 1-402.

Shen, L., Gao, T., Zhao, J., Wang, L., Wang, L., Liu, L., Chen, F., Xue, J. (2014). Factory-level measurements on CO_2 emission factors of cement production in China, Renewable and Sustainable Energy Reviews, Volume 34, 337-349, ISSN 1364-0321, http://dx.doi.org/10.1016/j.rser.2014.03.025.

Shokoya, O. S., Mehta, S. A., Moore, R. G., and Maini, B. B. (2005). Effect of CO_2 Concentration on Oil Recovery in Enriched Flue Gas Flood. PETSOC-2005-246, Canadian International Petroleum Conference, 7-9 June, Calgary, Alberta.

Sohrabi, M., Riazi, M., Jamiolahmady, M., Ireland, S., and Brown, C. (2009). Enhanced Oil Recovery and CO_2 Storage by Carbonated Water Injection. IPTC-14070, International Petroleum Technology Conference, 7-9 December, Doha, Qatar.

Stausland, J. (2014). Generating a Regression Model Proxy for CO_2 storage. MS thesis, Norwegian University of Science and Technology, Trondheim, Norway.

Taber, J. J., Martin, F. D., and Seright, R. S. (1997). EOR Screening Criteria Revisited—Part 2: Applications and Impact of Oil Prices. SPE Reservoir Engineering 12, 199-205.

Thomas, S. (2008). “Enhanced Oil Recovery –An Overview”, Oil and Gas Science and Technology – Rev. IFP, Vol. 63, No. 1, 9-19.

W. S. Dodds , L. F. Stutzman , B. J. Sollami. (1956). “Carbon Dioxide Solubility in Water”. Ind. Eng. Chem. Chem. Eng. Data Series, 1, 92–95.

Wang, Y, Orr F.M.Jr. (1997). Analytical calculation of minimum miscibility pressure. Fluid Phase Equilibria, Vol.139, 101–124.

Wang, Y., Orr F.M.Jr. (1998). Calculation of Minimum Miscibility Pressure, SPE-39683, SPE/DOE Improved Oil Recovery Symposium, 19-22 April, Tulsa, Oklahoma.

Whitson, C.H. (1983). "Characterizing Hydrocarbon Plus Fractions". SPEJ, Vol. 23, No. 4, pp. 683-694.

Whitson, C.H. and Brule, M.R. (2000). Phase Behaviour, Monograph Vol.20 SPE HENRY L. DOHERTY SERIES, Richardson, Texas.

Wolcott, J., Schenewerk, P., Berzins, T. and Karim, F. (1995). A parametric investigation of the cyclic CO_2 injection. J. Petrol. Sci. Eng. 14:1, 35-44.

Zhang, D.X., and Song, J. (2014). Mechanisms for geological carbon sequestration. International Union of Theoretical and Applied Mechanics, Vol.10, 319–327.

Zhang, Y. P., Sayegh, S. G., Huang, S., and Dong, M. (2006). Laboratory Investigation of Enhanced Light-Oil Recovery By CO/Flue Gas Huff-n-Puff Process. PETSOC-2004-021, Canadian International Petroleum Conference, 8-10 June, Calgary, Alberta.

CURRICULUM VITAE

PERSONAL INFORMATION

Surname, Name: Bender, Serdar
Nationality: Turkish (TC)
Phone: +90 555 624 97 96
Email: serdar.bender@gmail.com

EDUCATION

University of Texas at Austin, Austin, Texas, USA
M.Sc. in Petroleum Engineering (2011)

Middle East Technical University, Ankara, Turkey
B.Sc. in Petroleum Engineering (2008)

PROFESSIONAL EXPERIENCE

Year	Place	Enrollment
2011-Present	TPAO	Reservoir Engineer
2009-2011	UT Austin	Research Assistant
2008-2009	TPIC	Production Engineer

PUBLICATIONS

1. Bender, S. 2011. Co-optimization of CO_2 Sequestration and Enhanced Oil Recovery and Co-optimization of CO_2 Sequestration and Methane Recovery in Geopressured Aquifers. MS thesis, University of Texas at Austin, Austin, Texas.

2. Bender, S., (2013, November 26). Simulation and Optimization of IWAG Injection in the Batı Kozluca Heavy Oil Field, ACI 3rd Optimising Enhanced Oil Recovery Conference, Doha, Qatar.

3. Bender, S., and Yilmaz, M. (2014, April 12). Full-Field Simulation and Optimization Study of Mature IWAG Injection in a Heavy Oil Carbonate Reservoir. 2014 SPE Improved Oil Recovery Symposium, Tulsa, Oklahoma.

4. Bender, S., (2014, October 20). Reservoir Simulation Studies of CO_2 Flooding to Optimize Recovery from Carbonate Reservoirs. 3rd Global Innovative EOR Techniques Conference, Abu Dhabi, UAE.

5. Bender, S., (2015, May 29). EOR Projects in the Middle East Region. International Petroleum and Natural Gas Congress and Exhibition of Turkey, Ankara, Turkey.

6. Bender, S., and Akın, S. (2016, September 19). Flue Gas Injection for EOR and Sequestration: Case Study. Journal of Petroleum Science & Engineering, Under Review.